Universidad
Carlos III de Madrid

PhD Thesis

MILLIMETER-WAVE AND TERAHERTZ OPTICAL HETERODYNE PHOTONIC INTEGRATED CIRCUITS FOR HIGH DATA RATE WIRELESS COMMUNICATIONS

Author: Robinson Cruzoe Guzmán Martínez

Director: Dr. Guillermo Carpintero del Barrio

DEPARTMENT OF ELECTRONIC TECHNOLOGY

Leganés, May 2016

Universidad
Carlos III de Madrid

TESIS DOCTORAL

MILLIMETER-WAVE AND TERAHERTZ OPTICAL HERTERODYNE PHOTONIC INTEGRATED CIRCUITS FOR HIGH DATA RATE WIRELESS COMMUNICATIONS

Autor: D. Robinson Cruzoe Guzmán Martínez

Director: Dr. Guillermo Carpintero del Barrio

DEPARTAMENTO DE TECNOLOGÍA ELECTRÓNICA

Mayo de 2016

TESIS DOCTORAL

MILLIMETER-WAVE AND TERAHERTZ OPTICAL HETERODYNE PHOTONIC INTEGRATED CIRCUITS FOR HIGH DATE RATE WIRELESS COMMUNICATIONS

Autor: Robinson Cruzoe Guzmán Martínez

Director: Prof. Dr. D Guillermo Carpintero del Barrio

Firma Del Tribunal Calificador

Presidente: _____

Vocal: _____

Secretario:_____

Calificación:

_____

En Leganés, a ____ de _____ 2016

Este documento es el resultado de 7 años de trabajo, grandes experiencias las cuales me hicieron crecer tanto en lo personal como en lo laboral.

No es hasta el momento que te sientas y piensas en que ya es hora de dar otro paso y que esta etapa tiene y debe llegar a su fin. En esta vida cada ser debe recorrer diferentes caminos con innumerables experiencias, buenas o malas, pero que al fin al cabo son ganancia en la vida del ser mismo. Por eso siempre he tenido en mi mente, un verso de la Biblia el cual me inspira a seguir adelante a pesar de las pruebas y los días que se me presente. Ya que sin esas pruebas, no podría crecer como persona.

Esfuérzate y sé valiente. Solamente esfuérzate y sé muy valiente. Mira que te mando que te esfuerces y seas valiente; no temas ni desmayes, porque Jehová tu Dios estará contigo en dondequiera que vayas (Josué 1:6-:7; 1:9).

Gracias mi Señor Jehová, Dios Todopoderoso y Omnipotente por ayudarme, guiarme y darme las fuerzas, la sabiduría, la paciencia, el entendimiento y el conocimiento necesario para recorrer este camino, y obtener un logro más en mi vida, ya que sin ti no lo hubiera podido lograr. La Honra y la Gloria sean para ti por siempre y para siempre.

A mi esposa, Alexandra por darme aliento y apoyo en aquellos días que se acercaban para entregar el documento, diciéndome un poco más que tú puedes.

A mi hija Lydia Marie Guzmán Martínez como ciudadana Suiza, o Lydia Marie Guzmán Roudier como ciudadana Colombiana, el haber nacido y que ha sido una de las grandes bendiciones que solo Dios puede dar al hombre. Cada vez que llego a mi casa, después de un día de arduo trabajo, me recibe con una sonrisa. Una experiencia y un sentimiento que no puede ser descrito, y que solo aquellos que son padres lo pueden saber.

A mis padres y hermanos por su apoyo, y constante aliento para seguir adelante en este proyecto.

A mi tutor Guillermo Carpintero, por brindarme la oportunidad de pertenecer al grupo de investigación, por transmitirme conocimientos durante este tiempo

Hay otros actores, a los cuales les agradezco sus aportaciones varias. A Carlos Gordon por haber compartido tantas noches de trabajo en el laboratorio cuando era necesario, hasta algunos sábados también. Y de su filosofía de que el chándal pega con todo, hasta que llegas a una reunión de trabajo, y te dices a ti mismo, "Huy, como que soy el niño diferente".

A Luis Jorge, a él le gusta que le llamen mejor "Mex", por aquellos días en los cuales levantaba un cartel en el cual estaba escrita la palabra No para poderme responder cuando estaba en su mundo de fantasía de manga japonés, o viendo películas y series en cuevana, o viendo videos japoneses en youtube mientras el programa se estaba ejecutando. Además cuando me gritaba, oiga Don, "grande perro", para indicarme que algo en ingles estaba incorrecto.

A Julio Posada por ser aquella persona que Dios uso para yo poder llegar aquí a estas tierras, y poder cumplir esta meta. Como además de poder hacer parte de los 300.

A todos los 300, que a pesar de que mi estilo de juego, que algunas veces es un poco rudo dependiendo de cómo se desarrolla el mismo, que por tratar de derribarme sufrieron alguna lesión, pero sobre todo por darme la oportunidad de poder compartir con ellos desde el primer día que llegué España.

Abstract

The data rate of wireless communications systems has been increasing because of the new applications that today's society are applying. The prospective data rate for wireless communications in the marketplace will be 100 Gbps within 10 years. Therefore, to enable such data rates the use of millimetre and terahertz (THz) waves, whose frequencies range from 100 GHz to 1 THz, for broadband wireless communications is very suitable and efficient. At frequencies above 100 GHz, GaAs and InP based devices and integrated circuits (ICs) have been key players in THz communications research, because of high cut-off and maximum frequencies of transistors.

In fact, the photonics-based transmitter has become more effective to achieve higher data rates of over 20 Gbps. This could be realized thanks to the availability of telecom-based high-frequency components such as lasers, modulators and photodiodes (O-E converters). The use of optical fiber cables enables us to distribute high-frequency RF signals over long distances, and makes the size of transmitter frontends compact and light. Regarding the photonics-based receiver, photodiode is the photonic component best suited to be a signal downconverter. It is used an enveloped detector, so an easy modulation format such as on-off keying shifting (OOK) can be used to recover the transmitted data.

Most common optical continuous wave (CW) signal generator is based on an optical heterodyning, using a dual-wavelength optical source. In this technique, two optical wavelengths λ_1 and λ_2 are mixed on a photodiode or a photoconductor to generate an electrical beat note with its frequency being determined by the difference of the two

optical wavelengths. There are different solutions to implement the dual wavelength source. The most straightforward source involves combining the light from two independent different single-frequency semiconductor lasers.

The most straightforward approach to implement these signal generation schemes is to assemble the required discrete components. However, the optical fiber connections that are required introduce many problems, including path length variations due to thermal variations. A novel approach, that is becoming readily available nowadays, is to use photonic integration techniques. Photonic integration allows placing all of the required components onto a single chip. This has several advantages, starting from eliminating fiber coupling losses among the different components. Besides, a reduced size of the components gives a result a cost-effective solution.

Acronyms

AWG	Arrayed Waveguide Grating
AWGL	Arrayed Waveguide Grating based Laser
BB	Building Block
BER	Bit Error Rate
DBR	Distributed Bragg Reflector
DFB	Distributed FeedBack
EC	External Cavity
ECLD	External Cavity Laser Diode
EOPM	Electro-Optical Phase Modulator
ESA	Electrical Spectrum Analyzer
FPR	Free Propagation Region
FSR	Free Spectral Range
FWHM	Full-Width at Half-Maximum
GIP	Generic Integration Platforms
InGaAs	Indium Gallium Arsenide
InP	Indium Phosphide
LNA	Low Noise Amplifier
LW	Linewidth

MIR	Multimode Interference Reflector
mmW	Millimeter wave
MPW	Multi-Project Wafer
MZM	Mach-Zehnder Modulator
OOK	On-Off Keying
PHS	Phase Shifter
PIC	Photonic Integrated Circuit
SOA	Semiconductor Optical Amplifier
THz	Terahertz
UTC-PD	Uni-Travelling Carrier Photodiode

Index

Introduction

1.1 Introduction

Over recent decades, data rates in both wired and wireless communications systems have been increasing exponentially. Based on current trends, multi-gigabit-per-second wireless communications will be needed in order to cope with future needs [1]. Figure 1.1 shows the growth of the data rates in wired (fiber optic) and wireless communication links. Extrapolating the current trend in data rate growth, it is expected that wireless data will represent a significant proportion of total backbone traffic and that much faster wireless transmission rates will be required to support more sophisticated, bandwidth-intensive applications [2]. An important aspect to be highlighted from Figure 1.1 is the gap that exists between the data rates among wired and wireless communication systems. Wired technology (which includes fiber optic and coaxial cables) have already achieved a 100 Gbps data rate in 2010, whilst wireless technology is still increasing, achieving a maximum data rate of 100 Gbps using 16-QAM modulation format in 2013 [3]. It is expected that by 2020, the wireless data rates will reach more than 100Gbps.

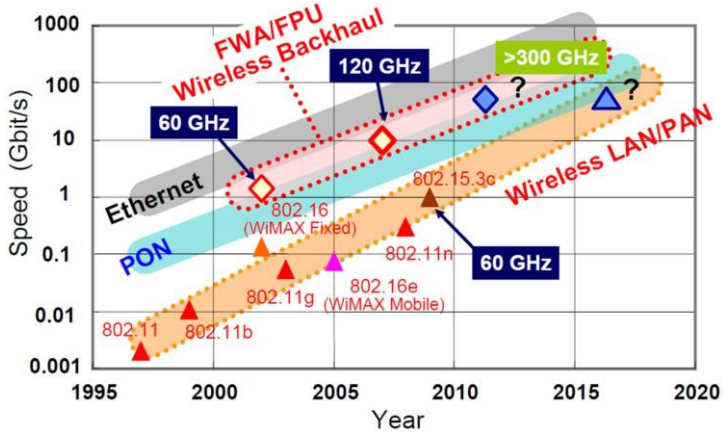

Figure 1.1. Data rate have been increasing exponentially in the last decades

The growth rate shown in Figure 1.1 has been coined as Edholm's law, describing that the demand for bandwidth in wireless short-range communications has doubled every 18 months over the last 25 years [4].Within the current frequency bands allocated for wireless communications, at 2.4 and 5 GHz, the available bandwidths are 40 and 160 MHz, respectively, with data rates up to 600 Mbps which are too narrow for broadband services. It is therefore necessary to consider a suitable solution to overcome the data rate limitation [5]. This has been termed as the bandwidth problem. In a recent interview to the father of the cellular phone, Martin Cooper, he stated that the bandwidth problem will only be solved through the creation of new spectrum [6]. To date, different approaches have been considered to increase the data rates of wireless data links, the most promising ones being: a) to increase the complexity of the modulation formats (higher order modulation formats), b) use free-space optical communications, or c) increase the frequency of carrier waves to the millimeter and Terahertz range) [5].

Higher order modulation formats have been shown to require very high spectral efficiency modulation formats to enable 100 Gbps wireless data rates using electronic or/and photonic technology. The 8.6 GHz bandwidth available in the unlicensed (60 GHz) [7] and 10 GHz (2 x 5 GHz, or 8 x 1.25 GHz) in the "lite license" (E-band, 71-76 and 81-86 GHz) [8] have shown that these spectrum allocation is enough to transmit a gigabit of data (1 Gbps or GigE) with simple modulation schemes such as BPSK, but using a 64-QAM [9] or higher order modulation formats full duplex data rates of 10 Gbps (OC-192, STM-64 or 10GigE) have been realized using electronic technology with a maximum transmitter output power up to 10 dBm [10]. There are several drawbacks to this kind of modulation format, mainly the need for

modulation/demodulation systems which increase the cost, the power consumption and introduce processing delays [11].

Free-space optical communications, currently using the visible and near-infrared (NIR) regions of the spectrum, offer a competitive wireless solution for point-to-point wireless links. Recent reports have demonstrated 100Gbps speeds [12], employing higher order modulation formats such as QPSK, QAM and polarization multiplexing systems. The main drawback of this technology is its dependence on the atmospheric conditions, especially to fog and rain, but also to humidity fluctuations which cause the scintillation effect [4]. This effect generates real refractive index fluctuations which can destroy the flat phase front of an IR light beam when it passes a few kilometres of air.

A very competitive approach is to increase the carrier wave frequency into the millimeter and terahertz range, where large frequency bands are still unregulated, offering the required bandwidth for broadband communications. As shown in Figure 1.2, these frequencies lie in a region of the electromagnetic radiation spectrum between photonics on the one hand (infrared range) and electronics (millimeter wave range) on the other, having coined the term "THz Gap" for this region.

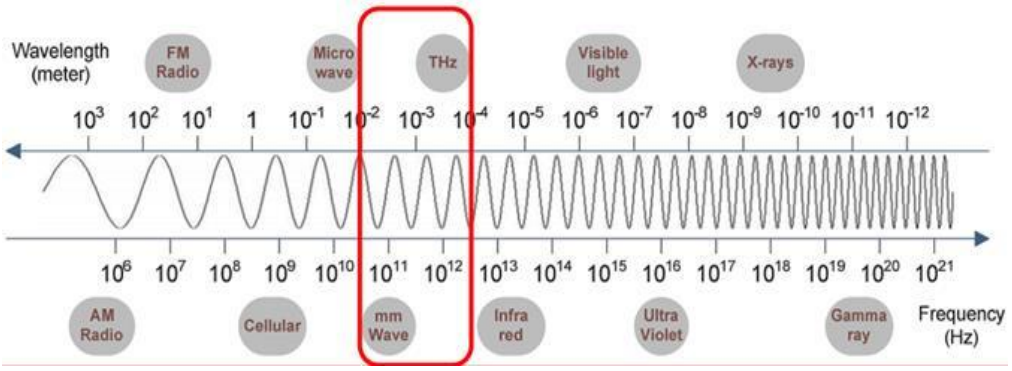

Figure 1.2. The THz Gap in the Spectrum of the Electromagnetic Radiation

The special characteristics of this range, where resonance frequencies of different compounds are located, makes it suitable for a wide range of applications beyond broadband communications [13], metrology [14], bioscience, spectroscopy [15], remote sensing [16] and imaging for security applications [17]. One of the main drawbacks of this approach is that it is hard to make Terahertz sources that deliver sufficient power, required as the Terahertz waves in atmosphere experience high losses. This challenge can be addressed through the source as well as through the development of compact receiver modules with a high responsivity and broad bandwidth.

Figure 1.3 represents the propagation losses over the millimeter-wave and Terahertz frequency range, including the atmospheric attenuation for different weather conditions [18], [19], [20], attenuation peaks due to oxygen and water vapor absorption peaks, which define transmission windows on which future wireless links could be operated Currently, a lot of research concentrates on wireless communication at millimeter-waves in the unlicensed 60 GHz band between 57-64 GHz and the W-band between 75-110 GHz.

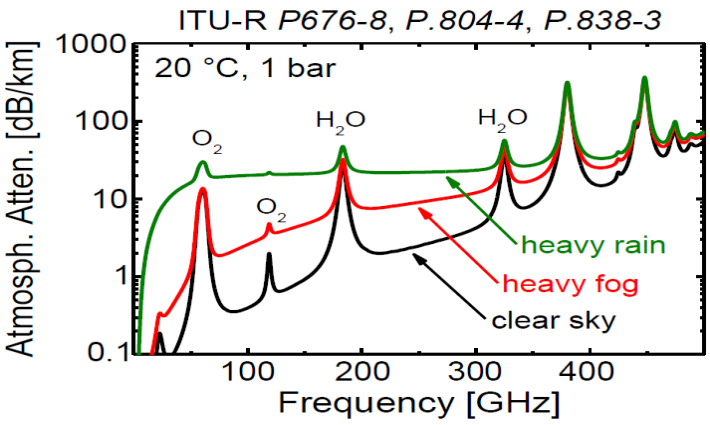

Figure 1.3. Propagation losses over the millimeter-wave and Terahertz frequency range, including the atmospheric attenuation in the range 0-500 GHz under different weather conditions according to ITU standards [18], [19], [20], attenuation peaks due to oxygen and water vapor absorption peaks.

Besides, the bands above 275 GHz remain unregulated, with several tenths of GHz of available bandwidth, being very attractive for data rate up to 100 Gbps and beyond.This allows using simple modulation formats, such as On-Off Keying (OOK), which eliminate coding delays [21]. However, as the free-space path loss is governed by the Friis' equation, which states that the loss increases with the square of the carrier frequency and the square of the link distance, wireless links at carrier wave frequencies above 100 GHz usually are directional, line-of-sight, point-to-point links.

Two different approaches for the millimeter-waves and terahertz signal generation can be done. The first approach is based on electronic up-conversion where two different configurations can be developed. The first configuration is the easiest way of generating mmW and THz signals in which a continuous wave (CW) signal generator followed by some frequency multipliers to increase the input frequency are used. In the second configuration, an optical data signal is transmitted over fiber and then received at a photodetector. After photo detection, the baseband data signal is up-converted to the millimeter-wave carrier frequency by a broadband electronic mixer implemented with millimeter-wave monolithic integrated circuits (MMIC). There have been several demonstrations of broadband wireless links, being NTT Microsystem Integration Laboratories the first to report a successful field trial of a wireless link operating at 120 GHz, showing a 10 Gbps data rate using electronic based technology [22]. Other demonstration at 220 GHz has been reported in [23].

The second approach is based on photonic technology. The photonics-based transmitter has proven to be effective to achieve higher data rates of up to 1 Gbps and above. This could be realized thanks to the availability of telecom-based high-frequency components such as lasers, modulators and photodiodes (O-E converters). The use of

optical fiber enables us to carry high-frequency RF signals over long distances making as well the size of the transmitter frontends compact and light. There have been several demonstrations reported at 120 GHz with data rate up to 3 Gbps [24]. Recently, 100 Gbps data rate on a wireless sub-THz communication system using photonic generation of the carrier wave at 237.5 GHz has been reported [3].

In this thesis, we present a novel approach developing a high capacity wireless link operating in the millimetre wave range using photonic integrated technology. Photonic-based systems present two main drawbacks, their size and cost. Photonic integrated solutions allow to reduce the size implementing multiple functions on a chip, as well as the cost, using multi-project wafer runs to reduce development costs.

There are several photonic techniques used for the generation of signals with frequencies in the mmW and THz range. The following section will introduce some of the most common, with emphasis on the techniques suitable for photonic integration.

1.1.1 Photonic techniques for the optical signal generation.

As we have already highlighted, increase the carrier wave frequency into the millimeter and terahertz wave region is a cost effective solution to broadband wireless links [25]. The difficulty to generate, amplify and modulate signals within these frequency ranges has been addressed combining electronics and photonics, emerging the field of microwave photonics (MWP). This field is a crossroad between photonics and radio-frequency (RF) engineering that combines the best of both worlds to enable key functionalities that are either too complex or not available on the RF domain alone [26].

It is commonly accepted that photonic techniques will play special relevance for frequencies starting about 100 GHz, and into the terahertz range, up to 10 THz. Photonic technologies have pioneered the access to this range, providing unique advantages in terms of quality of the generated signal (low phase noise, wide frequency tuning range) and modulation bandwidth [21], [27], [28]. To date, several wireless communication links that have been reported operating above 100 GHz use different photonic generation techniques for the carrier wave signal [29].

A photonic signals generation system is usually composed to two main building blocks, as shown in Figure 1.4, which are an optical frequency synthesizer (OFS) and an opto-electronic converter (OE). The OFS is responsible for the generation of a photonic signal, that when shined onto the OE, converts the optical signal into an electrical signal with the desired frequency. For the optical frequency synthesizer, there are two main photonic signal generation techniques, pulsed or optical heterodyne [29].

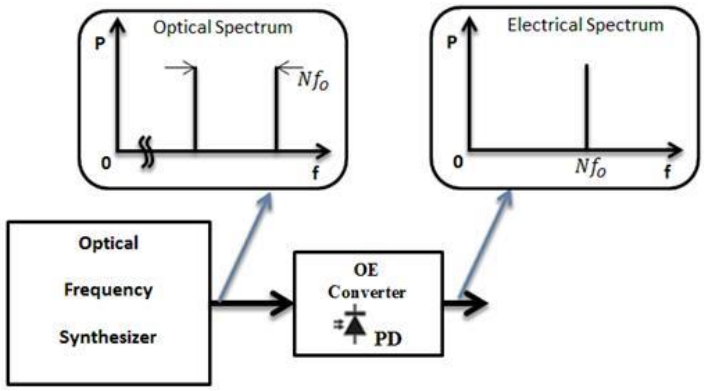

Figure 1.4. Photonic Signals Synthesis Technique

A schematic diagram of a system using a pulsed signal generation technique is shown in. Figure 1.5 shows the block diagram of a pulsed source. The optical signal is a train of short optical pulses, equally spaced in time by the pulse repetition period. Its

inverse is the repetition rate frequency (f_{ML}). The optical spectrum of such a source are optical modes around the fundamental optical frequency (f_O), spaced by the repetition rate frequency (f_{ML}). A high speed optical modulator is then used to introduce the data signal, which can be noticed as an increase in the linewidth of the optical modes. When shined onto the OE converter, an electrical signal is generated with its frequency given by the repetition rate of the pulses.

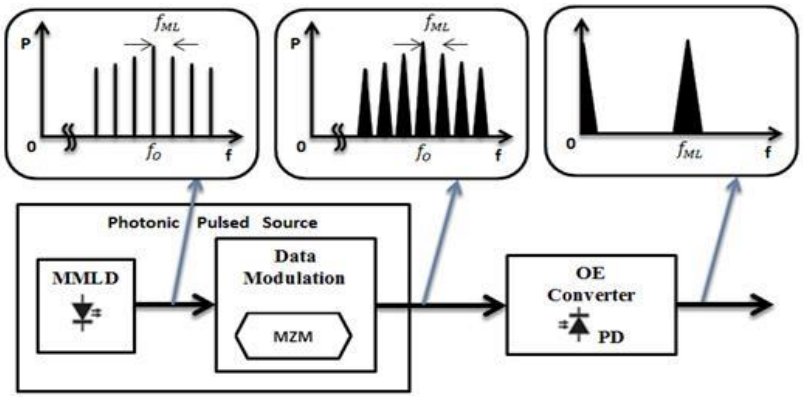

Figure 1.5. Pulsed Source Technique

A common form to implement this technique is using Mode Locked Laser Diodes (MLLD), either in passive or hybrid regimes [29]. The repetition rate frequency (f_{ML}) is determined by the resonator cavity length, and usually has a poor tunability, typically from 100 MHz to 1 GHz [30], [31].The phase noise of passively mode-locked lasers based on Fabry-Perot lasers is relatively high with an optical linewidth and frequency drift less than 200 kHz and 200 kHz/hour respectively [30]. The case of active mode locking, in which the laser is driven with an electronic oscillator, the phase noise is much lower (<–75dBc/Hz at an offset frequency of 100 Hz) [32], presenting an excellent stability.

Optical heterodyning is the simplest signal generation technique, where two optical frequencies f_1 and f_2 are mixed, creating two new signals, one at the sum $f_1 + f_2$ and the other at the difference $f_1 - f_2$. Typically only the difference frequency is observed at the output of the OE, often refer to as difference frequency of beat frequency. There are different forms to implement an optical heterodyne source.

An optical heterodyne signal is usually achieved combining the output of two laser diodes through a 50/50 optical coupler as shown in Figure 1.6. An electrical beat note signal or radio-frequency signal is then generated at the output of the photodetector with a frequency corresponding to the wavelength spacing of the two optical waves. While this approach provides an excellent frequency tuning range, from a few tenths of MHz to 10 THz [33], the main problem is that, its frequency stability is generally poor. The phase noise is –75 dBc / Hz at an offset frequency of 100 MHz, and the frequency drift is more than 10 MHz/hour [32]. It is due to the fact that both lasing modes are not correlated.

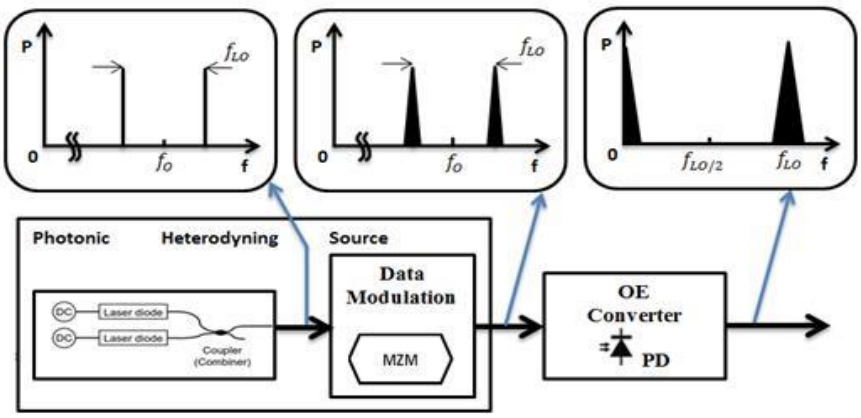

Figure 1.6. Optical heterodyning using two laser diodes

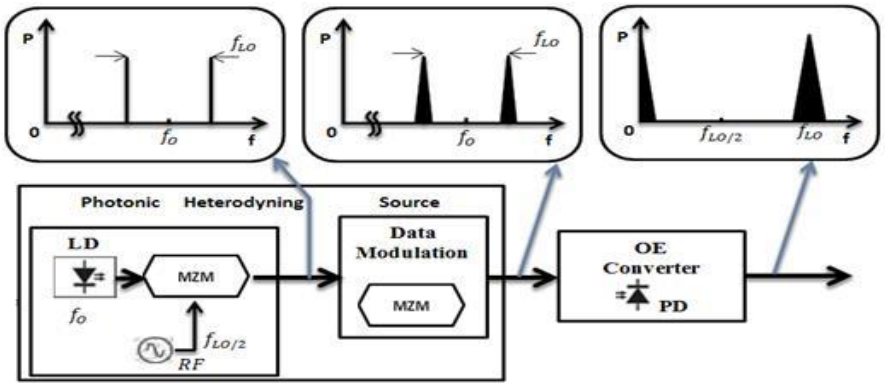

Figure 1.7. Double side band suppression carrier (DSB-SC) Heterodyning Source Technique

In order to increase the stability of the generated signal, a common approach is to use double sideband signal with a suppressed carrier (DSB-SC), shown in Figure 1.7. It employs a single frequency laser, emitting at the optical frequency f_o, and a Mach-Zehnder Modulator (MZM) driven by the local oscillator frequency (f_{LO}) at half of the required transmission frequency [28]. An extra data modulator is necessary for the data modulation.

The difference between these two aforementioned optical heterodyne techniques is that the lasing modes generated in the DSB-SC have the same frequency drift, phase noise and frequency stability which are related to the features of the local oscillator. The main drawback is that the tunability is limited by the frequency range available by the local oscillator. Regarding two laser sources optical technique, it has a wider tunability range than the DSB-SC, besides, the generated lasing mode has different characteristic due to the fact that they come from different laser source

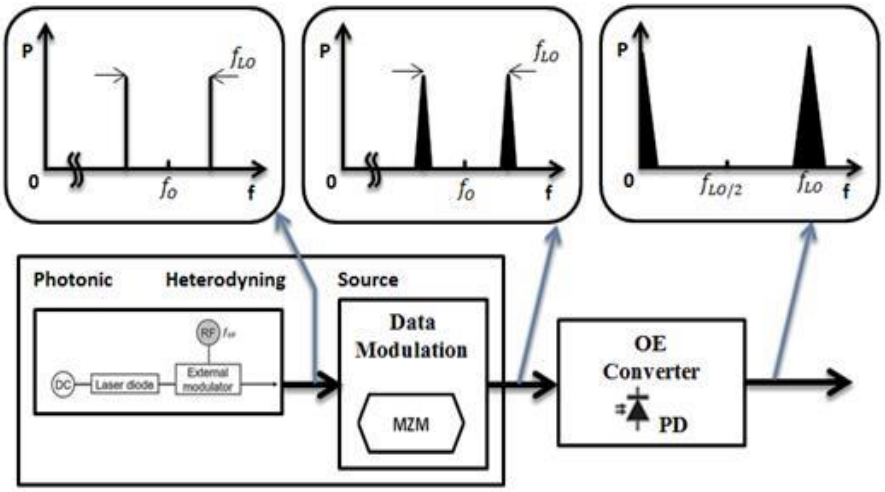

Figure 1.8. Combination of a continuous-wave (CW) laser and an external modulator

Another method is the combination of a continuous-wave (CW) laser and an external modulator, as shown in Figure 1.8. In such scheme, the modulator has to offer wide frequency bandwidth, which is limited by the driver electronics, and the state of the art that is approximately 110 GHz [34]. On the other hand, it has excellent phase noise or stability of the generated signal as it depends on the RF synthesizer. Figure 1.8 shows the experimental arrangement of a continuous-wave (CW) laser and an external modulator

The last method of optical heterodyne is an optical *frequency comb generator (OFCG)*, which is one of the most sophisticated photonic signal generation schemes that satisfy all the requirements of bandwidth and tunability greater than 2 THz [35], power output is high determined by the laser diode and the stability or phase noise determined by electronics. Recent results have demonstrated that it is possible to integrate a comb source with >2 THz bandwidth and <10 Hz frequency error between comb lines using an InGaAsP/InP quantum well (QW) [35].

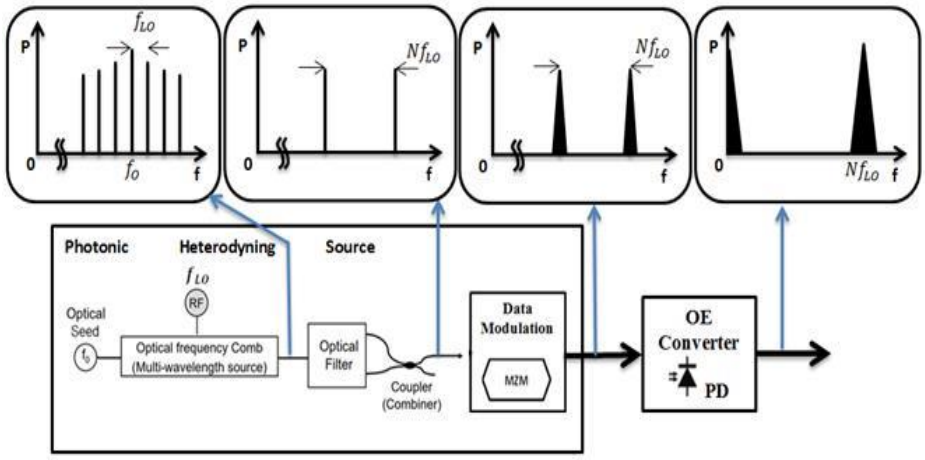

Figure 1.9. Block diagram, MMW/THz-wave generator with an OFCG

For signal generation, the OFCG is followed by an optical filter block, which selects two wavelengths from the OFCG spaced by the frequency desired for the synthesithed signal and it is necessary the optical-to-electrical (O-E) converter, or photo mixer at the end to complete the total signal generation. Figure 1.9 sketches the structure for signal generation, the OFCG, the optical filter and the (O-E) converter in the block diagram.

Signal generation using photonic techniques have several advantages over electronic techniques in bandwidth, tunability and stability or phase noise, all of which are key parameters that are used to characterize a signal source. The ***bandwidth*** is related to the amount of information that can be transferred through a communication channel. A band of a given width can carry the same amount of information regardless of where that band is located in the frequency spectrum. Therefore, bandwidth is the frequency range occupied by a modulated carrier wave. The ***tunability*** refers to the ability of the source to change the frequency of the generating signal controlled by some external command. The ***tuning range*** is then the range of frequencies within which is possible to adjust the frequency of the signal. The ***output power*** is the amount of energy that is delivered by the transmitter, which is directly related to the achievable transmission

distance. Finally, the frequency generated by a signal source is not perfectly stable, but rather exhibits some variation due to noise, which leads to a finite linewidth of the signal. This noise is characterized by the ***phase noise*** (or Stability).

Each photonic generation technique has its own performance in terms of the above parameters. Table 1.1 shows a comparative among different photonic-based signal generation techniques. Pulsed sources are represented by mode-locked laser diodes (MLLD) [30], [31], and for optical heterodyne, we account for: a) continuous-wave (CW) laser and an external modulator [34], b) two laser diodes [32], [33], and c) Optical Frequency Comb Generator (OFCG) [35].

Photonic Signal Synthesis Techniques	**Method**	**Bandwidth**	**Tunability**	**Power Output**	**Stability / Phase Noise**
Pulsed Sources	a) Mode-Locked Laser Diode (passive/active)	Good Passive > 1 THz Active > 200 GHz	Bad from 0,1 to 1 GHz	High	Excellent for active Bad for passive
Heterodyning Sources	b) CW LD + external modulator	Good around 100 GHz	Good approximately 110 GHz	High	Excellent determined by electronics
	c) Heterodyning two LDs (with a short lasing cavity)	Excellent 0,1 to 10 THz	Excellent from 0,1 to 10 THz	High	Poor, bad Frequency drift large linewidth
	d) Optical comb (OFCG) + filter	Excellent > 2 THz	Excellent > 2 THz	High	Excellent determined by electronics

Table 1.1. Comparison among mmWs/THz-waves generation methods [36]

Pulsed sources have the capability of generating an optical output power greater than the heterodyning sources. It is because of many lasing modes are generated into the lasing cavity of laser. However, in free-running operation or passive mode-locked regime not all the generated pulses are locked in phase. Therefore, the frequency stability, the phase noise, the electrical linewidth and the frequency drift are greater than the heterodyning technique. Active mode-locked regime allows us to enhance and improve the performance of the pulsed source which depending on the external RF signal generator. The major drawback of this kind of photonic technique is that its tunability does not allow us to have a broad tuning range of the lasing modes. Regarding heterodyning sources which having an optical output power less than the pulsed sources, they have the advantage of providing a broad tuning range of the lasing modes. By using longer laser cavity, the frequency stability, the phase noise and the electrical linewidth can be reduced becoming smaller than the pulsed sources working in free-running operation.

In summary, the best photonic technique to generate millimeter-wave and terahertz signals with a broad tuning range of the lasing modes is the heterodyne technique. However, the pulsed sources are very useful for applications where high optical output power is required. The most straightforward approach to implement these photonic signal generation schemes is to assemble such topologies using the required optical components such as laser, modulators, optic fibre, etc. However, the optical fibre connections that are required introduce many problems, including path length variations due to thermal variations. A novel approach, that is becoming readily available nowadays, is to use photonic integration circuits (PICs).

Photonic integration allows placing all of the required optical components onto a single chip. This has several advantages, starting from eliminating fibre coupling losses among the different components. Besides, a reduced size of the components gives a result a cost-effective solution. Therefore, optical heterodyning sources where two independent laser sources are used can be developed. Multiwavelength transmitters developed and presented in this thesis could become key components for data communication and telecommunication applications, for example in radio-over-fiber and wireless data transmission link systems. One of the most promising configurations, in terms of the circuits scalability and further possibility of high scale on-chip integration, as well as attractive from the performance perspective (including high output power, narrow optical linewidth, high speed modulation), are AWG-laser based transmitters where arrays of fixed and tunable lasers can be integrated.

This work addresses the development of multiwavelength photonic transmitters, operating in dual-wavelength regimen using the generic integration approach. We demonstrate that photonic multiwavelength sources can be made in indium-phosphide-based generic technologies using building blocks. In this thesis we propose two different multiwavelength transmitter structures that could be applicable in wireless data transmission link systems.

1.2 Outline

This thesis describes the design of multi-wavelength photonic integrated circuits (PICs) for the millimeter-wave and terahertz signal generation for high data rate wireless communication systems using the optical heterodyne technique. These laser sources will work in a dual-wavelength mode in order to use the optical heterodyne technique.

Chapter 2 describes the optical heterodyne technique for the millimeter-wave and THz signal generation. Several kinds of optical sources, in order to make up a dual-wavelength laser source, are described. An analytical study of an arrayed waveguide grating as a key component for the design of multiwavelength laser sources is described in this chapter as well. Taking advantage of the use of passive and active optical components, some structures and topologies can be developed and implemented. These lasers provide high accuracy in wavelength selection using only one passive intracavity filter within the Fabry-Perot cavity formed between both mirrors at the end of the chip. Closely spaced longitudinal modes may cause mode hops, but, on the other hand, the long extended cavity of the laser contributes to achieving a narrow optical linewidth. AWG lasers are also susceptible to operation in several free spectral ranges. The linewidth and the several kind of noise source presented as the lasers are working will be studied in this chapter. In addition, the optical heterodyne technique for the measurement of the optical linewidth and the electrical beat-note linewidth of each optical lasing mode and the heterodyne beat-note will be studied as well.

Chapter 3 discusses the development characterization of a monolithically integrated AWG-based laser source using cleaved facet as mirrors, which use the basic structure of

an AWG-based laser. A drawback of the AWG-based laser is that, they have a long Fabry-Perot cavity, which may require the placing of a boost amplifier within the circuit – at the common arm of the AWG - in order to compensate inherent losses into the laser cavity. The AWG source has an extended cavity configuration which provides a narrow optical linewidth compared with other laser sources such as DBR and DFB lasers. An analytical study of the central channels placed on the input port will be studied also.

Chapter 4 presents an implementation of an on-chip integrated AWG-based laser using multimode interference reflectors (MIR). The MIRs are used as mirrors of the Fabry-Perot laser cavity instead of the cleaved facets of the chip. These on-chip mirrors can be positioned freely, thus reducing the length of the laser cavity. The AWG source has an extended cavity configuration which provides a narrow optical linewidth. The relatively long laser cavity might introduce some intrinsic loss that can be compensated with a booster amplifier placed out of the Fabry-Perot laser cavity. Electro-optical phase modulators (EOPM) are integrated into two channels to have a fine tune of the lasing modes of each of them.

Chapter 5 presents a high data rate wireless communication system using the aforementioned dual-wavelength lasers. The Bit error rate (BER) measurement is done in order to measure the quality of the wireless link. Different wireless link topologies to measure the BER in this experiment are used. In addition to this, the characterization of the optical and electrical components is a key point in order to assess the performance of each of them.

Finally, Chapter 6 presents the conclusions of the Thesis and proposes the future working lines.

This research was supported by the European Commission (EC) under FP7 ICT European project iPHOS [37] and by the Dutch Ministry of Economic Affairs under Smartmix project Memphis [38]. We acknowledge cooperation with foundry partners: Oclaro Ltd. [39] and COBRA [40]; software partners: PhoeniX Software [41], Photon Design [42].

1.3 References

[1] T. Kleine and T. Nagatsuma, “A review on terahertz communications research,” J. Infrared Millim. Terahertz Waves, Vol. 32, n°. 2, pp. 143–171, 2011.

[2] Timothy P. McKenna, Jeffrey A. Nanzer, and Thomas R. Clark Jr. “Photonic Millimeter-Wave System for HighCapacity Wireless Communications”. Johns Hopkins APL Technical Digest, Volume 33, Number 1. 2015, www.jhuapl.edu/techdigest.

[3] S. Koenig, D. Lopez-Diaz, J. Antes, F. Boes, R. Henneberger, a. Leuther, a. Tessmann, R. Schmogrow, D. Hillerkuss, R. Palmer, T. Zwick, C. Koos, W. Freude, O. Ambacher, J. Leuthold, and I. Kallfass, “Wireless sub-THz communication system with high data rate,” *Nature Photon*., Vol. 7, no. 12, pp. 977–981, Oct. 2013.

[4] J. Federici and L. Moeller, “Review of terahertz and sub-Terahertz wireless communications”, *J. Appl. Phys*., Vol. 107, no. 11, pp. 1–22, 2010.

[5] A.J. Seeds, H. Shams, M.J. Fice, C.C.Renaud, "TeraHertz Photonics for Wireless Communications", *J. Lightwave Technology*, 33(3), pp.579587, 2015.

[6] Communicators with Martin Cooper Interview, December 4th, 2014.

[7] N. Guo, R. C. Qiu, S. S. Mo, & K. Takahashi, “60-GHz millimeter-wave radio: Principle, technology, and new results,” *EURASIP Journal on Wireless Communications and Networking*, 48-48. 2007

[8] C. Stallo, E. Cianca, S. Mukherjee, T. Rossi, M. De Sanctis, & M. Ruggieri, “UWB for multi-gigabit/s communications beyond 60 GHz,” Telecommunication Systems, 52(1), 161-181, 2013.

[9] L. Riche, “The performance of high-order quadrature amplitude modulation schemes for broadband wireless communication systems,” 2012.

[10] http://www.etsi.org/images/files/ETSIWhitePapers/etsi_wp9_e_band_and_v_band_survey_20150629.pdf

[11] Y. Xiao, &J. Rosdahl, “Throughput and delay limits of IEEE 802.11,” *Communications Letters*, IEEE, 6(8), 355-357, 2002.

[12] N. Cvijetic, Dayou Qian, Jianjun Yu, Yue-Kai Huang, and Ting Wang, "100 Gb/s per channel free-space optical transmission with coherent detection and MIMO processing," *in Proc. 35th Eur. Conf. Opt. Commun*., pp. 1–2 , 2009.

[13] A. Hirata, "120-GHz Wireless Link Using Photonic Techniques for Generation, Modulation, and Emission of Millimeter-Wave Signals", *IEEE J. Lightwave Technology*, Vol. 21, pp. 2145-2153, 2003.

[14] S. Diddams, D. Jones, J. Ye, S. Cundiff, J. Hall, J. Ranka, & R. Windeler, "Direct RF to optical frequency measurements with a femtosecond laser comb", *IEEE Transactions on Instrumentation and Measurement*, Vol. 50, no. 2, pp. 552-555, 2001.

[15] M. Tonouchi, "Cutting-edge terahertz technology", *Nature Photon*., Vol. 1, pp. 97-105, 2007.

[16] H. Song, N. Shimizu, T. Furuta, K. Suizu, H. Ito, & T. Nagatsuma, "Broadband-frequency-tunable sub-terahertz wave generation using an optical comb, AWGs, optical switches, and a uni-traveling carrier photodiode for spectroscopic applications", *J. Lightwave. Technology*. 26, pp. 2521-2530, 2008.

[17] J. Federici, "THz imaging and sensing for security applications—explosives, weapons and drugs", *Semiconductor Science Technology*, Vol. 20, pp. 268-266. 2005.

[18] ITU, "Recommendation P.676-9, Attenuation by atmospheric gases", 2012.

[19] ITU, "Recommendation P.840-4, Attenuation due to clouds and fog", 2009.

[20] ITU, "Recommendation P.838-3, Specific Attenuation Model for Rain for Use in Prediction Methods", 2005.

[21] T. Nagatsuma, S. Horiguchi, Y. Minamikata, Y. Yoshimizu, S. Hisatake, S. Kuwano, N. Yoshimoto, J. Terada, and H. Takahashi, "Terahertz wireless communications based on photonics technologies," *Opt. Express* 21, pp. 23736-23747, 2013.

[22] A. Hirata, R. Yamaguchi, T. Kosugi, H. Takahashi, K. Murata, T. Nagatsuma, N. Kukutsu, Y. Kado, N. Iai, S. Okabe, S. Kimura, H. Ikegawa, H. Nishikawa, T. Nakayama, and T. Inada, "10-Gbit/s wireless link using InP HEMT MMICs for generating 120-GHz-band millimeter-wave signal," *IEEE Trans. Microw. Theory Tech.,* vol. 57, no. 5, pt. 1, pp. 1102–1109, May 2009

[23] I. Kallfass, J. Antes, T. Schneider, F. Kurz, D. Lopez-Diaz, S. Diebold, H. Massler, A. Leuther, and A. Tessmann, "All Active MMIC-Based Wireless Communication at 220 GHz," *IEEE Trans. THz Sci.Technol.,* vol. 1, no. 2, pp. 477-487, 2011.

[24] A. Hirata, T. Kosugi, H. Takahashi, R. Yamaguchi, F. Nakajima, T. Furuta,... & T. Nagatsuma, "120-GHz-band millimeter-wave photonic wireless link for 10-Gb/s data transmission," Microwave Theory and Techniques," IEEE Transactions on, 54 (5), 1937-1944, 2006.

[25] A. Stohr, "Photonic millimeter-wave generation and its applications in high data rate wireless access," *IEEE Top. Meeting on Microwave Photonics (MWP)*, 5-9 Oct. 2010.

[26] J. Capmany and D. Novak "Microwave photonics combines two worlds" *Nature Photonics* , Vol 1, pp. 319-330, June 2007.

[27] T. Nagatsuma and K. Kato, "Photonically-assisted 300-GHz wireless link for real-time 100-Gbps transmission," in *2014 IEEE MTT-S International Microwave Symposium (IMS)*, pp.1-4, 1-6 June 2014.

[28] A. Stohr, A. Akrout and others, "60 GHz radio-over-fiber technologies for broadband wireless services," *Journal of Optical Networking*, Vol. 8, n°. 5, pp. 471-487, 2009.

[29] G. Carpintero, R. Guzman, C. Gordon, G. Kervella, M. Chtioui, & F. Van Dijk, "Photonic Integrated Circuits for Radio-frequency signal generation". 2015.

[30] K. Sato, "100 GHz optical pulse generation using Fabry-Perot laser under continuous wave operation", *Electron Letters*, Vol. 37, pp. 763-764, 2001.

[31] K. Sato. "Active mode locking at 50 GHz repetition frequency by half- frequency modulation of monolithic semiconductor lasers integrated with electro absorption modulators", *Appl. Phys. Lett.* , Vol. 69, pp. 2626-2628, 1996.

[32] A. Hirata, M. Harada, K. Sato & T. Nagatsuma, "Low-Cost Millimeter-Wave Photonic Techniques for Gigabit/s Wireless Link", Publication *IEICE Transactions on Electronics* , Vol. E86-C, No.7, pp.1123-1128, 2003.

[33] Z. Fan, "Optical Generation of a mHz-Linewidth Microwave Signal Using Semiconductor Lasers and a Discriminator-Aided Phase-Locked Loop", *IEEE Trans. Microwave Theory and Tech*., Vol. 45, pp. 1296-1300, 1997.

[34] D. Chen, H. Fetterman, A. Chen, W. Steier, L. Dalton, W. Wang, & Y. Shi "Demonstration of 110 GHz electro-optic polymer modulators", *Applied Physics Letters*, 70(25), 3335-3337, 1997.

[35] A. Coldren , S. Parker, A Sivananthan, M. Lu, & L. Johansson, "Integrated Phase-locked Multi-THz Comb for Broadband Offset Locking", University of California at Santa Barbara, 2012

[36] T. Nagatsuma, N. Kukutsu & Y. Kado, "Photonic Generation of Millimeter and Terahertz Waves and Its Applications", *Automatika,* Vol. 5, pp. 51-59, 2008.

[37] www.iphos‐project.eu

[38] Memphis, "Merging Electronics and Micro & Nano-Photonics in Integrated Systems", http://www.smartmix-memphis.nl.

[39] Oclaro Technology Ltd., Caswell, United Kingdom, http://www.oclaro.com.

[40] https://www.tue.nl/en/university/departments/electrical-engineering/research/research-institutes/research-institute-cobra-and-research-center-for-integrated-nanophotonics/

[41] PhoeniX Software, http://www.phoenixbv.com.

[42] Photon Design, http://www.photond.com.

Optical Heterodyne Photonic Integrated Sources

2.1 Optical heterodyne technique

Optical heterodyning is one of the most versatile optical techniques that can be used to generate millimeter and Terahertz wave signals. It only requires two optical wavelengths, spaced by the frequency of the signal that we are aiming to generate. The simplicity of this technique enables multiple realizations which, at the end, differ in the characteristics of the two optical wavelengths. These in turn determine those of the generated electrical signal. Most of the realizations usually offer a wide tuning range, as there has been a great effort in the development of tunable lasers which allow changing the frequency simply by tuning the wavelength on one of the two optical sources. The generated frequencies by means of this photonic technique are limited only by the photodetector bandwidth [1].

In its simplest form, using two independent lasers to generate each of the two wavelengths, we find that the major drawback of the heterodyne technique is the strong influence of laser phase noise, as the two wavelengths are not correlated. The linewidth of the generated mmW/THz signal is at best the sum of the optical linewidths. As the data rate increases, the tolerance for noise decreases, having developed different techniques to reduce the generated signal phase noise. Optical techniques include optical phase locked loops (OPLL) [2], [3], as well as optical injection locking (OIL) [1]. The main issue of these stabilization techniques is that both result in complex optical systems which increase the cost of the signal source [4].

2.1.1 Optical heterodyne technique based millimeter-wave and terahertz signal generation.

As we have discussed, a simple and cost-effective approach to signal generation based on the optical heterodyne technique is to couple two telecom-based semiconductor lasers using a fiber optic combiner, as shown in Figure 2.1. The optical heterodyne signal $E_T(t)$, is the sum of the two optical sources, $E_1(t)$ and $E_2(t)$, which can be expressed as:

$$E_1(t) = A_1 \cos(\omega_1 t + \phi_1) \qquad \text{Eq. 2.1}$$

$$E_2(t) = A_2 \cos(\omega_2 t + \phi_2) \qquad \text{Eq. 2.2}$$

where A_1 y A_2 are the amplitude terms, ω_1 y ω_2 are the angular frequency terms, and ϕ_1 y ϕ_2 are the phase terms of the two optical waves

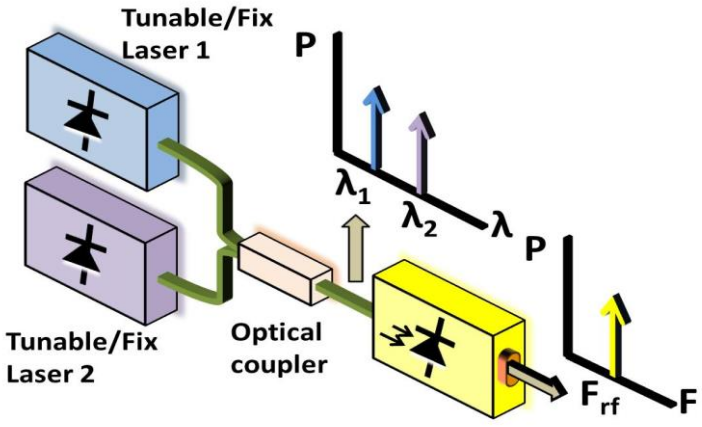

Figure 2.1. Dual-wavelength source based photonic heterodyne technique to generate mmW and THz signals. Both lasers work in free running mode.

The electrical signal is generated on a high speed photodiode, which acts as an envelope detector of the optical frequencies. Its role is to down-convert the optical frequencies into the electrical domain. Considering the dependency between generated

photocurrent $i_{ph}(t)$ and the injected optical signal onto the photodiode, $|E_T(t)|^2$, the photocurrent can be expressed as:

$$\begin{aligned}|E_T(t)|^2 = \; & 0.5{A_1}^2[1+\cos(2\omega_1 t+\phi_1)] \\ & + 0.5{A_2}^2[1+\cos(2\omega_2 t+\phi_2)] \\ & + A_1A_2\big[\cos\big((\omega_1+\omega_2)t+\Delta\phi\big) \\ & + \cos\big((\omega_2-\omega_1)t+\Delta\phi\big)\big]\end{aligned} \qquad \text{Eq. 2.3}$$

From Eq. 2.3 and considering that the photodiode cut-off frequency is well below the optical frequencies (≈ 193 THz for a 1550 nm laser diode), the photodetector can respond to the average power and the difference frequency, which can be expressed as:

$$I_{PD}(t) = R_{PD}\left[P_1(t)+P_2(t)+2\sqrt{P_1(t)P_2(t)}\cos(\Delta\omega t+\Delta\phi)\right] \qquad \text{Eq. 2.4}$$

In this expression, the first two terms correspond to the direct intensity detection and the third term is the heterodyne mixing term. $\Delta\omega$, $(\omega_2 - \omega_1)$ is the angular frequency difference between the two optical sources. The heterodyne mixing term is the responsible for the electrical radio-frequency signal generation, limited only by the photodetector bandwidth. The fact that the two lasers are independent, introduces different light polarization differences, temperature drift, phase noise variations, all intervening to define the linewidth of the electrical signal. This is represented by the phase fluctuation factor, $\Delta\phi = \phi_2 - \phi_1$ is related to the independent noise sources generating the optical linewidth on each optical source.

Tunable lasers used for the generation of millimeter-wave and Terahertz signals have been reported in the literature [5], [6], [7], [8], [9]. Different laser structures have been proposed to implement tunable lasers.

2.2 External cavity laser diode

External cavity lasers (ECLD) have the key advantage of enabling tuning the optical wavelength, though an adjustable optical element. Most often, a diffraction grating is used for this purpose, which provides frequency-selective optical feedback and narrows the optical linewidth. Typical values for an external cavity laser diode are linewidths below 1 MHz and remarkable tuning range of hundreds of nm.

A schematic diagram of such a laser structure is shown in Figure 2.2, which is composed of an active semiconductor gain medium, a collimating lens and an output mirror which form an external cavity

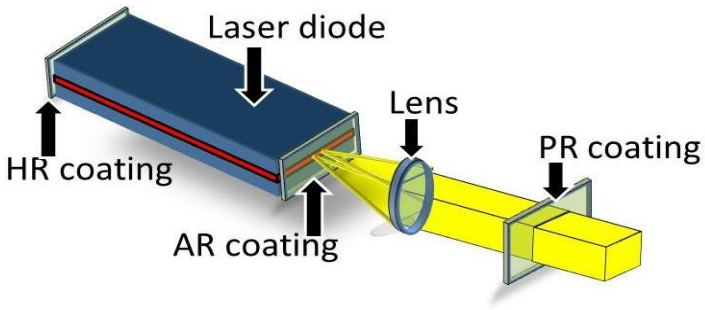

Figure 2.2. Simple setup of an laser diode with external cavity. The laser diode is highly- reflective coated on one side of the facet, whilst the other end is anti-reflective coated. The laser resonator extends to the output mirror which is partially-reflective coated.

The main advantages of the optical feedback from an external cavity are the enhancement of single longitudinal mode operation, the spectral line-narrowing, the improved frequency stability, and the wavelength tunability [10], [11], [12], [13]. This structure is complex, with critical mechanical tolerances for optimum performance, in particular with respect to variations in external cavity length and alignment [14]. In addition, the active semiconductor gain medium facets and the external reflector form a

double cavity configuration, which is more likely to exhibit unstable behavior than the solitary laser [15], [16]. The most common element used as output mirror is a diffraction grating, and two well-known approaches are commonly employed.

The first approach uses a Littrow configuration, as shown in Figure 2.3. The grating is aligned such that the first order diffraction from the grating is coupled directly back into the laser while the zeroth-order diffraction is reflected as the output beam. The lasing wavelength is selected by the angle of the incident laser beam with respect to the grating, known as the Littrow angle θ. The Littrow configuration offers the advantage of high efficiency and power but also faces problems of mode-hopping and beam angular displacement as the grating angle is adjusted

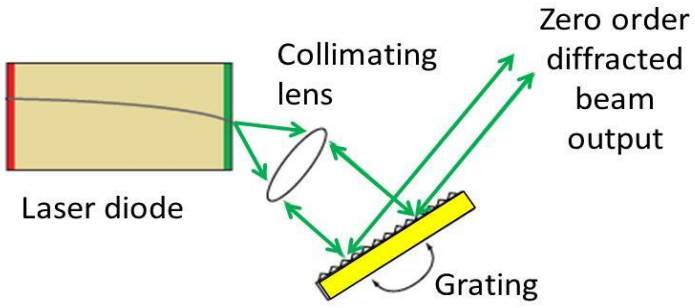

Figure 2.3. Schematic diagram of a tunable external cavity laser in Littrow configuration.

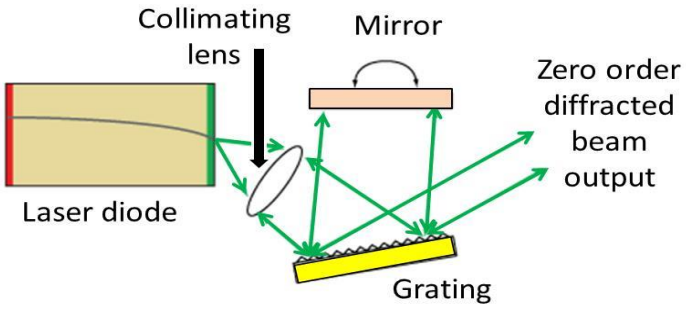

Figure 2.4. Schematic diagram of a tunable external cavity laser in Littman-Metcalf configuration.

The alternative configuration is the Littman-Metcalf [17], [18], [19] shown in Figure 2.4. The first order diffraction beam goes to an additional mirror, which then reflects the beam back to the grating and into the diode laser as optical feedback. Tuning is achieved by varying the mirror angle instead of the grating angle, allowing the grating, and thus the zeroth order output beam, to remain fixed as the wavelength is changed. Relative to the Littrow configuration, the Littman-Metcalf configuration overcomes the problems of mode-hopping and beam angular displacement but does not share as high output efficiency. Furthermore, the additional components involved and its design complexity prevent it from surpassing the widespread prevalence of the relatively simpler yet adequately effective Littrow arrangement.

One drawback to the Littman-Metcalf design is that the internal losses are higher than in the Littrow configuration, and hence, the output power of the laser is typically lower. The increase in internal losses is mainly due to the loss of the zero-order beam reflected from the tuning mirror and the increased loss due to the decrease in the efficiency of the grating when used to reflect light at a large angle of incidence.

2.3 Integrated tunable lasers

. Currently, there are two main integrated structures to achieve a tunable lasers, distributed Bragg reflector (DBR) and distributed feedback lasers (DFB).

2.3.1 Distributed Bragg reflector lasers.

A Distributed Bragg Reflector (DBR) laser diode is a wavelength tunable single-frequency laser. The DBR laser structure is fabricated with surface features that define a monolithic structure. It is based on passive grating reflectors forming one or both mirrors of the laser resonator, integrated on-chip, as shown in Figure 2.5.

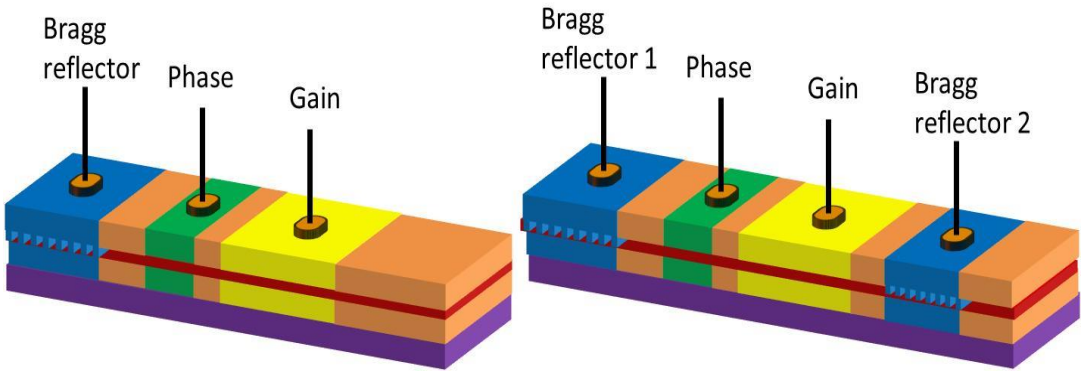

Figure 2.5. Illustration of a tunable single-frequency three sections (on the left side) and four sections (on the right side) DBR laser. The first DBR laser configuration consists of a gain section, a phase section and a grating mirror section. For the four sections DBR laser, the back mirror and front mirrors provide frequency selective reflectivity to select the lasing wavelength. The different bias value pumped into the front mirror, back mirror, and phase segments allows controlling the wavelength of the laser.

The DBR mirror is designed to reflect only a single longitudinal mode. The first approach is a DBR laser in which a Fabry-Perot resonator defined by a partially reflective cleaved mirror at one end and a passive DBR mirror on the opposite end to provide wavelength dependent feedback. An alternative approach is to use passive DBR

mirror structures to define both mirror structures of the resonator. As the grating reflectors are formed along a passive waveguide section, we need a smooth transition between the active and passive waveguides without introducing unwanted reflections [20].

The DBR lasers can be tuned either by adjusting the active section current or by changing the operation temperature of the laser. Tuning by temperature changes usually exhibits mode-hopping. An additional tuning control can be introduced by including an additional phase section within the laser cavity. The tuning range of DBR lasers is in the order of a few nm. Mode-hop-free tuning over a larger wavelength region is possible by coordinated tuning of the Bragg grating, the gain section, and the phase section. Typical cavity lengths are about 1mm or 2 mm, and the optical linewidths are around 10 MHz.

2.3.2 Distributed feedback lasers

In distributed feedback (DFB) lasers, which also use grating mirrors, the grating is embedded within the gain section [20], as shown in Figure 2.6. Because the DFB laser is designed to experience feedback all along the gain ridge, no end mirrors are needed. However, in the perfectly symmetric case, opposing reflections at the Bragg wavelength are anti-resonant, or destructive, and lasing does not occur at the Bragg wavelength. However, two lasing modes equally spaced and around the Bragg wavelength are produced, the difference between the two modes being known as the stop band. A phase shift in its center causes it to lase at the Bragg frequency.

DFB lasers preceded the DBR laser; one of the reasons is due to its simplicity and relative ease of fabrication, as it does not require the active-passive transition between the active section and the grating mirror.

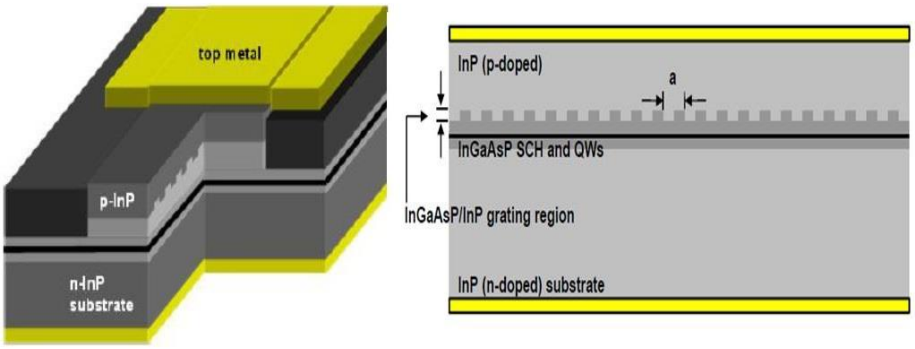

Figure 2.6. Illustration of a tunable single-frequency DBF laser. The entire length of a DBF laser is fill with active material embossed with a grating..

A change in the refractive index alters the wavelength selection of the grating structure and thus the wavelength of the laser output, producing a wavelength tunable laser. The linewidth is typically a few hundred MHz, and wavelength tuning is often possible over several nanometers. Altering of the current powering the laser will also tune the device as a current change causes a temperature change inside the device. In fact, the free spectral range of the DFB is much higher than the DBR. The mode hop free tunability in a DFB is generally higher than in a DBR, and this is often cited as a clear advantage of the DFB over the DBR. However, when it occurs it is not deterministic, and it does so in such a manner that it leaves a gap in the tuning range [21]. Mode-hop-free emission wavelength tuning achieved via laser current variation for different temperature values

2.4 AWG-based multiwavelength laser

2.4.1 Arrayed waveguide grating

An arrayed waveguide grating (AWG) is a passive optical component, which as shown in Figure 2.7, formed of an input waveguide, a set of output waveguides. These waveguides are coupled to an array of waveguides through two star couplers (also knows as free propagation regions – FPRs). First, proposed by M. Smit [22], it has received different denominations, such as PHASAR (acronym for optical phased array), or WGR (acronym for waveguide grating router), the acronym AWG is the most commonly used nowadays. As a passive optical component, it has been demostrated on different material platforms, from Indium Phosphide technology [23], [24], [25], [26], as well as silica-on-silicon [27], silicon-on-insulator [28], lithium niobate [29] and polymer [30].

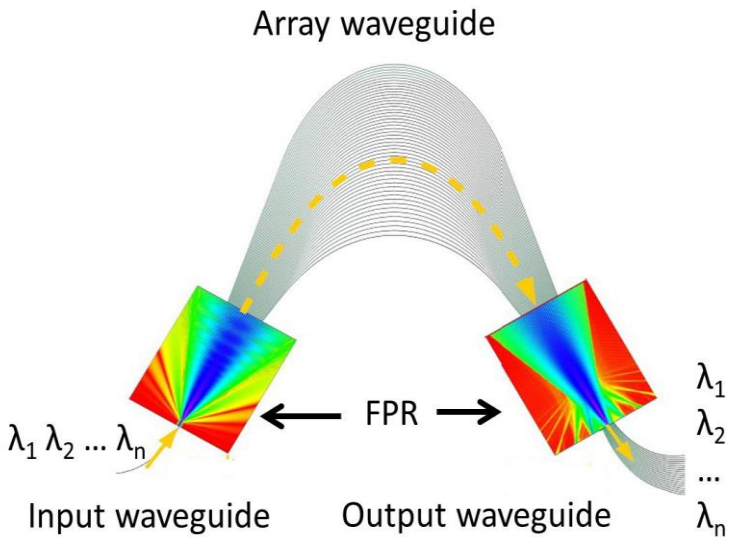

Figure 2.7. Schematic of an AWG. A set of incoming wavelengths are coupled into the input waveguide and demultiplexed at the output waveguides on the other side of the AWG.

The main function of AWG is as wavelength multiplexer/demultiplexer, initially intended for dense wavelength division multiplexed link (DWDM). The functionality of this component can be briefly described as follows.

The optical signal at the input waveguides carries multiple wavelengths λ_1 - λ_n which enter into the FPR, where light is diffracted illuminating the array of waveguides. The light is propagated through each one of the waveguides of the array, reaching to the second FPR. The length of each waveguide on the array is chosen so that the optical path length difference between adjacent waveguides, dL is an integer multiple of a central wavelength λ_c. For this wavelength only, the fields in the individual arrayed waveguides will arrive at the input of the output coupler with equal phase, and the field distribution at the output of the input coupler will be reproduced at the input of the output coupler. Different wavelength will experience different phase shift, and therefore the wavelengths are spatially separated at the output, reaching different output waveguides. An example of the transmission function of a 4-channel AWG is shown in **Error! Reference source not found.**.

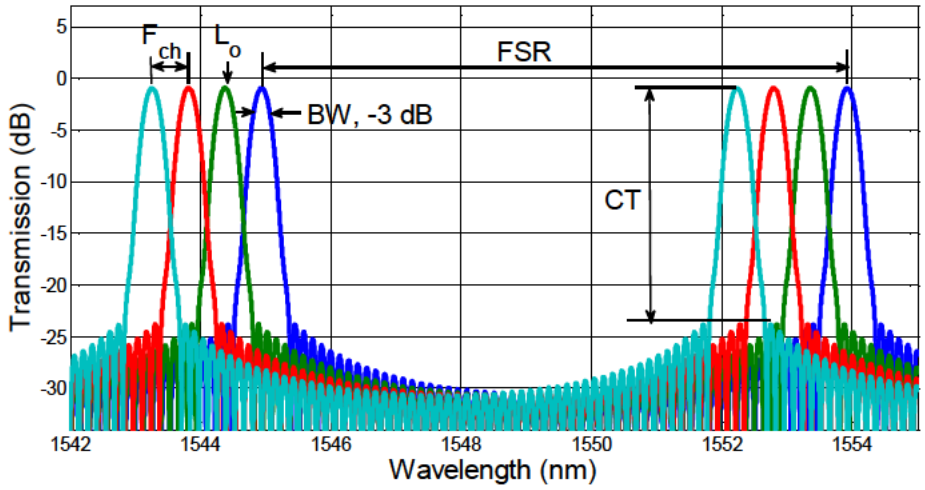

Figure 2.8. Example of the transmission functions of a 4-channel AWG. Channel 1, 2, 3and 4 are light blue, red, green and dark blue, respectively.

The difference in frequency between two adjacent channels is called channel spacing (F_{ch}). The -3dB bandwidth of the channel is a constant value, which depends on the channel spacing. The response of an AWG is periodic, which means that two wavelengths that are spaced by the Free Spectral Range (FSR) will be delivered through the same output waveguide of the AWG.

Another important parameters of an AWG is the crosstalk (*CT*).The crosstalk is the coupling of optical power into a channel from the adjacent ones. Besides, this coupling of optical power between adjacent channels can be reduced by having a narrower channel passband of AWG [31], also a side mode suppression ratio (SMSR) value greater than 25 dB between the main lasing mode and adjacent ones within the channel passband can be achieved, as shown in Figure 2.9. As a passive device, the geometric dimensions play a key role in order to establish the characteristics of the optical transfer function.

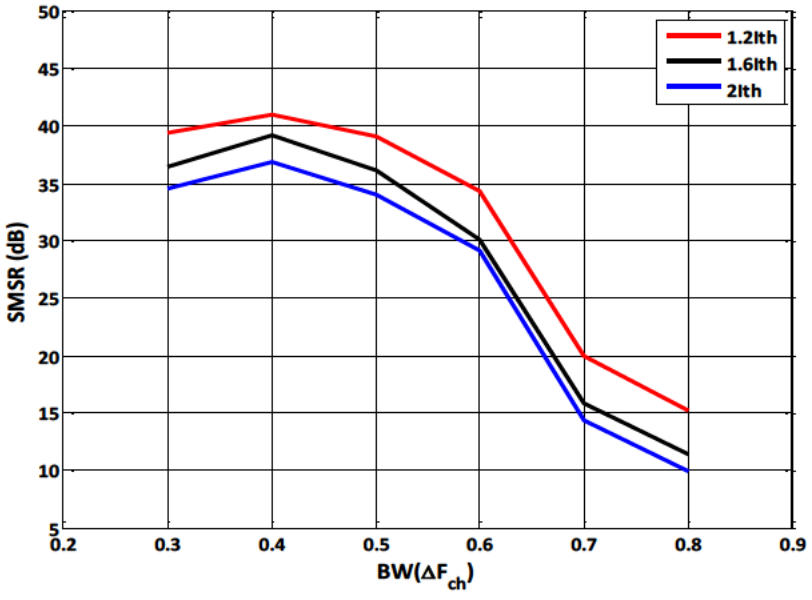

Figure 2.9. SMSR among longitudinal modes in the AWGL. The channel bandwidth (BW) is scaled to the channel spacing on the AWG.

2.4.2 AWG-based lasers

Combining an arrayed waveguide grating (AWG) with a set of semiconductor optical amplifiers (SOA), located at the channel waveguides, and defining a Fabry-perot cavity, is a straightforward manner to build a monolithically integrated multiwavelength laser. In this way, we achieve an arrayed waveguide grating laser (AWGL), which can be regarded as a set of multiplexed extended cavity lasers (ECL). The number of wavelengths that can be generated simultaneously from such a laser depends on the number of output channels and semiconductors optical amplifiers integrated into the device.

We have developed AWG-lasers based on InP technology, on multi-project wafer runs (MWP), from different technology platforms, mainly such as OCLARO and SMARTPhotonics.

An AWGL has several advantages over the other multi-wavelengths and tunable lasers,amng which are:.

- It can deliver light multiple wavelengths simultaneously and efficiently within the common output waveguide.
- Has long-term wavelength stability better than other optical devices due to the fact that the wavelength selection is dominated by a passive optical component.
- Has a built-in wavelength control mechanism which is easier than compared to other multi-section tunable lasers which depend on accurate control of tuning of bias currents.

Figure 2.10 shows the basic structure of such a laser structure, in which we have included only two channels. The AWG is a passive optical component which acts as an intra-cavity wavelength filter, establishing the lasing wavelengths by filtering the Fabry-Perot modes in the laser cavity formed between the two mirrors placed at both end of the lasing cavity.

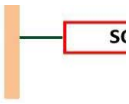

Figure 2.10. Schematic of the basic arrayed waveguide grating-based laser configuration with two channels. M1 and M2 mirrors can be either made by a high reflective (HR) coated or a partially reflective (PR) coated depending on the configuration of the AWGL.

As the length of the Fabry-Perot cavity, determined mainly by the size of the AWG becoming in the order of several millimeters, thus the generated modal spacing of these Fabry-Perot modes can be as low as tenths of GHz. All these lasing modes are filtered by the AWG, which selects the lasing wavelength being the mode closer to the lowest attenuation from channel passband. The resonator mirrors, M1, and M2, can be modified by applying metal or dielectric coatings, like highly-reflective (HR) and/or partially-reflective (PR) coatings. Alternatively, (partial) reflectors can be made using: loop reflectors [32], distributed Bragg reflectors [33] or reflectors based on multi-mode interference (MIR) [34]. The MIRs shall be studied in Chapter 4.

Photonic integration technology allows designing many different variations of structures from this AWG-based laser basic structure. Several architectures and structures have been developed by other authors [35], [36], [37]. Moreover, the photonic

integration allows us to add different optical components such as phase shifters (PHS), electro-optical phase modulators (EOPM) or Mach-Zehnder modulators (MZM). These can be located within the Fabry-Perot resonator, in order to achieve advanced functions, from data modulation to fine tunning of the lasing mode of a given channel [38]. However, adding these components has the drawback of increasing the lasing cavity length, resulting in a closer spacing of the Fabry-Perot modes. The output optical power can also be increased by placing an SOA working as a boost amplifier [26] either in the output waveguide of the common arm, or outside the laser cavity.

2.4.3 AWG-based laser simulation

In order to analyze the different possible implementations of the AWG laser structure, it would be very helpful to have a design tool to calculate the expected response in terms of the AWG's parameters. The current commercially available design tools, for which libraries of components are being developed for the Generic Integration Platforms (GIP), so far do not contain a model for the AWG. This is an extremely complex component, and its function is really key to determine the behavior of the AWG laser.

Within this work, we have developed an AWG model based on transmission matrix equivalent of a Finite Impulse Response (FIR) filter bank to be incorporated into Photon Design PICWave software [39]. An S-matrix circuit from PICWave software allows us to use an S-matrix spectrum to define the response of an active or passive optical component as a function of wavelength. This S-matrix circuit contains a FIR section which, can model a device with an arbitrary spectral profile. One of the advantages of this component is that, it does not have a physical size defined by the user, but instead

provides a way of importing a frequency-domain model. The software will read this matrix in a wavelength dependent scattering matrix of the component and automatically generate an equivalent time-domain model for inclusion in the PICWAVE circuit simulator. This scattering matrix is developed using MATLAB software and loaded the circuit which allows combining a rigorous optical propagation analysis with fast photonic circuit modelling.

In order to assess our model, four channel AWGL is developed with one SOA per channel and a waveguide at the common port. The AWG characteristics were:

- Central wavelength, λ_c, = 1550 nm.
- Channel spacing, F_{ch}, = 100GHz.
- Free spectral range, FSR = 900GHz.
- Channel bandwidth = 0.55*$F_{ch.}$

Figure 2.11 shows the transmission function of the designed AWG, which is developed from another MATLAB script. Some AWG's physical parameters are needed to simulate the transmission function of the AWG such as input and output waveguide width, gap of the waveguide in the array, etc. We have selected an AWG channel passband which is 55% of the AWG channel spacing.

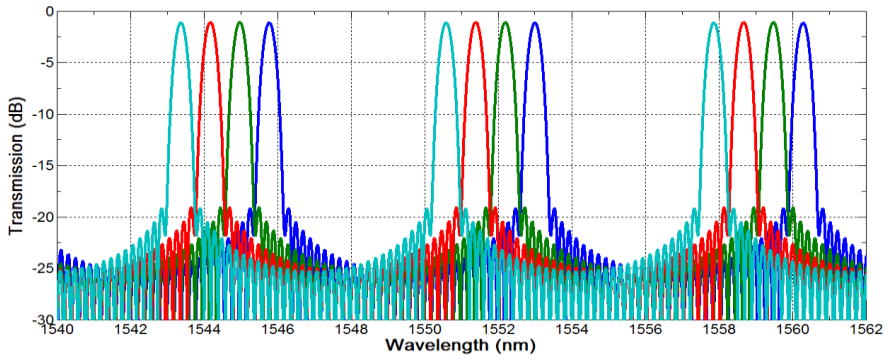

Figure 2.11. AWG transmission response simulated in MATLAB. Channel 1, 2, 3and 4 are light blue, red, green and dark blue, respectively. The design center wavelength is 1550 nm

After having tested this initial step, the next step is to input the above-mentioned AWG parameters into the MATLAB script in order to generate the scattering matrix of an FIR filter bank equivalent to the AWG transmission function evaluated before. The generated file is then loaded into the S-matrix circuit, having it four input ports and one output port. Each channel can be evaluated independently, connecting or not, other components to the input ports.

The schematic block diagram of one channel waveguide AWG, implemented in PICWave, is shown in Figure 2.12, the model includes different building blocks from OCLARO technology platform, among which we find deep etched passive waveguides (SG), semiconductor optical amplifiers (SOAs), and shallow to deep etch transitions (WG-SG). Moreover, two *mirrors* blocks are added to simulate the cleaved facet mirrors. This model allows us to simulate the AWG's response and also has been used to calculate an estimation of the threshold current, the optical spectrum response at different bias current values of the channel and the differential quantum efficiency. One note on this performance is that we did not include the AWG insertion losses.

The value of this model is that it allows us to analyze some of the key issues of the AWG in the device performance, as the influence of the AWG channel passband in the side mode suppression ration among these closely spaced modes.

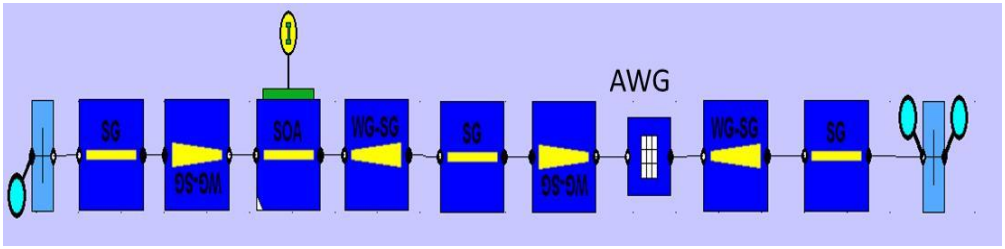

Figure 2.12. Block diagram of one channel AWGL implemented in the PICWave simulator

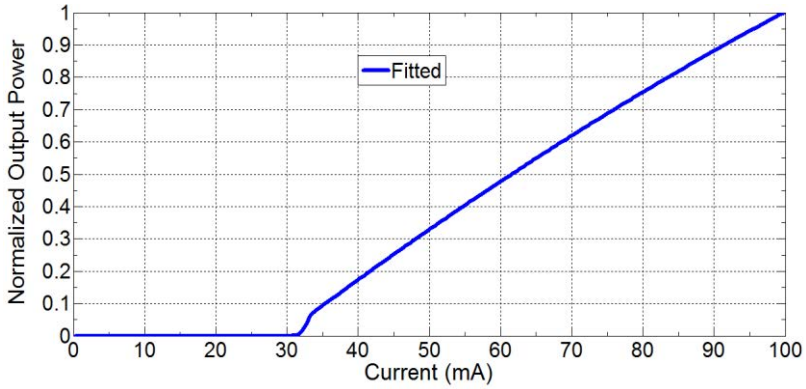

Figure 2.13. Light vs Current curve of an AWGL simulated in PICWave.

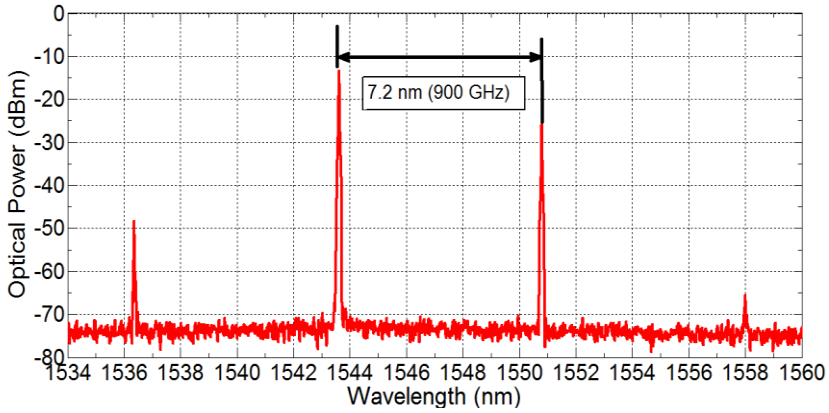

Figure 2.14. Optical spectrum response of the AWG-based laser simulated in PICWave. The simulation center wavelength is 1550 nm. Higher and lower FSR orders are generated due to the modal gain curve of the active section of the channel.

With this model we have been able to simulate the *light-current* (*L-I*) characteristic of the device, is shown in Figure 2.13, which provides the threshold current value. For this purpose, we have swept the channel SOA current from 0 to 100 mA. The resulting threshold current is 29.3 mA and the differential quantum efficiency ($\frac{dP}{dI}$ [W/A]), estimated from the slope is 0.0086 W/A. The resulting optical spectrum response is presented in Figure 2.14, in which we observe lasing at multiple FSR, mainly due to the modal gain curve of the active section of the channel. This SOA's modal gain curve needs to be fitted in order to be used by the time domain model. This is done in PICWave using a *Wide-Band Gain Fitting*. The Wide-Band Gain Fitting allows us to

maintain the accuracy of the fitted curves over a very wide range of wavelength in accordance with our simulation window, as shown in Figure 2.15.

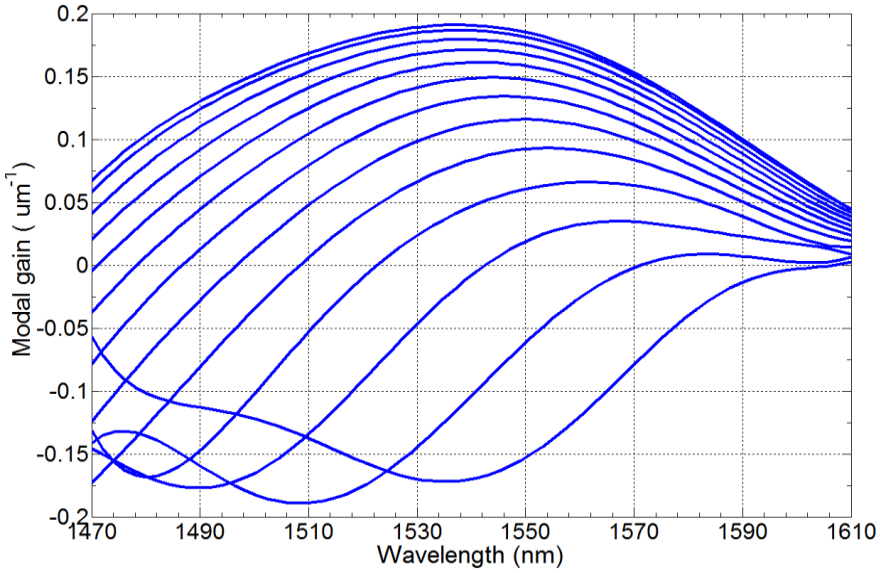

(a)

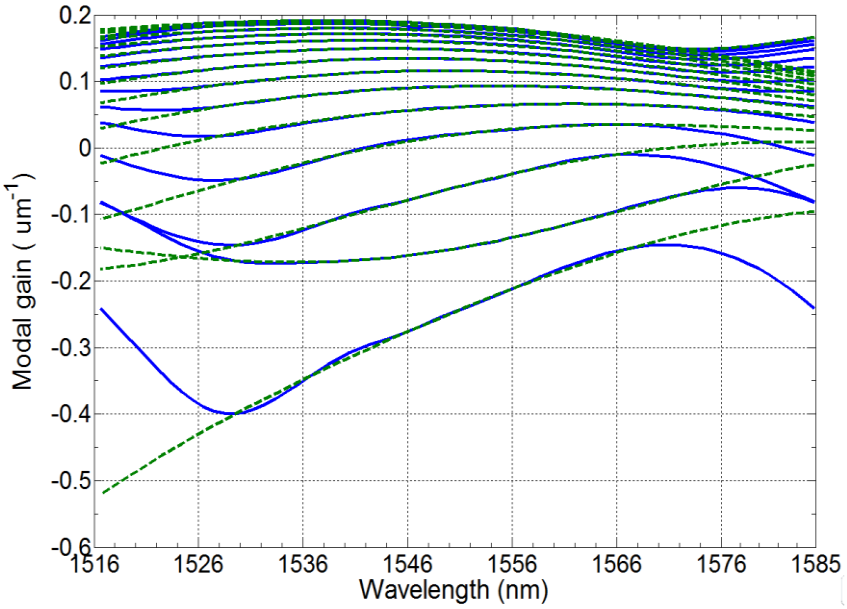

(b)

Figure 2.15. (a) SOA's modal gain curve from OCLARO. (b) Imported modal gain curve (green) and modal fitted curve (blue) plotted against wavelength for different carrier densities over 70 nm simulation window.

2.5 Dual-wavelength optical laser sources

The different laser structures that we have discussed enable emission on a single optical frequency. What is really important about some of the options that we have discussed is that enable to develop integrated dual-wavelength laser sources. Some of the advantages and disadvantages of using these sources to use them for dual-wavelength source are shown in Table 2.1.

Optical laser source	Advantages	Disadvantages
Tunable external cavity laser	• Narrow optical linewidth less than 100 KHz • High optical power • Wide wavelength tuning range	• Some external components are added to the system. • A bulky system compared with other lasers. • The optical modes are not correlated • Temperature changes affect in a separated way each laser source
Distributed Bragg reflector laser	• Wide wavelength tuning range. • Single optical mode independent of the injected current into the gain section.	• Phase fluctuations. • Poor frequency stability. • The optical modes are not correlated. • Single optical mode is dependent of the injected current into the gain section • Optical linewidth greater than 500HKz. • Temperature changes affect in a separated way each laser source
Distributed feedback laser	• Wide mode-hop free wavelength tuning range(greater than DBR laser) • Only one electrical contact for the wavelength tuning	• Phase fluctuations. • Poor frequency stability. • The optical modes are not correlated. • Single optical mode is dependent of the injected current

		into the gain section • Optical linewidth greater than 1 MHz • Temperature changes affect in a separated way each laser source
AWG based laser	• It is able to generate as many wavelengths simultaneously as can be possible. • A specific lasing wavelength corresponding to the selected channel's SOA shall be generated at the common output of the chip. • Frequency spacing between two individual channels can be from some tenths to cents of GHz and beyond • The frequency spacing between the adjacent channels is fixed by the AWG's channel spacing design. • A temperature change affects all the optical components into the chip at the same time, by yielding a wavelength shifting in all the channels with the same shifting. • Both optical modes are correlated at the chip output.	• AWG's size increases the Fabry-Perot laser cavity, giving as result lasing wavelength spacing in the order of tenths of GHz • Lasing wavelengths can appear at higher or lower FSR orders • Placing another optical components, the Fabry-Perot cavity increases from tenths of GHz to cents of MHz, depending on the length of these optical components • A longer optical pathway can reduce the direct modulation of high data rates.

Table 2.1. Advantages and disadvantages of different separated optical laser sources in order to make up a dual-wavelength laser source.

2.6 Optical and electrical linewidth

A key parameter of a signal that is to be used as communication carrier wave is its linewidth. The linewidth is the width (typically the full width at half-maximum) of its electrical spectrum, arising from the phase noise (random fluctuations of the signal phase). It has been demonstrated that with carrier waves with linewidths around several MHz can be used with direct envelop detection methods [40]. However, when coherent detection is desired, narrower linewidths below 100 KHz are required [41].

In the optical heterodyning signal generation scheme, the linewidth of the generated electrical signal strongly depends on the optical linewidth of the two modes that are mixed. The linewidth of any laser source is defined in terms of the full width at half maximum (FWHM) of the optical power spectrum. The broadening of the laser line shape is mainly due to the various noise mechanisms which yield fluctuations in the phase of the optical field. This section provides an introduction of some noise mechanisms which can cause a broadening of the linewidth of laser sources.

2.5.1 Schawlow-Townes and Henry linewidth.

One of the most characteristic phenomena taking plce within the active regions of laser diodes is the spontaneous emission. This process continuously adds incoherent photons to the laser mode, causing amplitude and phase fluctuations. In a semiconductor laser, both are linked through the change in the refractive index with carrier variations, an effect that is accounted for in the spectral linewidth through the

Henry factor (also known as linewidth enhancement factor $\alpha = {\Delta n'}/{\Delta n''}$ [1]), which increases the theoretical Schawlow and Townes value [42]. Therefore, the linewidth of a semiconductor laser diode according to Henry is then given by [43].

$$\Delta\vartheta_{Laser} = \frac{\vartheta_g^2 h\nu\eta_{sp}\alpha_m(1+\alpha^2)g}{8\pi P_o} \qquad \text{Eq. 2.5}$$

where $h\nu$ is the energy of the laser line, g is the gain of the active section of semiconductor laser diode, n_{sp} is referred to as the spontaneous emission factor, ϑ_g is the group velocity, P_o is the output power of the laser, α is the Henry's linewidth enhancement factor and α_m is defined as the mirror loss given by the following equation

$$\alpha_m = \frac{Ln\left(\frac{1}{r_m}\right)}{L_{cav}} \qquad \text{Eq. 2.6}$$

$$g = \frac{Ln\left(\frac{1}{r_m}\right)}{\eta L_{cav}^2} \qquad \text{Eq. 2.7}$$

where L_{cav} is the cavity length, r_m defined as the reflectivity value of the mirrors on the chip facet and η is the quantum efficiency. Using Eq. 2.6 and Eq. 2.7 in Eq. 2.5 we have that

$$\Delta\vartheta_{Laser} = \frac{\Delta F_{laser}^2 h\nu\eta_{sp} Ln\left(\frac{1}{r_m}\right)(1+\alpha^2)}{\pi\eta P_o} \qquad \text{Eq. 2.8}$$

ΔF^2_{laser} is the modal spacing frequency into the laser cavity. This expression is extremely useful, as it clearly shown that the linewidth can be decreased either through

[1] $\Delta n'$ and $\Delta n''$ as the deviation of the real- and the imaginary part of the refractive index

increasing the laser cavity length or increasing the emitted optical power. This dependence has been verified on integrated dual DFB sources [44].

Other phenomena which play a role into determining the optical linewidth are the internal temperature fluctuations within laser diode caused by photon and carrier fluctuations [45]. As we are aiming to single frequency laser diodes, we will not take into account the noise arising from side modes close to the main lasing mode [46], [47], but this effect can be considered negligible if the side-mode suppression ratio exceeds 20 dB.

2.5.2 External technical noise

Usually, the most important source of noise in laser diodes is originated at external noise sources, mainly the voltage and current sources. Other external sources are temperature noise, electromagnetic coupling and mechanical vibrations which are present in any setup. Injection of current and voltage noise is caused by instabilities of the current and voltage source or by electrical pick up from the measurement environment. Instabilities at the output of the current and voltage sources are mainly caused either by the noise of the sensing resistor which monitors the injected current and voltage to semiconductor laser diode or the ripple noise generated by the internal power supply of the equipment.

[2] $\Delta F_{laser} = \frac{c}{2*n_g*L_{cavity}}$. Where c is light speed and n_g is effective refractive index in the medium.

2.5.3 Optical linewidth measurement setup.

There are different methods to determine the optical linewidth of a single frequency laser source. One of the most common is the delayed self-heterodyne technique [48], for which we have used the setup shown in Figure 2.16. This method uses the wave interference principle.

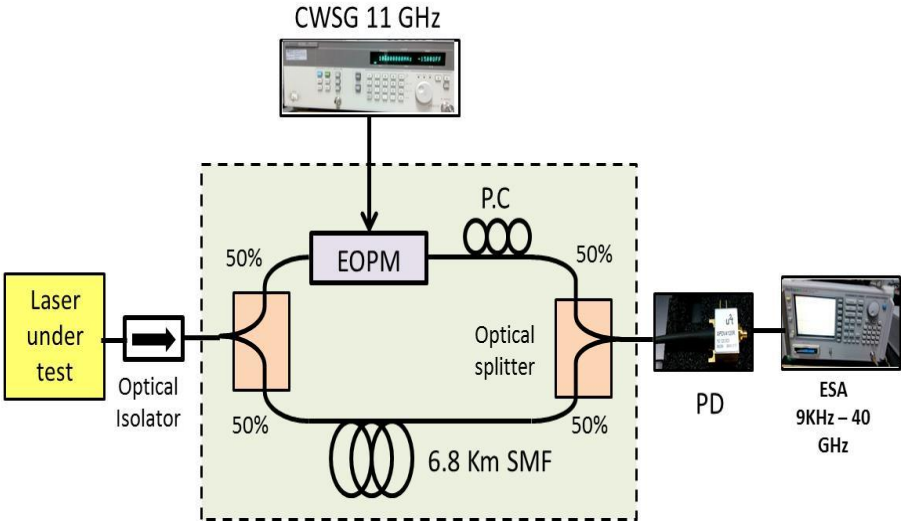

(a)

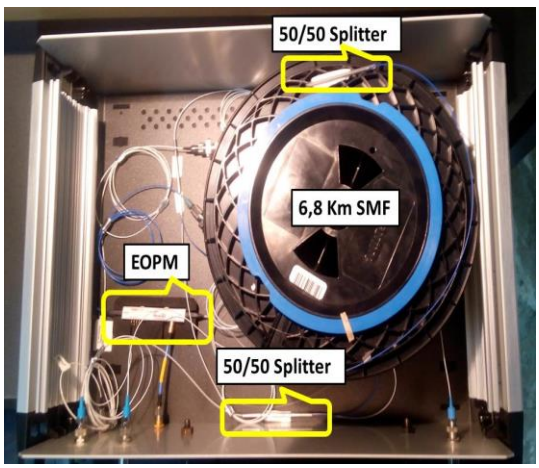

(b)

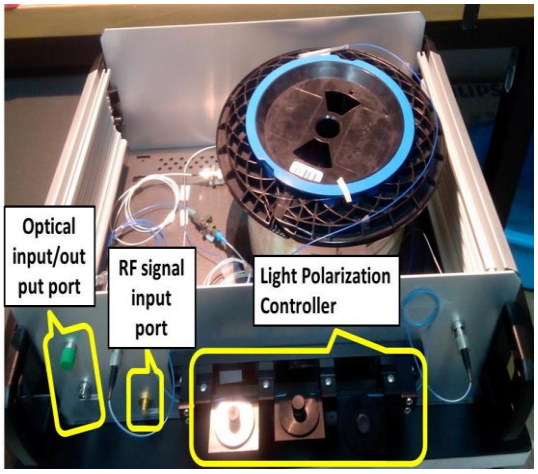

(c)

Figure 2.16. (a) Block diagram for the linewidth measurement. Delayed self-heterodyne linewidth measurement setup (dash-line green square). (b) Upper view of the optical components used in the linewidth measurement setup. (c) Frontal view of the setup.

This setup breaks the coherence of the optical wave emitted by the laser using a long fiber, the length of which determines the frequency resolution for the linewidth measurement. The self-heterodyne method is able to shift information from high spectral frequencies to frequencies that can be measured with electronics components.

The optical signal is passed through an optical isolator (OI), to avoid that back-reflections affect the linewidth of the laser. A 50/50 fiber splitter is used to divide the light input into two identical branches. An electro-optical phase modulator (EOPM) is used to create sidebands, spaced by the injected modulation frequency, at 11 GHz. On the other branch, a single-mode optical fiber reel with a 6.8 km length breaks the coherence of the light source. A manual light polarization controller (PC) is added in order to match the polarization of light from both branches.

The two arms are combined with another 50/50 coupler, and are mixed on a photodiode. The EOPM shifts the detection frequency away from DC, where the electrical spectrum analyzer does not work well. The two optical signals that incident on the photodiode (PD) are down-converted to frequency difference that EOPM generates, centered at the local oscillator input frequency.

2.5.4 Electrical linewidth of signals generated by optical heterodyning

When an electrical signal is generated through optical heterodyning, there is a direct relation between the optical and electrical linewidths. We have already discuss the experimental method to measure the optical linewidth. For the electrical linewidth, it must be taken into account the high frequency range that we are aiming for. The setup used for this measurement is shown in Figure 2.17. A high-speed PIN photodiode (PD) provided by U2T is used as an optical-electrical signal converter, with 3 dB cut-off

frequency of 100 GHz. A harmonic mixer (HM) with a frequency range from 75 to 110 GHz, E-band, to down-converts the high-frequency signal to baseband is used.

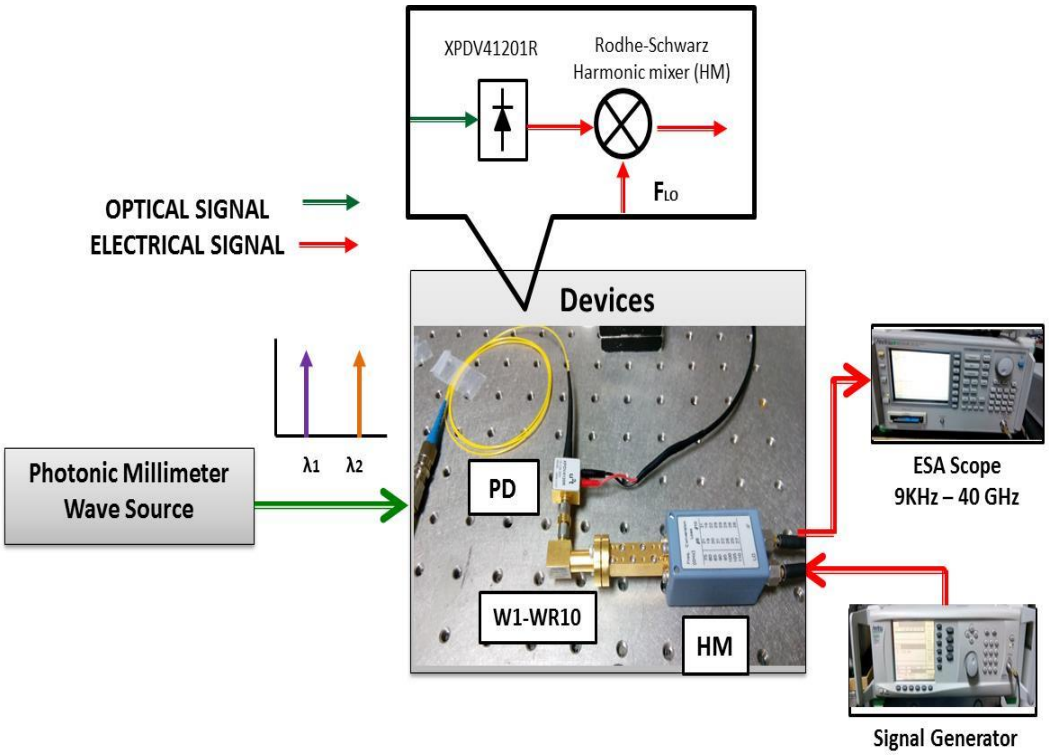

Figure 2.17. Block diagram used for the electrical beat-note linewidth measurement of the mixing of two optical lasing modes coming from the photonic mmW source under test.

The two optical lasing modes generated by the photonic millimeter wave source, are carried through a single mode fiber towards the XPDV4120R PIN photodiode. They are mixed into the PIN-PD generating a radio frequency (RF) beat-note signal at its output. The outgoing RF signal generated by the PIN-PD is the frequency spacing of the two optical modes. A W1 type connector ought to be used for connecting the PD's output to other electrical components such as RF amplifier or horn antennas.

A W1-WR10 transition to connect the PD's output to the harmonic mixer input waveguide is used. In order to down-convert the RF beating signal generated by PIN-PD into a measurable signal which can be detected and recorded by the available

electrical spectrum analyzer's (ESA) frequency range, a Rodhe-Schwarz FS-Z110 harmonic mixer is used. Two different harmonic orders can be used to generate a baseband electrical signal; it is an image of the incoming original signal in the harmonic mixer input waveguide.

In this work, a 404 MHz baseband electrical signal is generated at the harmonic mixer head output by selecting the tenth harmonic. Therefore, in order to select this harmonic order, an external continuous wave (CW) signal generator connected to the local oscillator input port is used. The frequency range of the whole setup is from 70 to 110 GHz with 32 dB maximum losses.

2.7 Conclusions

In this chapter, an analytical study of optical heterodyne technique as one of the photonic optical techniques used for the millimeter-wave and THz signal generation was done. The optical heterodyne technique is the easiest way to generate an electrical radio-frequency signal from a few MHz to cents of GHz and beyond. The basic idea of this photonic technique is to use two separated single mode optical laser sources with a wide wavelength tunability range in order to achieve the desired electrical radio-frequency signal. The electrical radio-frequency signal is the result of the beating of the two optical modes into a photodetector or photo mixer, and this one is related with the wavelength spacing between these optical modes. Several kinds of optical laser sources can be used in order to get this photonic optical technique such as tunable external cavity lasers, distributed grating reflector lasers, distributed feedback lasers, and AWG based lasers. Each optical source has its own advantage and disadvantage when are used to make up a dual-wavelength laser source.

In this thesis, AWG based laser was selected in order to build a dual-wavelength laser source. The main feature of an AWG is that this optical component is a passive filter, filtering the incoming lasing modes. This study allowed for the identification of the main design parameters in the design of an AWG. The designed AWG can be fabricated on generic InP technology platform, so much so that most of the AWG commercial fabricated for communications systems, mainly in WDM networks are fabricated on Silica technology platform.

The design of an FIR-filter bank using MATLAB software in order to generate a closer transmission response of the AWG was developed. The next step was to place the

AWG into the Fabry-Perot cavity of a laser and to do an analytical study of the different kind of AWG-based laser structures and topology can be made into a chip, by using cleaved facet as mirrors and other optical components in order to build a multiwavelength laser which can generate as many wavelengths simultaneously as are needed. This analytical approach allowed for the simulation of and AWG-based laser in PICWave software, where some active and passive optical components are used.

The linewidth measurement of a laser source is a very important parameter so that the usefulness of a carrier signal is defined by the linewidth so it is necessary to take into account the linewidth requirements for THz data transmission systems. The linewidths around MHz are useful for direct envelop detection methods. However when we use coherent detection we have to consider the MHz linewidth limitation, due to the fact that lower linewidths are required for higher order modulation schemes A delayed self-heterodyne optical technique in order to measure the -3 dB optical linewidth of each channel of the AWG-based laser was designed and built in the lab.

2.8 References

[1] J. J. O"Reilly, P. M. Lane, and M. H. Capstick , "Optical Generation and Delivery of Modulated mm-waves for Mobile Communications" in *Analogue Optical Fibre Communications*,1995

[2] Yang Jing Wen, Hai Feng Liu, Dalma Novak, and Yoh Ogawa. "Millimeter-Wave Signal Generation from a Monolithic Semiconductor Laser via Subharmonic Optical Injection". *IEEE Photonics Technology Letters*, Vol. 12, No. 8, pp. 1058-1060. 2000.

[3] Langley L. N., Elkin M. D., Edge C., Wale M. J., Gliese X., Huang X., and Seeds A. J. "Packaged Semiconductor Laser Optical Phase-Locked Loop (OPLL) for Photonic Generation. Processing and Transmission of Microwave Signals", *IEEE Transactions On Microwave Theory and Techniques*, Vol. 47, No. 7, pp. 1257‑1264, 1999.

[4] A. García Juárez, I. Zaldívar Huerta, A. Baylón s, M. del Rocío Gómez, L. García, A. Leal and A. Vera. "Wired/Wireless Photonic Communication Systems Using Optical Heterodyning". Advances in optical communications. Chapter 7.

[5] Tadao Nagatsuma, Shogo Horiguchi, Yusuke Minamikata, Yasuyuki Yoshimizu, Shintaro Hisatake, Shigeru Kuwano, Naoto Yoshimoto, Jun Terada, and Hiroyuki Takahashi. "Terahertz wireless communications based on photonics technologies", *Optic Express*, Vol. 21, No. 20, October 2013.

[6] A.J. Seeds, H. Shams, M.J. Fice, C.C.Renaud, "TeraHertz Photonics for Wireless Communications", *J. Lightwave Technology*, 33(3), pp.579587, 2015

[7] F. van Dijk, A. Accard, A. Enard, O. Drisse, D. Make, and F. Lelarge, "Monolithic dual-wavelength DFB lasers for narrow linewidth heterodyne beat-note generation," in *Proc. Int. Top. Meet. Microw. Photon. Jointly Held With Asia-Pacific Microw. Photon. Conf.*, pp. 73–76. 2011.

[8] G. Carpintero, K. Balakier, Z. Yang, R. Guzman, A. Corradi, A. Jimenez, G. Kervella, M. Fice, M. Lamponi, M. Chtioui, F. van Dijk, C. Renaud, A. Wonfor, E. Bente, R. Penty, I. White, and A. Seeds, "Microwave photonic integrated circuits for millimeter-wave wireless communications," *J. Lightw. Technol.*, Vol. 32, No. 20, pp. 3495–35011, Oct. 2014.

[9] F. van Dijk, A. Accard, A. Enard, O. Drisse, D. Make, and F. Lelarge, "Monolithic dual-wavelength DFB lasers for narrow linewidth heterodyne beat-note generation," in *Proc. Int. Top. Meet. Microw. Photon. Jointly Held With Asia-Pacific Microw. Photon. Conf.,* 2011, pp. 73–76.

[10] M. W. Fleming and A. Mooradian, "Spectral characteristics of external-cavity controlled semiconductor lasers", *IEEE J. Quantum Electron*., Vol. QE-17, pp. 44-59, Jan. 1981

[11] K. R. Preston, K. C. Woollard, and K. H. Cameron, "External cavity controlled single-longitudinal-mode laser transmitter module", *Electron. Lett*., Vol. 17, pp. 931-933, Nov. 1981.

[12]] S. Saito, 0. Nilsson, and Y. Yamamoto, "Oscillation center frequency tuning, quantum FM noise, and direct frequency modulation characteristics in external grating loaded semiconductor lasers", *IEEE J. Quantum Electron*., Vol. QE-18, pp. 961-970, June 1982

[13] F. Favre. D. le Guen. and J. C. Simon. "Optical feedback effects I_ upon laser diode oscillation field spectrum*", IEEE J. Quantum Electron*., Vol. QE-18, pp. 1712-1717, October. 1982.

[14] F. Favre and D. le Guen, "Emission frequency stability in single-mode-fiber optical feedback controlled semiconductor lasers", *Electron. Lett*., Vol. 19, pp. 663-665, August. 1983.

[15] R. Lang and K. Kobayashi, "External optical feedback effects on semiconductor injection laser properties", *IEEE J. Quantum Electron*., Vol. QE-16, pp. 347-555, Mar. 1980.

[16] D. M. Fye, "Relationship between carrier-induced index change and feedback noise in diode lasers", *IEEE J. Quantum Electron*., Vol QE-18, pp. 1675-1678, Oct. 1982.

[17] K.C. Harvey and C.J. Myatt. "External-cavity diode laser using a grazing-incidence diffraction grating". *Optics Letters,* Vol 16, pp 910‑912. 1991.

[18] M.G. Littman and H.J. "Metcalf. Spectrally narrow pulsed dye laser without beam expander". *Applied Optics* Vol 17, pp 2224‑2227. 1978.

[19] K. Liu and M.G. Littman. Novel geometry for single-mode scanning of tunable lasers. *Optics Letters* Vol 6, pp 117‑118. 1981

[20] L. Coldren, S. Corzineand M. Masnovic. "Diode lasers and photonic integrated circuits", second edition. Chapter 3.

[21] http://www.photodigm.com/difference-between-dbr-and-dfb-lasers

[22] M. Smit, "New focusing and dispersive planar component based on an optical phased array", *Electronics Letters*, Vol. 24, No. 7, pp. 385-386,1988.

[23] C. van Dam, "InP-based polarization independent wavelength demultiplexers", PhD thesis, Delft University of Technology, The Netherlands, 1997.

[24] Y. Barbarin, X. Leijtens, E. Bente, C. Louzao, J. Kooiman, and M. Smit, "Extremely small AWG demultiplexer fabricated on InP by using double-etch process," in Tech. Digest Integr. Photon. Res. (IPR'04), p. IThG4, San Francisco, USA, June-July 2004.

[25] B.W. Tilma, "Integrated tunable quantum-dot laser for optical coherence tomography in the 1.7 μm wavelength region," Ph.D. thesis, Technische Universiteit Eindhoven, The Netherlands, 2011.

[26] K. Ławniczuk, "Multiwavelength transmitters in generic photonic integration technologies," PhD thesis, Technische Universiteit Eindhoven, The Netherlands, 2014.

[27] C. Richard Doerr and K. Okamoto, "Advances in Silica Planar Lightwave Circuits", *Journal of Lightwave Technology*, Vol. 24, No. 12, 2006.

[28] P. Dumon, W. Bogaerts, D. Van Thourhout, G. Morthier, R. Baets, P. Jaenen, S. Beckx, J. Wouters, T. Farrell, N. Ryan, E. Grivas, E.; Kyriakis-Bitzaros, E.; Halkias, G.; McKenzie, I., "A nanophotonic 4 x 4 wavelength router in silicon-on-insulator", *Optical Fiber Communication Conference*, 2006 (OFC '06), 5-10 March 2006.

[29] H. Okayama and M.Kawahara, "Waveguide array grating demultiplexer on LiNbO3," in *Technical Digest Integr. Photon. Res. (IPR '95)*, pp. 296-298, Dana Point, CA, 1995.

[30] M. Diemeer, L. Spiekman, R. Ramsamoedj, and M. Smit, "Polymeric phased array wavelength multiplexer operating around 1550 nm", *Electron. Lett.*, Vol. 32, pp. 1132-1133, 1996.

[31] R. C. Guzman, L. J. Orbe, G. Carpintero, A. Corradi, E.A.J.M. Bente "Travelling wave model of an AWG-based multiwavelength laser", in *Proceedings of the 16th ECIO*, 2012.

[32] P. Munoz, R. Garcia-Olcina, C. Habib, L. R. Chen, X. J. M. Leijtens, J. D. Domenech, M. Rius, J. Capmany, T.De Vries,M. J. R.Heck, L. Augustin, R.Notzel, andD. Robbins, "Multi-wavelength laser based on an arrayed waveguide grating and sagnac loop reflectors monolithically integrated on inp," *IET Optoelectronics*, Vol. 5, 2011.

[33] B. Docter, Deeply-Etched DBRMirrors for Photonic Integrated Circuits and Tunable Lasers. Eindhoven, The Netherlands: Ph.D. Thesis, Technische Universiteit Eindhoven, the Netherlands, 2009.

[34] E. Kleijn, M. Smit, and X. Leijtens, "Multimode Interference Reflectors: a new class of components for photonic integrated circuits," *J. Lightw. Technol.*, Vol. 31, no. 18, pp. 3055–3063, 2013.

[35] P. Harmsma, M. Smit, Y. Oei, M. Leys, C. Verschuren, and H. Vonk, "Multi-wavelength lasers fabricated using selective area chemical beam epitaxy," in Technical Digest Integr. Photon. Res. (IPR '99). 1999, pp. 17–19, Sta. Barbara, USA

[36] M. Zirngibl and C. Joyner, "High performance, 12 frequency optical multichannel controller", *Electron. Lett.*, Vol. 30, no. 9, pp. 700–701, Apr. 1994.

[37] C. Doerr, C. Joyner, L. Stulz, and J. Centanni, "Wavelength-selectable laser with inherent wavelength and single-mode stability", *IEEE Photon. Technol. Lett.*, Vol. 9, no. 11, pp. 1430–1432, Nov. 1997.

[38] W. Pascher, J.H. den Besten, D. Caprioli, X. Leijtens, M. Smit, and R. van Dijk, "Design and characterization of a traveling wave electro-optic modulator on InP", *URSI Conference*. Sept. 30–Oct. 2 2002, p.21, Miltenberg, Germany

[39] Photon Design, *http://www.photond.com*

[40] I. Aldaya, G. Campuzano, C. Gosset, and G. Castañón. "Phase-insensitive RF envelope detection allows optical heterodyning of MHz-linewidth signals." *IEEE Photon. Technol. Lett.*, vol. 25, no. 22, pp. 2193-2196, 2013.

[41] T. Ishikawa, H. Tanaka, M. Shibata, M. Tajima, Y. Oka, and T. Kaneko, "Narrow Spectral Linewidth Full-Band Wavelength Tunable Lasers for Digital Coherent Communication Systems."*Sei Technical Review*, no. 77, pp. 54-58, 2013.

[42] A. Schawlow and C. Townes, "Infrared and optical masers". *Phys. Rev*., 112, pp. 1940–1949, 1958.

[43] C. Henry, "Theory of the linewidth of semiconductor lasers". *IEEE J. Quantum Electron*., 18, pp. 259–264, 1982.

[44] F. Van Dijk, A. Accard, A. Enard, O. Drisse, D. Make and, F. Lelarge "Monolithic dual wavelength DFB for narrow linewidth heterodyne beat-note generation" in *Proccedings IEEE Int. Top. Meeting on Microwave Photonics (MWP),* pp. 73-76, 2011, (2001).

[45] J. Zoz and U. Barabas. "Linewidth enhancement in laser diodes caused by temperature fluctuations". *IEEE Proc.-Optoelectron.,* 141, pp. 191–193, 1994.

[46] U. Krüger and K. Petermann. "The semiconductor laser linewidth due to the presence of side modes". *IEEE J. Quantum Electron*., 24, pp. 2355–2358, 1988.

[47] S. Miller. "The effect of side modes on linewidth and intensity fluctuations in semiconductor lasers". *IEEE J. Quantum Electron*., 24, pp. 750–757, 1988.

[48] T. Okoshi, K. Kikuchi and A. Nakayama, "Novel method for high-resolution measurement of laser output spectrum". *Electron. Lett.*, Vol. 16, pp. 630-631, 1980.

Multiwavelength AWG laser using cleaved facet mirrors

3.1 Linear AWG based laser

The first photonic integrated circuit that we have developed as dual-wavelength source for optical heterodyning is an AWG laser with at least two channels.

The photonic integrated circuit was fabricated on the OCLARO InP active/passive integration technology platform. The device structure, as shown in Figure 3.1(a), consists of an AWG with a central wavelength at λ = 1550 nm, channel spacing $\Delta\lambda_{ch}$ = 0.8 nm (ΔF_{ch} =100 GHz) and the FSR is 7.2 nm (900 GHz). We observe up to sixteen channels, each with its corresponding 600 μm long SOA -labeled SOA N (with N = 1 to 16). It is important to highlight two points:

- The free spectral range of the AWG is smaller than the channel spacing multiplied by the total number of channels (900 GHz < 16 x 100 GHz). In this AWG, there is an overlap between channels 1 to and 9 to 16.
- The device employs the cleaved facet of the chip to define the Fabry-Perot cavity mirrors of the AWGL, using a PR coated with a reflection value of 32% approximately.What is really it means is that any element that we want to include in the chip, has to be included within the resonator cavity. For this device, the element that we have added is a 750 μm long SOA, located at the common output and used to boost the output optical power (Boost amplifier). The lasing mode spacing ΔF, generated by the longer laser cavity is around 4.7 GHz.

A microscope photograph of cleaved facet structure 16-channels AWGL is shown in Figure 3.1(b).

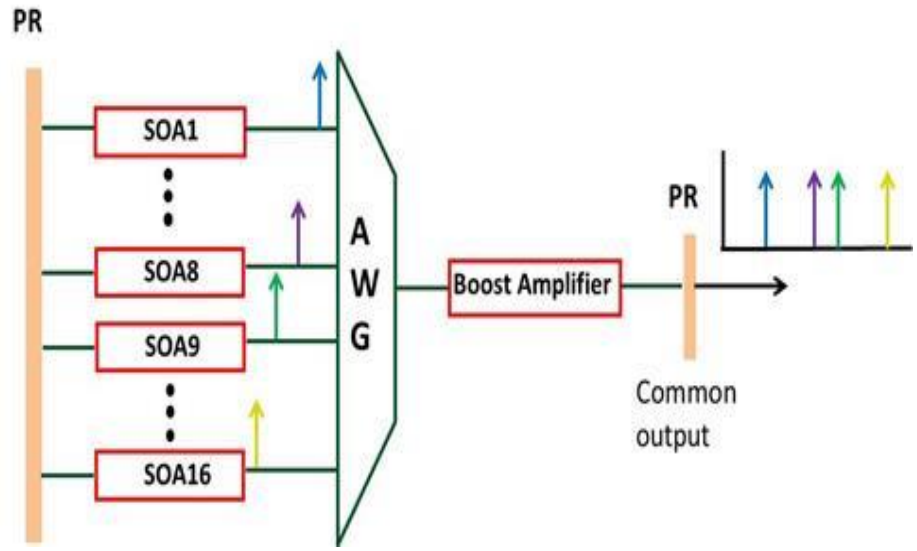

(a)

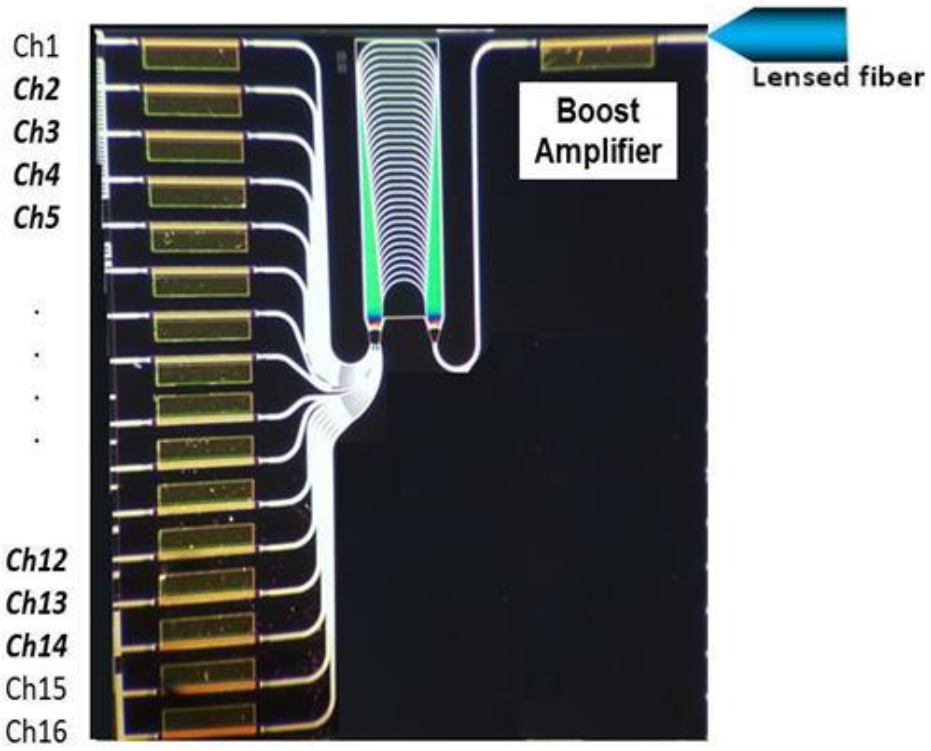

(b)

Figure 3.1. (a) Schematic of 16-channels AWGL. The cleaved facets of the chip use as mirror a partially reflective (PR) coated with a reflection value of 32% approximately. (b) Microscope photograph of cleaved facet structure of 16-channels AWGL.

The device can be used as an optical source of an optical heterodyne signal by activating two channel SOAs. This device allows to generate wavelengths that are spaced by an integer multiple of the channel spacing over the FSR range. The two wavelengths are combined on the AWG's common output, amplified by the Boost amplifier. This implies that we need to use the bias current of each channel to equalize the amplitude for each of the wavelengths, which also affects to the SMSR. Using the same Boost amplifier for the generated wavelengths at the common output of the AWG, it gives the advantage of having the same carrier densities and the same variations in amplified spontaneous emission (ASE).

In the present structure, the Boost amplifier must amplify the two channel wavelengths, experiencing the same variations that are caused at this SOA by changes in refractive index due to changes in temperature and carrier concentration.

However, the boost amplifier is a common gain media for the two wavelengths, inserted within the resonator, which means that gain competition can arise, leading to instabilities of the dual-mode lasing operation turning it impossible to have simultaneous emission of the two optical lasing modes.

Chusseau [1] state that a stable dual-wavelength regime is possible only when the coupling factor between the modes is weak. At a common SOA, the physical origin of the mode coupling is the short intra-band relaxation time that strongly couples the carrier populations [1], and for a quantum well (QW) gain media, dual-wavelength operation can only occur over a small range of injection currents and temperatures.

3.2 Measurements of LI curves and optical spectrum characteristics.

In Figure 3.2 (c) is shown a general block diagram of the arrenged setup for the L-I curve and optical spectrum measurements . To characterize this device, it is soldered onto a copper mount to place it on a probe station, where needle probes are used to bias the Channel and Boost SOAs A Peltier element, placed underneath the copper, stabilizes the mount temperature to 16 ºC for all the measurements. The light from the chip is collected using a lensed fiber.

A photograph of the probe station is shown inFigure 3.2 (a). Figure 3.2 (b) shows the access to the common arm mirror with a lensed fiber. The lensed fiber is aligned to the waveguide, . An optical isolator has been fusion spliced to the lensed fiber in order to reduce the undesired effects from back-reflections to the chip.

As shown in the Figure 3.2 (c), the setup that we use allows us to simultaneously measure the optical output power and the optical spectrum. This gives us Light-Current characteristic as well as the spectral content, to analyze the side mode suppression ratio (SMSR) [2].

A Thorlabs ILX PRO-8000 with eight current sources is used to bias several channels as well as the boost amplifier simultaneously. A high resolution optical spectrum analyzer (0.02nm) is used to record the spectrum.

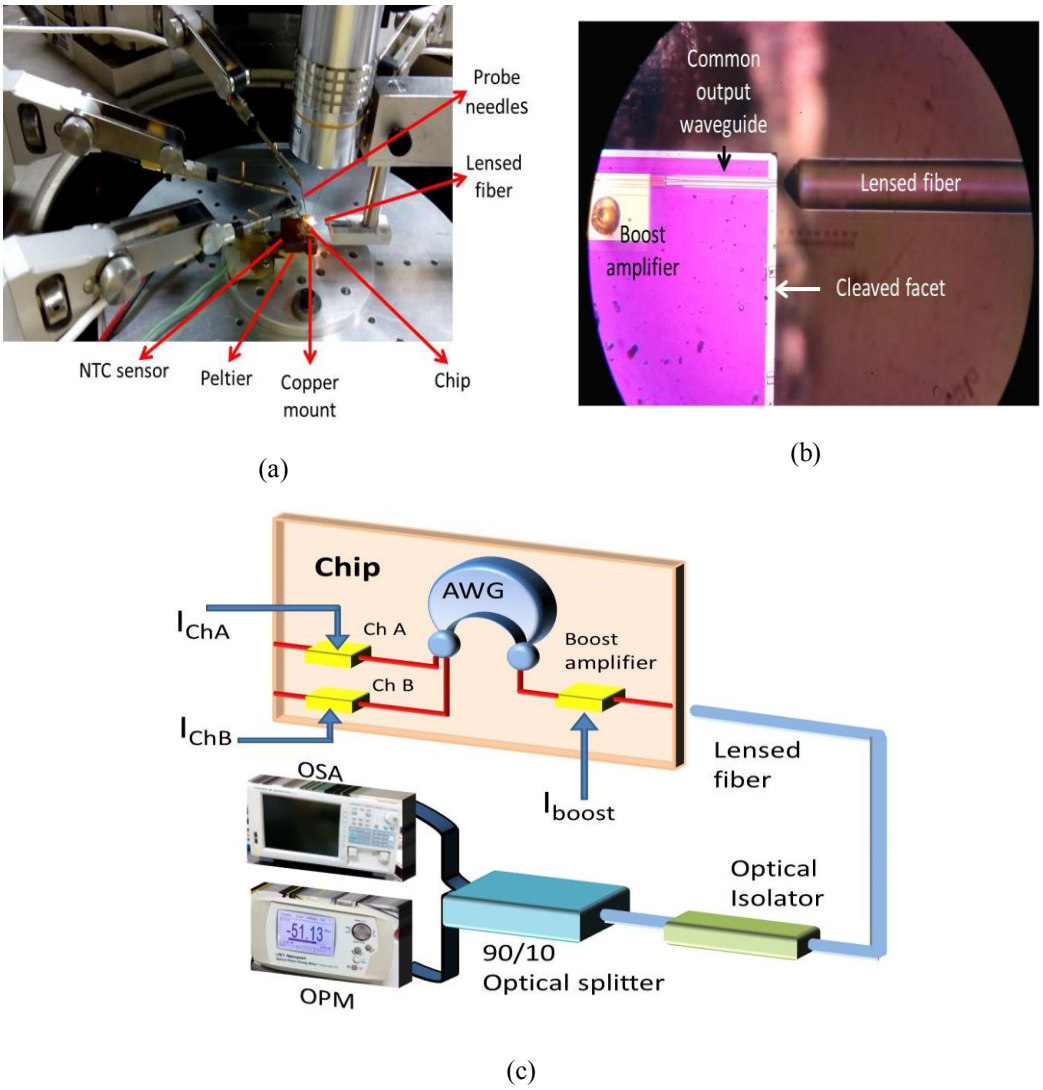

Figure 3.2. (a) Photograph of the probe station where the chip is placed to be characterized. (b) Microscope photograph of how the lensed fiber is placed and aligned close to the cleaved facet of the chip. (c) General block diagram of the arranged setup for the L-I curve and optical spectrum measurements.

3.2.1 Boost amplifier characteristics

The first test is to bias the boost amplifier only, without injecting any current into the channel's SOAs. Under this condition, we record the *Light-Current* characteristic curve sweeping the current injected into Boost SOA from 0 to 100 mA. The result is shown in Figure 3.3 (a). This figure reveals a typical *Light-Current* characteristic curve of a laser,

with a threshold current at about 24 mA and maximum output power of 550 µW. A dP/dI linear value of 7.6 µW/mA is founded.

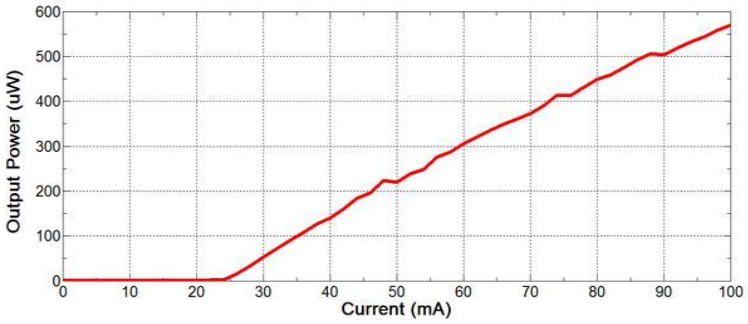

(a)

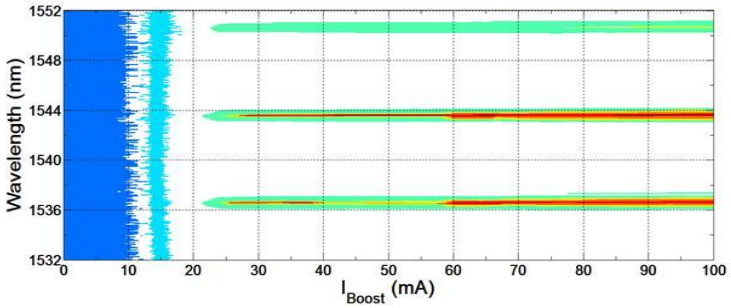

(b)

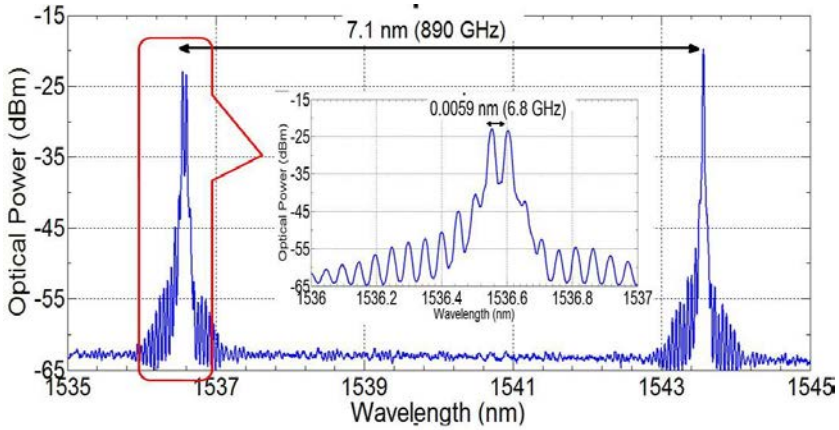

(c)

Figure 3.3. (a) LI curve of the boost amplifier. (b) Mapping of the detected output optical power spectrum at the common output of the chip. (c) Optical spectrum of the boost amplifier as is biased at 28 mA. The frequency spacing between both lasing modes is about 7.1 nm (890 GHz). The lasing mode spacing of the generated Fabry-Perot is around 0.0059 nm (6.8 GHz), which is equivalent to 5900 µm long. This length corresponds from cleaved facet at the common output of the AWG to the FPR where the channels SOAs are connected.

The mapping of the detected output optical power spectrum, shown in Figure 3.3 (b), shows lasing modes which are kept as the bias current is swept. The frequency spacing between both lasing modes is about 7.1 nm (890 GHz). In addition, lasing modes caused from undesired reflections at the free propagation region, where the channel SOAs are connected, let to establish an undesired Fabry-Perot cavity with the cleaved facet of the chip. It is because of small unwanted geometrical errors (in the order of nm) during the fabrication process of the chip [3] . The lasing modes generated by the Fabry-Perot cavity is about 0.0059 nm (6.8 GHz), which corresponds to 5900 μm long.

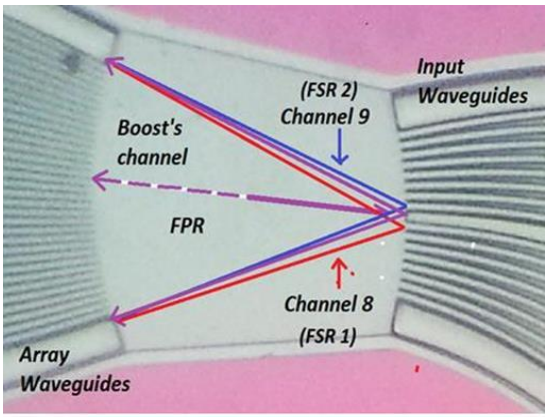

(a)

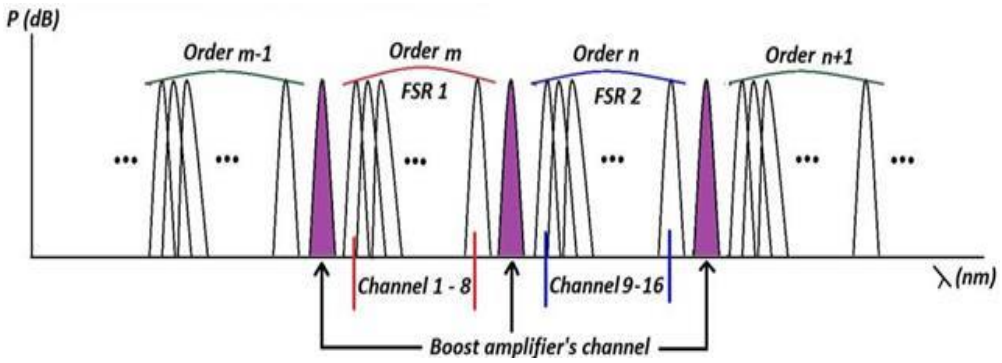

(b)

Figure 3.4. (a) Photograph of the FPR of the 16-channels AWG. Reflections are caused by the gap located between the waveguides of the channels #8 and #9 (violet line); which acts as a central mirror for the boost amplifier. (b) Transmission output spectrum of the device.

Figure 3.4 (a) shows the photograph of the FPR where the channels SOAs are connected. As can be observed, wider gap between the waveguides of channel #8 and #9 than the other channels is presented, acting as a mirror in order to establish a Fabry-Perot cavity. This phenomenon will generate an extra channel caused by the boost amplifier as it is biased, as shown in Figure 3.4 (b). Therefore, the frequency spacing between the channel #8 and #9 is about 200 GHz, this value is twice the channel spacing of the AWG.

This result suggests that when the boost amplifier is biased, the AWG acts as a frequency selective mirror. The resulting lasing modes compete for the Boost SOA gain against the modes created when the Channel SOA is activated. This turns the task to achieve a single mode emission into a complex one, usually restricting the current values that can be injected to values that set the same gain peak wavelength for all the SOAs in the resonator, the boost amplifier and the channel SOA.

3.2.2 Individual channel SOA characteristics

We now turn to analyze the behavior of the device when current is injected into a channel SOA, while the boost amplifier is kept at a fixed current level. The results shown in Figure 3.5 (a) were obtained injecting current into Channel #7 SOA at different Boost SOA values. As I_{boost} increases above 15 mA, the Channel threshold level decreases down to 10 mA. From the spectral results, we observe that the lasing modes that are generated at the Boost SOA undesired cavity occur at different FSR orders to those lasing when the channel SOA is biased

While $I_{boost} < 24$ mA, we need to bias the channel SOA to achieve lasing condition. As soon as $I_{boost} > 24$ mA, there is already lasing from the undesired resonator

established from the FPR and the facet, having an initial optical power level (around 50 μW for I_{boost} = 30 mA). As shown in Figure 3.5 (b), we need the channel current level to reach at least 12 mA to start lasing at the channel wavelength. This highlights the fact that the Boost SOA placed within the Fabry-Perot cavity reduces the threshold current level for the channel. Thus is clear that the Boost SOA helps to overcome the resonator losses of the structure. However, the interaction between these two, the channel SOA and the Boost SOA are far more complex.

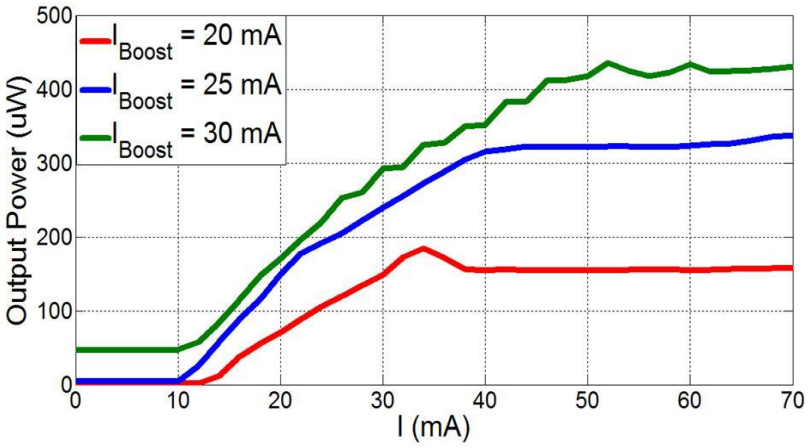

(a)

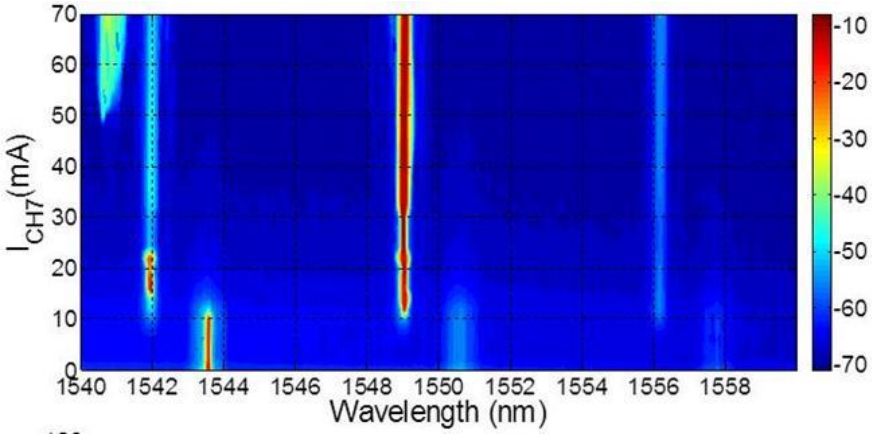

(b)

Figure 3.5. (a) *LI* characteristic curve. Channel 7 is swept from 0 to 70 mA. The output optical power is measured at the common output of the chip as the boost amplifier is biased at different current levels of 20 mA, 25 mA and 30 mA. (b) The detected output optical power spectrum. The boost amplifier is set to 30 mA. The channel 7 bias current is swept from 0 mA to 70 mA in 2 mA steps.

The interaction between them is clearly shown when we trace the optical spectrum at different values of the Channel SOA for a fixed Boost SOA current level, shown in Figure 3.6. As long as the Channel SOA current is below the Boost SOA, the emission is single mode. However, when this is no longer the case, multiple lasing modes appear with a modal spacing around 5.1 GHz. This is the Fabry-Perot cavity mode spacing.

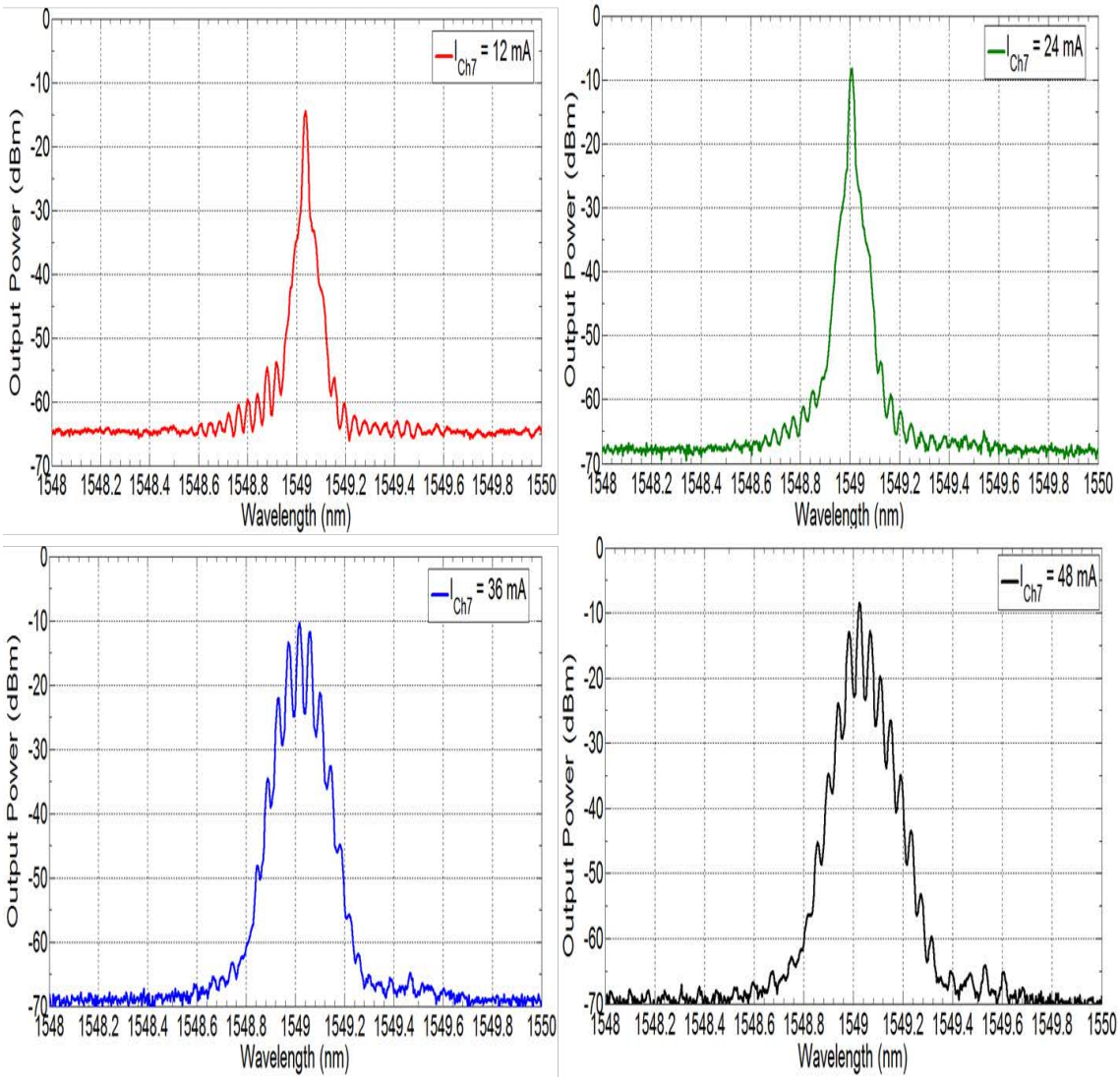

Figure 3.6. Optical spectrum of channel 7at different bias current levels of 12, 24, 36 and 48 mA. The boost amplifier is set at 30 mA. The modal spacing of the adjacent lasing modes is around 5.1 GHz as the channel 7 bias current level goes above 30 mA.

We suspect that there is a problem arising from the gain selection mechanism of the Fabry-Perot modes by the AWG when there are two different SOAs in the cavity.

Injecting different current levels to each one (above their individual threshold level), establishes a different location for their corresponding gain peak. As the lasing mode must stay within the channel passband of the AWG, and each SOA provides a different gain line-shape, a complex selection mechanism is established. Our experience is that the channel SOA current level cannot be greater than the Boost SOA bias current.

We have analyzed the threshold current for different channels, obtaining the results presented in Figure 3.7. We observe that the outer channels, such as channel 3, have higher threshold current levels than those for the inner channels, such as channel 8.

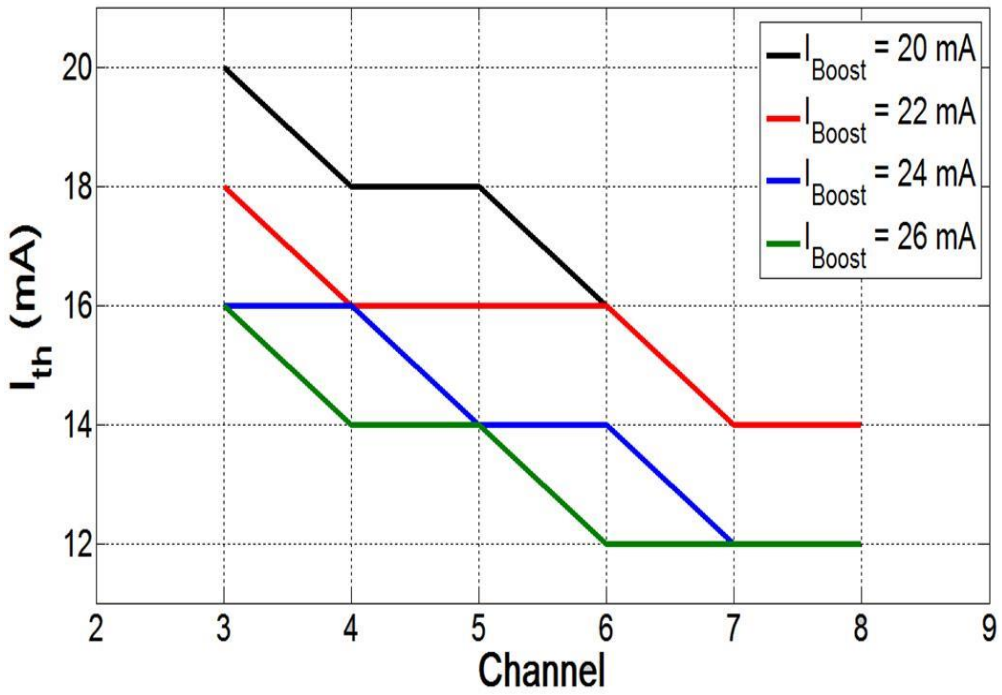

Figure 3.7. I_{th} vs Channel position curve. The boost amplifier is swept from 20 to 26 mA in order to know the performance of the threshold current level of the channels of the device.

3.3 Dual-wavelength mode operation

To achieve a dual-wavelength source from an AWGL we just need to turn on the bias current on two channels simultaneously. The wavelength spacing will depend on the channel spacing of the AWG, and how far apart these two channels are.

First we turned on two adjacent channels (Channels #7 and #8), generating two wavelengths spaced by the channel spacing frequency For this study, the bias current for Channel #8 is swept from 0 to 30 mA in 2 mA steps with Channel #7 bias current fixed to 16 mA and the boost amplifier fixed at four different values: 20, 22, 24 and 26 mA. The results are presented in Figure 3.8, showing that when the boost amplifier bias current is low (20 mA), we achieve a strong lasing mode (with SMSR > 30 dB) from Channel #7. As the bias current level of Channel #8 increases above 16 mA (Channel #7 bias), lasing at Channel 7 disappears to be replaced by lasing at Channel #8. This evolution is explained by the fact that the lasing from Channel 7 is weak with respect to the lasing mode of Channel 8. Dual-wavelength mode operation is only achieved when the both channels are balanced, around the channel #8 bias current at 16 mA.

The same situation is observed for the other cases, shown in Figure 3.8 (b), (c) and (d), where we observe a shift in the emission wavelength from #7 to #8 as the current increases. The range of the bias current levels over which we observe dual mode lasing moves upwards as the boost amplifier current increases. Dual-wavelength mode operations are achieved when the bias current of channel 8 is set at 16 and 18 mA, 18 and 20 mA and 20 and 22 mA when the boost current level is 22 mA, 24 mA and 26 mA respectively.

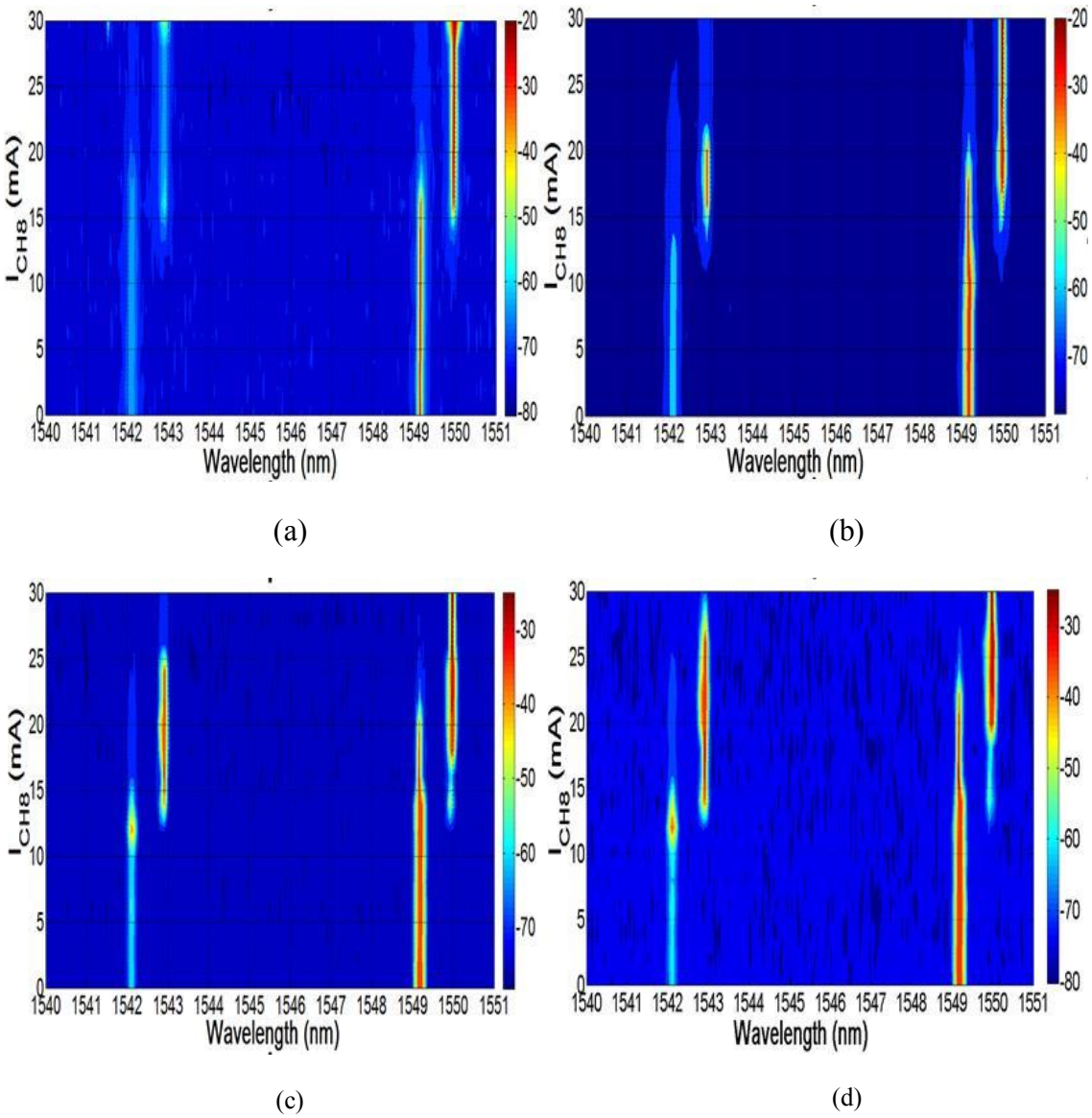

Figure 3.8. Output optical spectrum at the common output waveguide of the chip. The channel 7 is set a fixed current value of 16 mA whilst the channel 8 bias current is swept from 0 mA to 30 mA in 2 mA steps. The boost amplifier is set at 4 fixed bias current levels of 20 mA (a), 22 mA (b), 24 mA (c) and 26 mA (d).

To further analyze the interaction between SOA sections, Figure 3.9 shows the optical spectrum as the Channel #7 and #8 are kept at a fixed value (16 mA) and the bias into the boost amplifier is swept from 20 to 26 mA. At 20 mA, as in the previous case, we observe a dual-wavelength operation regime.

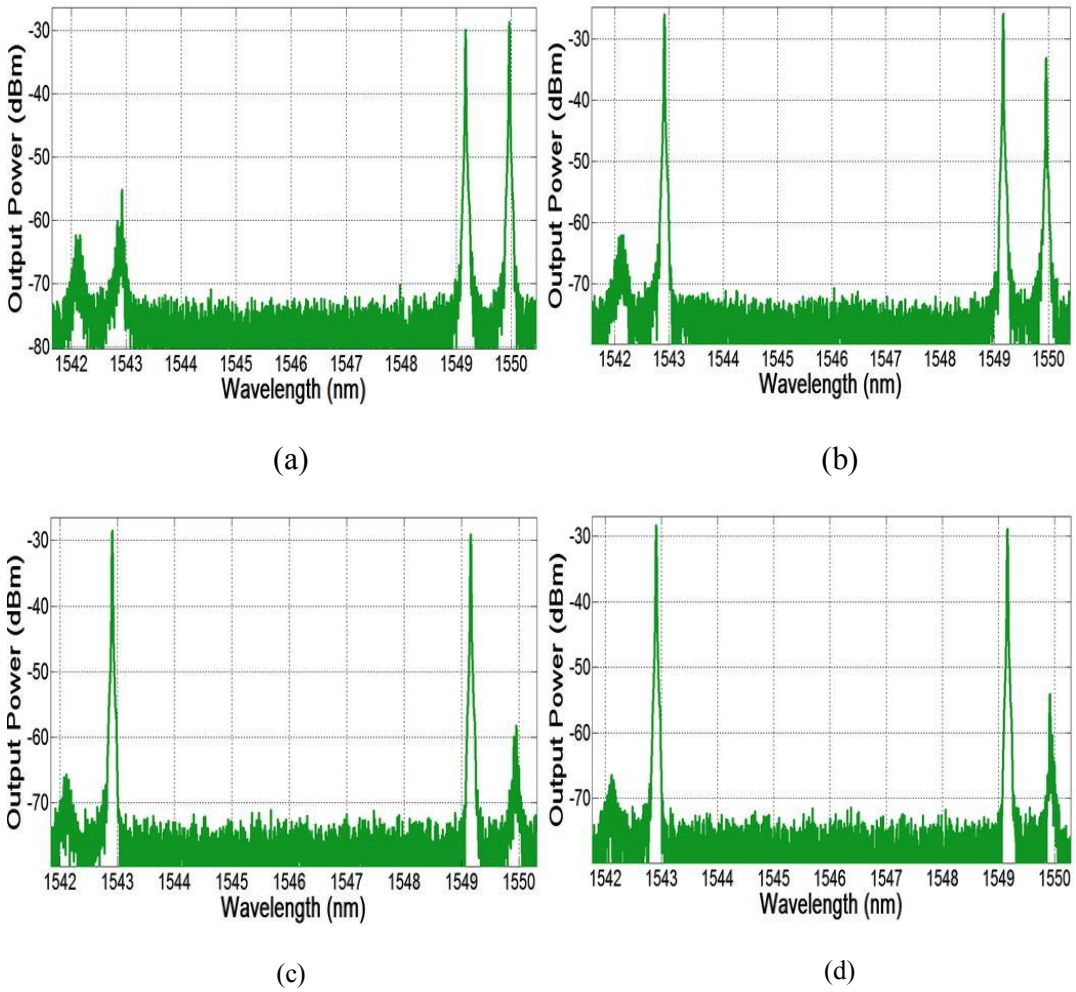

Figure 3.9. Output optical spectrum at the common output waveguide of the chip. The channels 7 and 8 are set a fixed current value of 16 mA. The boost amplifier is set at 4 fixed bias current levels of 20 mA (a), 22 mA (b), 24 mA (c) and 26 mA (d).

An extended map of the dual-wavelength mode operation regimes where two adjacent channels are selected is shown in **Error! Reference source not found.**. These maps demonstrate that in order to achieve dual-wavelength operation regimen, we must fulfill two different conditions.

- The bias current injected into each of the lasing channel should be similar.
- The bias current injected into each of the lasing channels needs to be above the bias current of the boost amplifier.

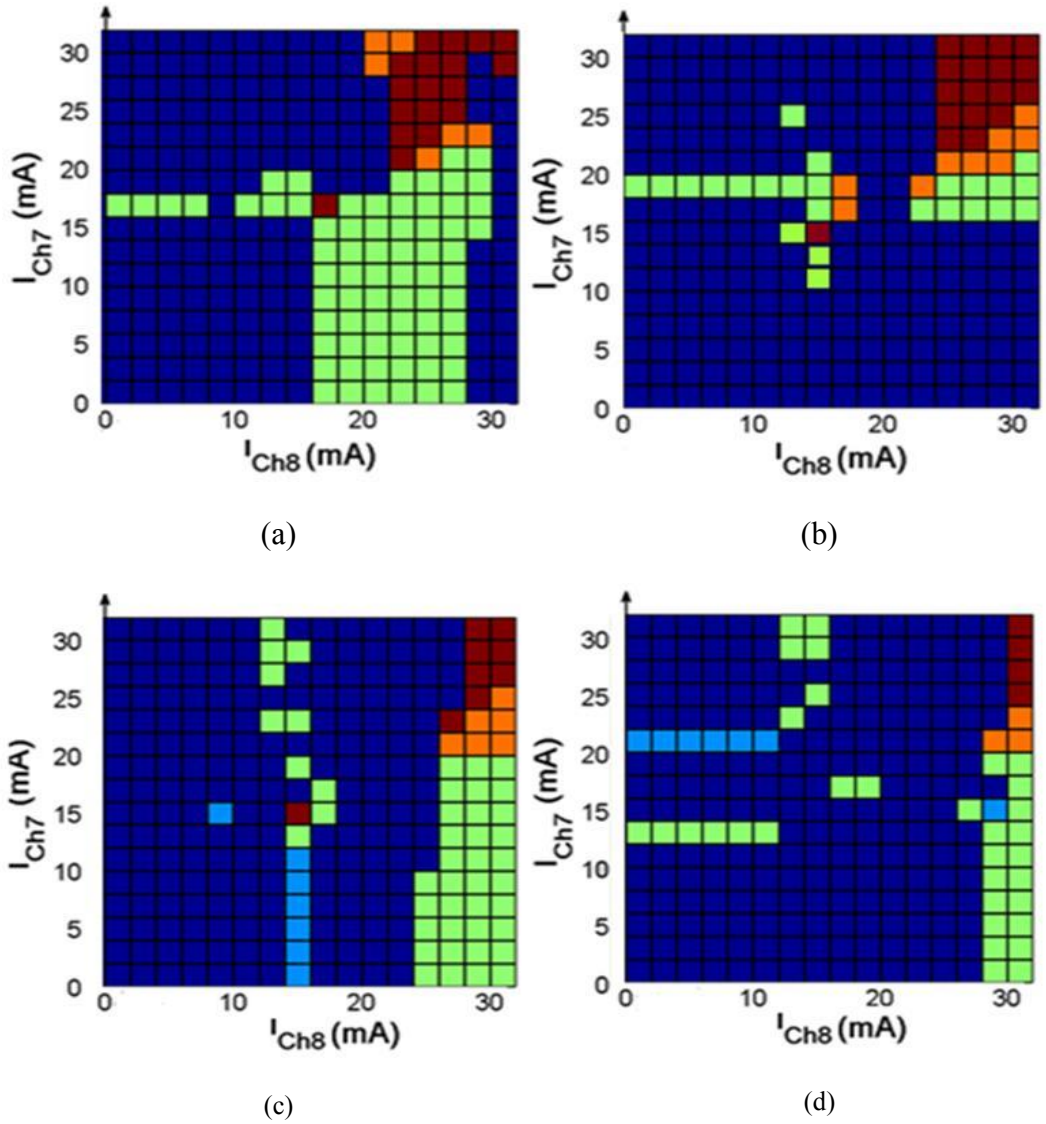

Figure 3.10. Mapping of the operation regions of the AWGL when the Channel #7 and #8 are swept from 0 to 30 mA at fixed Boost SOA bias level 20 mA (a), 22 mA (b), 24 mA (c) and 26 mA (d).Single-wavelength (light blue and green) and dual-wavelength (dark red and orange)

The dark red and orange color represents dual-wavelength mode operation regimes. For the dark red regions, the peak difference between the lasing modes is less than 3 dB, while for orange regions; this difference is higher than 3 dB. As the bias current of the boost amplifier increases the range of currents over which we observe dual-wavelength reduces.

In Figure 3.11, we present some dual wavelength operation regimes generated from this chip when the bias current of channel #7 is set at fixed current value of 30 mA whilst the bias current of channel 8 is set at four different fixed current values of 24, 26, 28 and 30 mA. We measured the frequency spacing between both, achieving 97 GHz, close to the design channel spacing of the AWG (100 GHz).

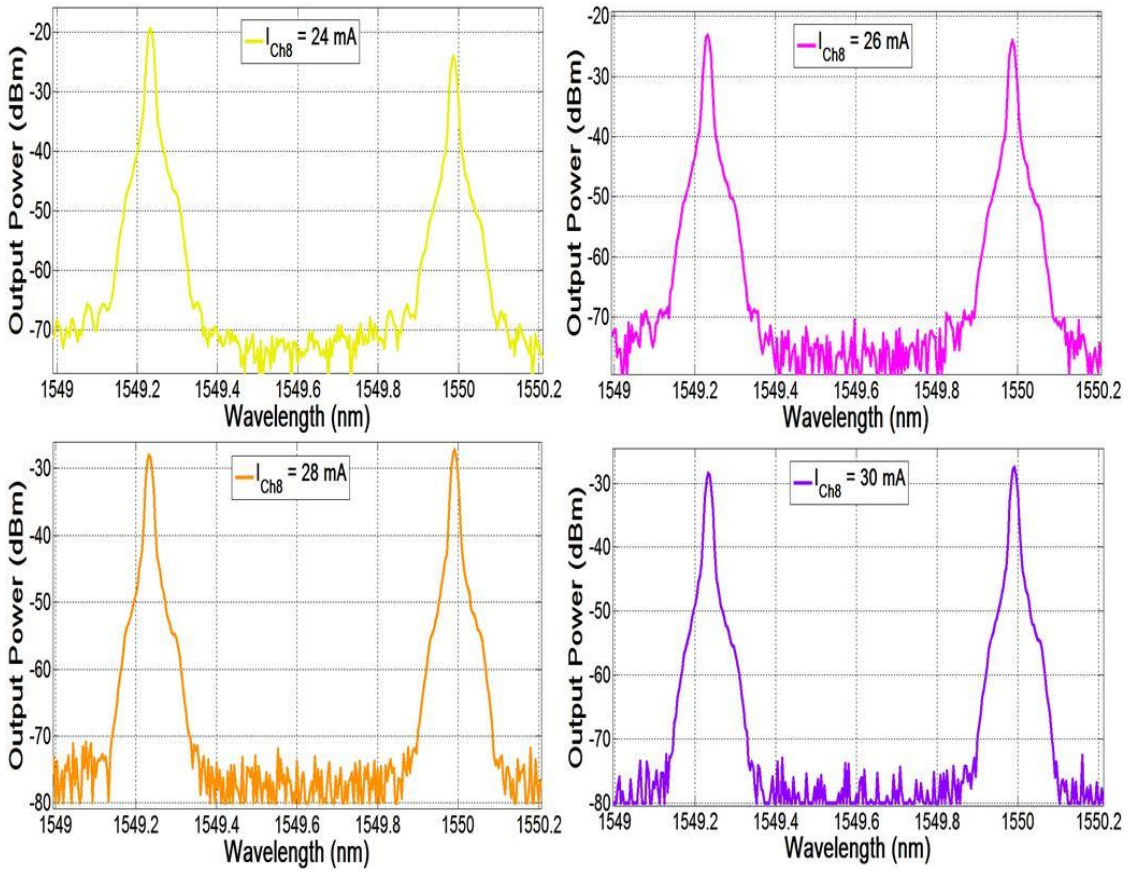

Figure 3.11. Output optical spectrum at the common output waveguide of the chip. The channel #7 is set a fixed current value of 30 mA whislt the channel #8 bias current is swept from 24 mA to 30 mA in 2 mA steps. The boost amplifier is set at 4 fixed bias current levels of 20 mA, 22 mA, 24 mA and 26 mA, respectively.

We have also analyzed the interaction among channels when these are not adjacent. First, we selected channel #5 and #7, expecting a channel spacing around 200 GHz. Figure 3.12 shows the mapping of dual-wavelength mode operation regimes. As can be seen, the dual-wavelength operation regime is smaller than the first scenario. In fact, the tuning of the bias current of each SOA is a bit more complex in order to achieve dual-

wavelength mode operation in the same FSR order of the AWG. Then we analyzed the case when the two channels are spaced three times channel spacing, using channel #5 and #8. In

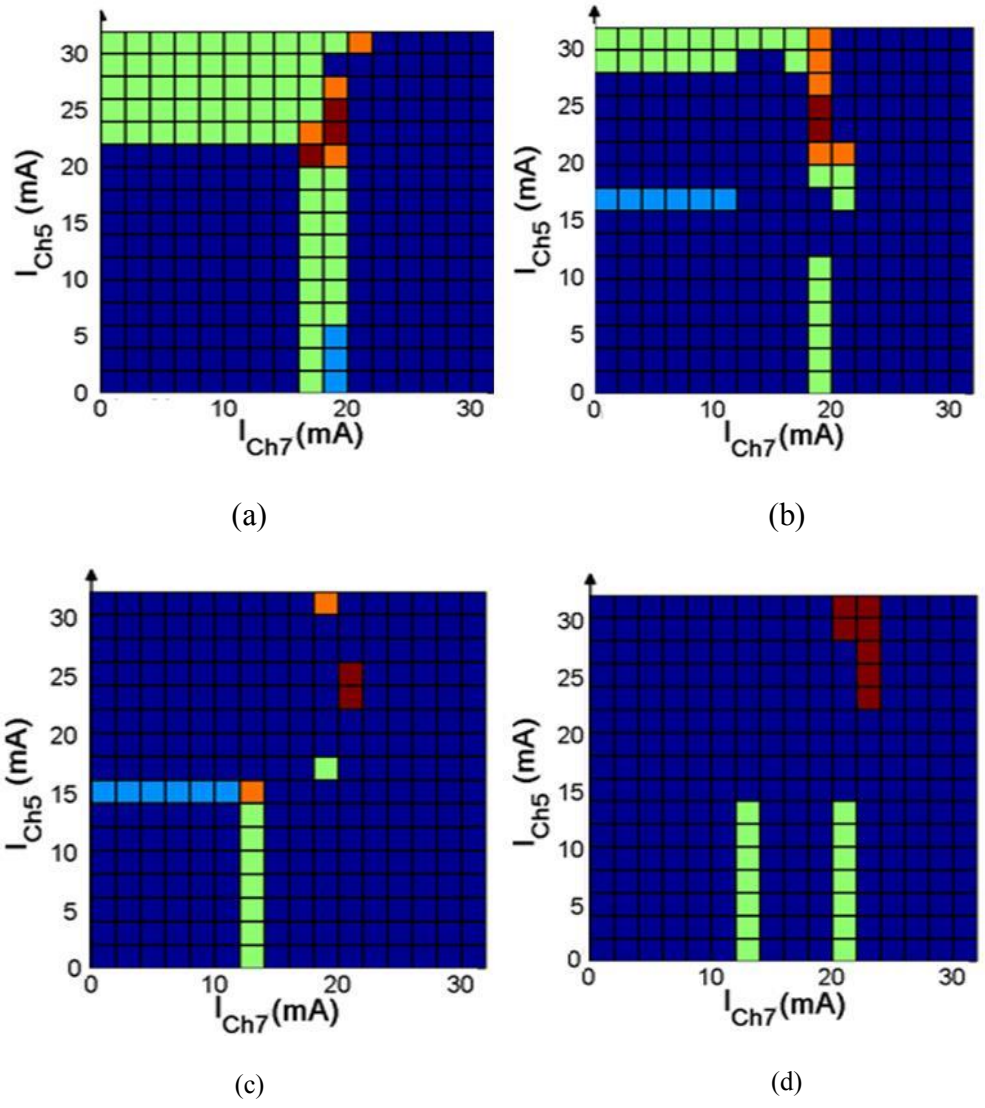

Figure 3.12. Mapping of the single-wavelength (light blue and green) and dual-wavelength (dark red and orange) mode operation regimes of the AWG. Channel 5 and 7 are swept from 0 to 30 mA whilst the boost amplifier is set at 4 fixed bias current levels of 20 mA (a), 22 mA (b), 24 mA (c) and 26 mA (d).

Finally, a third scenario is done, where two channels is selected having three times channel spacing between them i.e. 2927 GHz. For this case the channel 5 and 8 are chosen. In Figure 3.13 is shown the mapping of dual-wavelength mode operation

regimes. As can be seen, the dual-wavelength mode regime is greater than the second scenario. In fact, the single-wavelength mode operation regimes are greater than the first scenario. The condition to get dual-wavelength mode operation is that the bias current of one of the channels must be greater than the bias current injected into the boost amplifier, while the other channel's bias current should have the same bias current with a tolerance of ±4 mA.

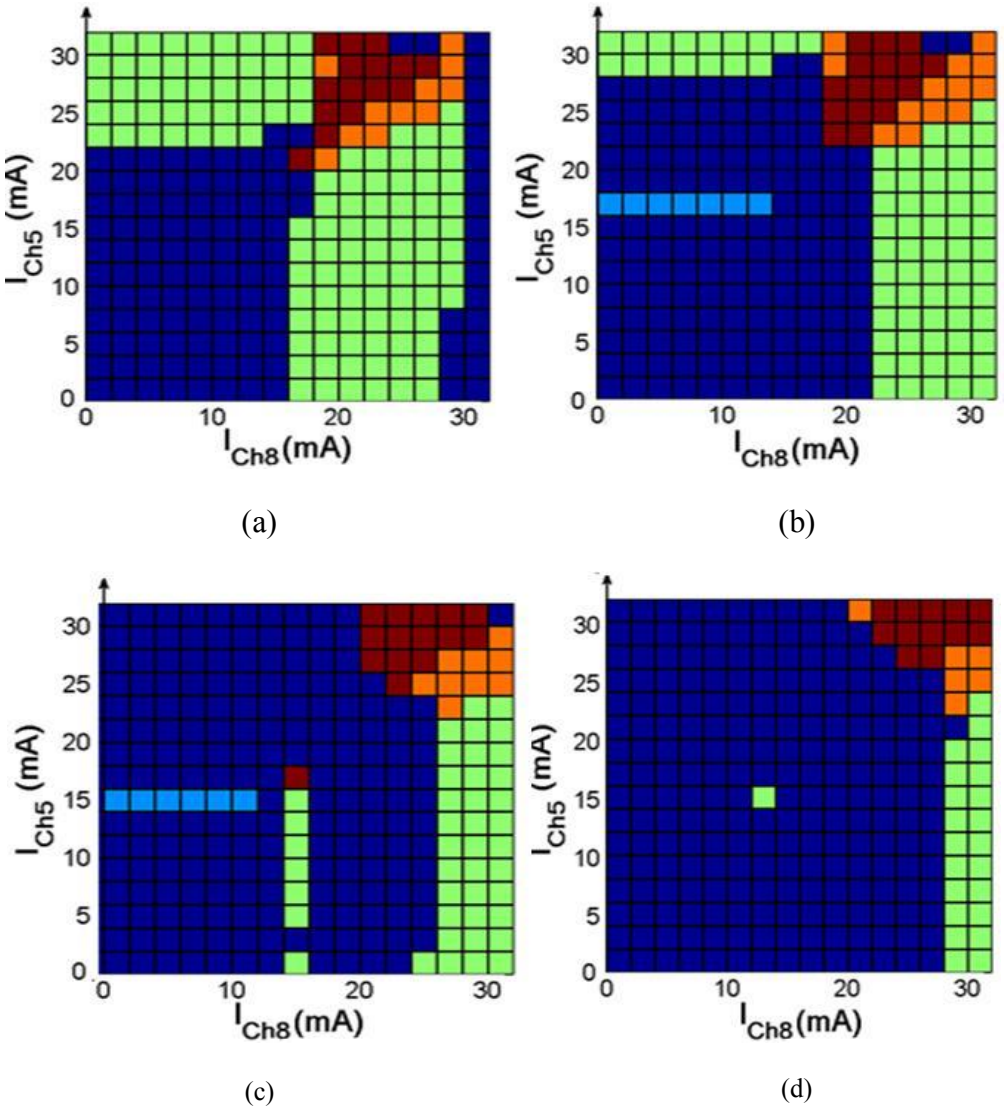

Figure 3.13. Mapping of the single-wavelength (light blue and green) and dual-wavelength (dark red and orange) mode operation regimes of the AWG. Channel 5 and 8 are swept from 0 to 30 mA whilst the boost amplifier is set at 4 fixed bias current levels of 20 mA (a), 22 mA (b), 24 mA (c) and 26 mA (d).

3.4 Linewidth measurements

The linewidth measurements on the AWGL were performed using two different current sources aiming to assess the effect of the electrical noise of the current sources. We have used the following current sources: PRO-8000 current source from ThorLabs (it was named source 1) and LDC-3724B low noise current source from ILX Lightwave (it was named source 2).

Two different tests were developed in this experiment in order to assess the trend of the linewidth. For each test, the channels SOAs were always biased using the source 1, whilst the boost amplifier was biased using both current sources.

First, we biased the channel SOA with a fixed current value while the bias current of boost amplifier is swept from I_{min} to I_{max}. The second test is the other way round. These two tests will also show us the interaction between the bias current of the channels SOAs and of the boost amplifier to achieve the lowest optical linewidth value, which it will be used for a real time wireless video transmission link.

Figure 3.14 and Figure 3.15 shows the recorded and measured optical linewidth of the channels #6, #7 and #8. Biasing the boost amplifier with the source 1, the minimum and maximum achieved optical FWHM (full-width half maximum) linewidth measurement is 336 and 852 KHz. These values correspond to the channel #6 and #8, respectively. When the boost amplifier is biased using the source 2, the minimum and maximum optical FWHM linewidth measurement is 150 and 1452 KHz, which are measured from channel #7 and #8, respectively.

Channel	Linewidth
6	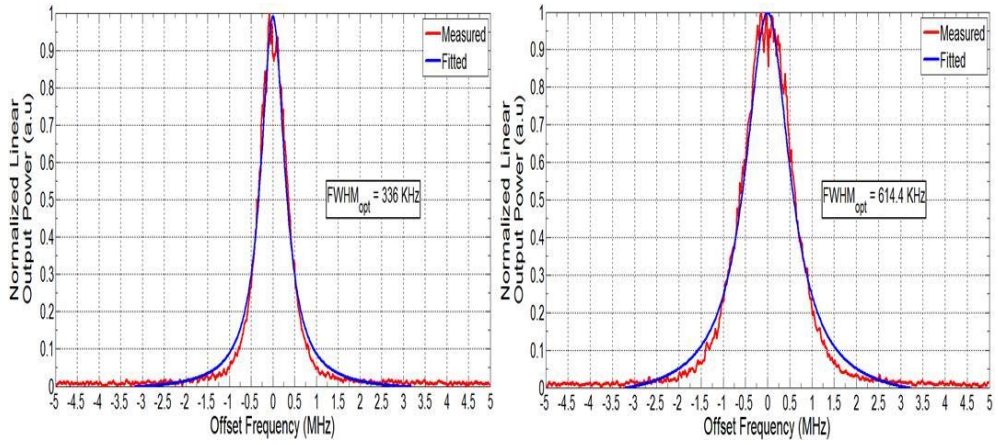
7	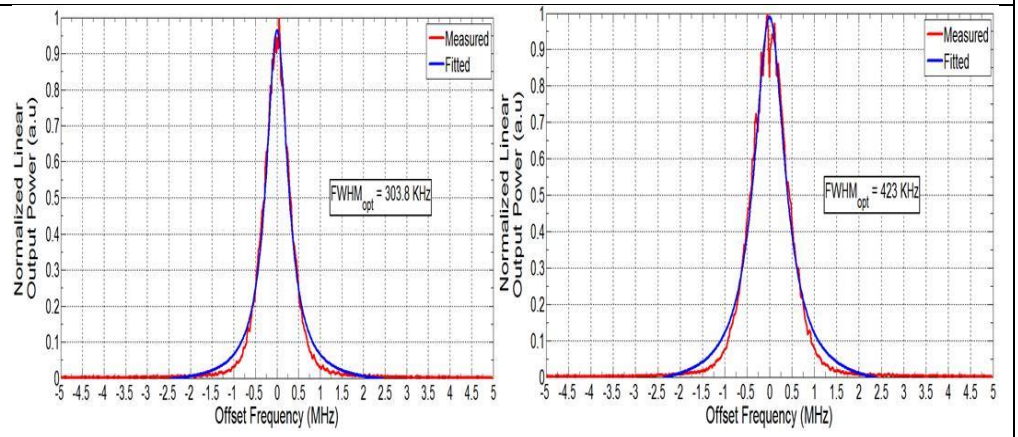
8	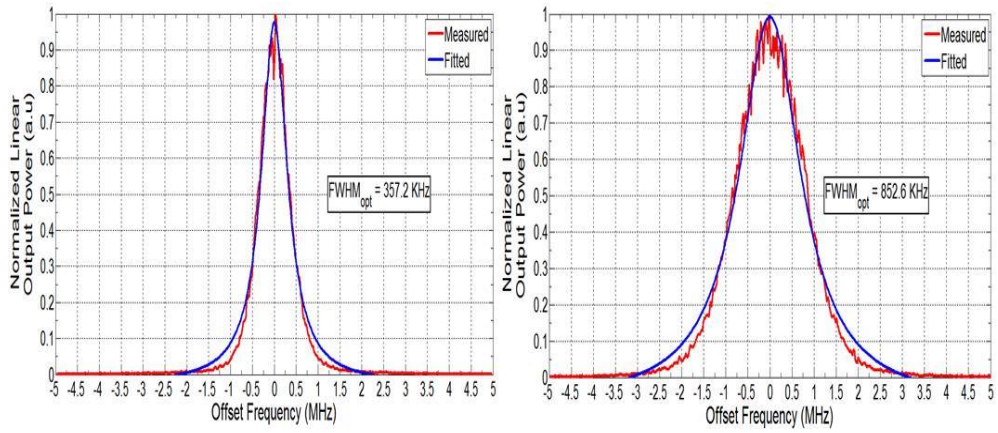

Figure 3.14. Linewidth of the channels 6, #7 and #8 of the AWGL. The bias current of channel SOA is set at fixed current value of 20 mA, whilst the bias current of boost amplifier take two different current values of 42 and 62 mA. Red line represents the recorded measure by the electrical spectrum analyzer while the blue line is the Lorentzian profile fitting. The channel SOA and boost amplifier are biased using the PRO-8000 current source.

Channel	Linewidth
6	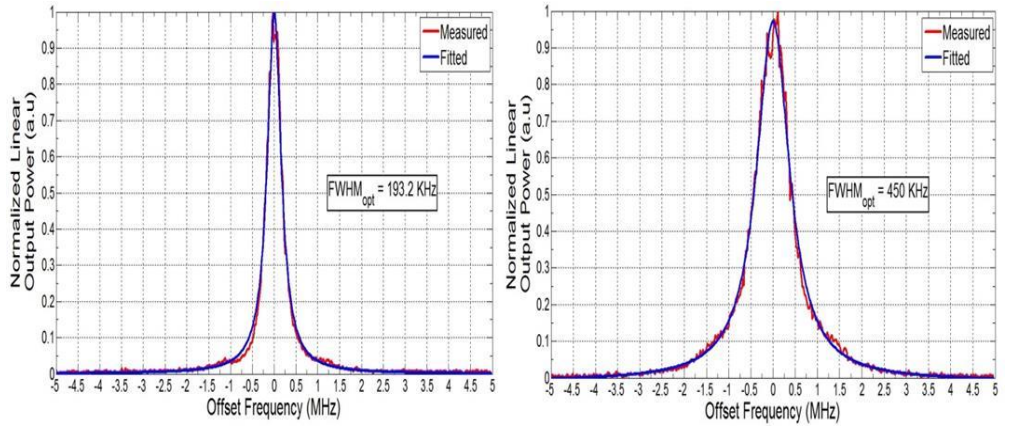
7	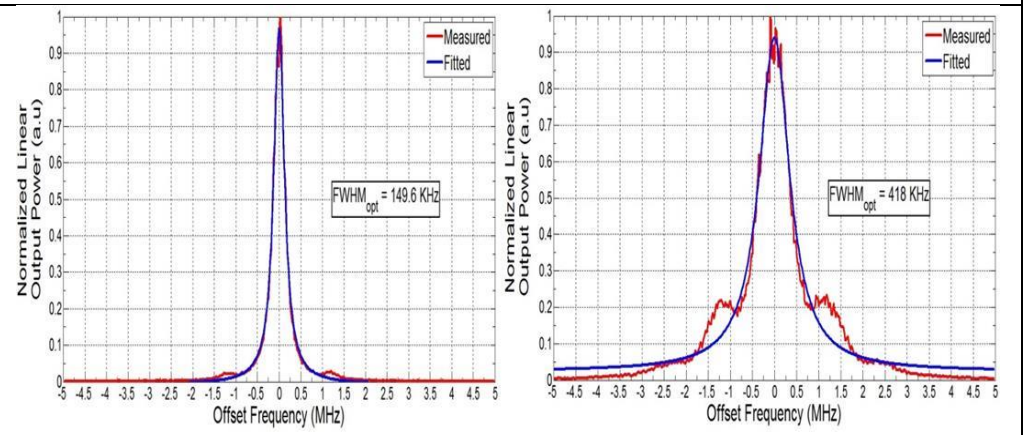
8	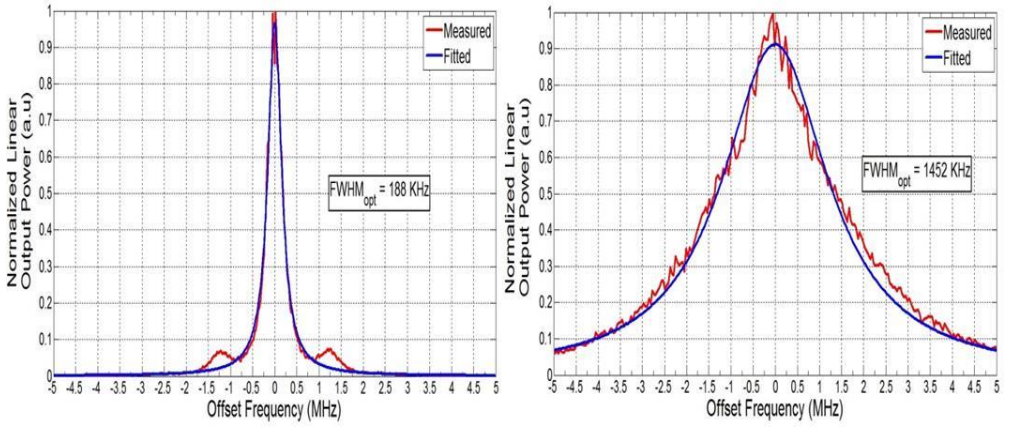

Figure 3.15. Linewidth measurements of 16-channel AWGL. The bias current of channel SOA is set at fixed current value of 20 mA, whilst the bias current of boost amplifier takes two different fixed current values of 42 and 62 mA. Red line represents the recorded measure by the electrical spectrum analyzer while the blue line is the Lorentzian profile fitting. The channel SOA and boost amplifier are biased using the PRO-8000 and LDC-3724B current source, respectively. Satellite peaks are present on each channel.

Figure 3.14 shows that no satellite peak appears in the linewidth of each channel as the source 1 is used. It is due to the fact that the electrical noise added by current source makes that the linewidth become wider and thus, hiding the real linewidth value. However, when the source 2 is used the linewidth value is reduced in a factor around 55%, as shown in Figure 3.15, but also it generates satellite peak on both sides of the maximum peak.

The generated satellite peaks in the measured Lorentzian profile are ripples spaced by the resonance frequency of noise of the source. The magnitude of these satellite peaks is dependent on the damping factor of the laser. Weak damping leads to stronger peaks [4]. However, the full width half maximum (FWHM) linewidth of the spectrum is the same, regardless of these satellite peaks. The trend of the linewidth for different bias settings of the boost amplifier as the channel SOA is set at fixed current value of 20 mA is shown in Figure 3.16.

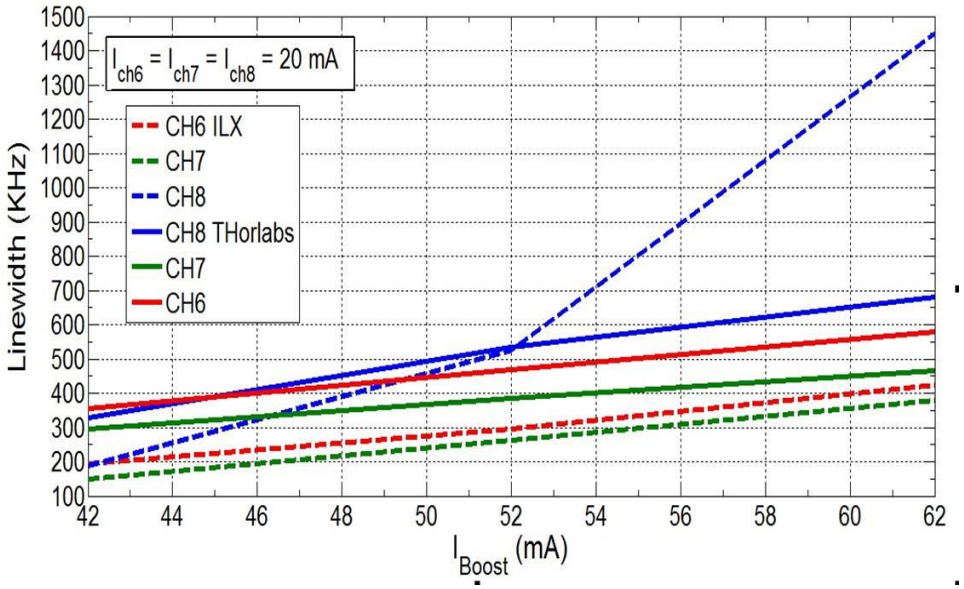

Figure 3.16. Linewidth vs I_{boost} curve. The bias current of the channel SOA is set at 20 mA whilst the current injected into the boost amplifier is swept from 42 to 62 mA in 10 mA steps. (Solid line) The channel SOA and boost amplifier are biased using the PRO-800 current source. (Dashed line) Only the boot amplifier is biased using the LDC-3724B current source.

Figure 3.16 shows the trend of the linewidth and the effect of noise of the current source as the bias current injected into the boost amplifier increases whilst the channel SOA is set at a fixed bias current. This study demonstrates that:

- Higher linewidth values are achieved when the bias current of the boost amplifier is increased as the channel bias point is set at a fixed value.
- Electrical noise can be reduced using an ultra-low noise current source getting the real linewidth value of any laser.

In fact, the best performance is achieved as the device is biased using the low noise current source, achieving a minimum FWHM linewidth less than 200 kHz, with the best result of 150 kHz from the channel 7.

For further analysis on the trend of the linewidth, a second test has been done. The current injected into the channel SOA is swept from 20 to 40 mA using always the source 1, while the boost amplifier is biased at a fixed current value of 50 mA. The boost amplifier is biased using the source 1 and 2.

Figure 3.17 show that the trend of the linewidth is the other way round. It means that, increasing the bias current of the channel SOA as the bias current of the boost amplifier is set at a fixed value, the linewidth can be reduced. The minimum achieved FWHM linewidth under this condition is less than 200 kHz, with the best result of 123 kHz from the channel 7, using the source 2. Therefore, we can state that the bias current of the boost amplifier must be greater that the channel SOA, but also a closer value to this in order to achieve the lowest linewidth value.

When the bias current of the channel #6 and #8 are set at 40 mA, several adjacent optical modes to the main lasing mode appears causing that the linewidth measurement become wider , achieving linewidth values greater than 1 MHz.

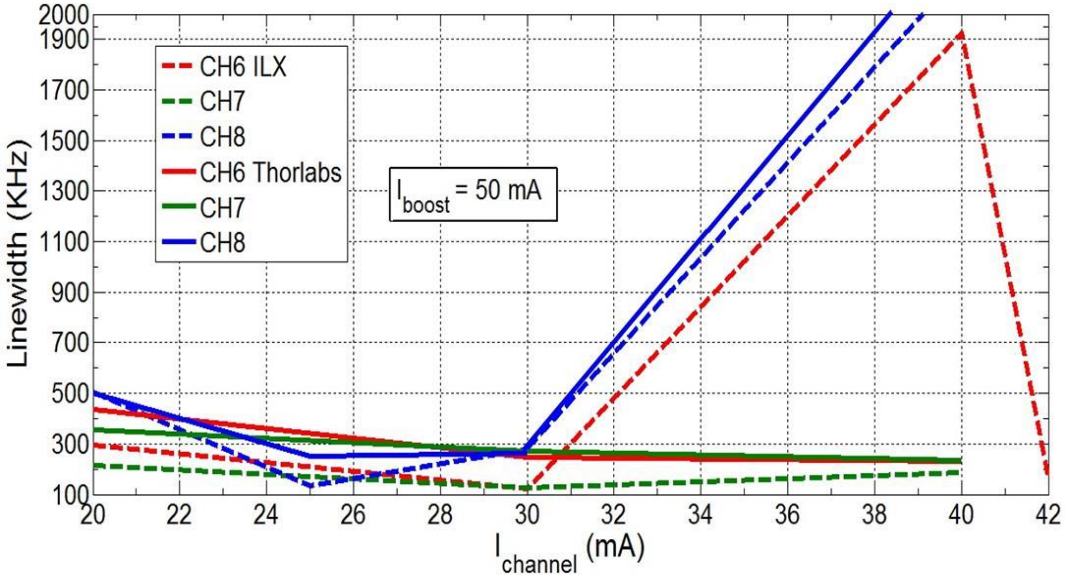

Figure 3.17. Linewidth vs $I_{channel}$ curve. The bias current of the boost amplifier is set at 50 mA whilst the current injected into the channel SOA is swept from 20 to 40 mA in 10 mA steps. (Solid line) The channel SOA and boost amplifier are biased using the PRO-800 current source. (Dashed line) Only the boot amplifier is biased using the LDC-3724B current source.

3.5 Conclusions

In conclusion, we have evaluated and demonstrated the performance of an AWGL for millimeter and Terahertz wave signal generation by optical heterodyning using two optical modes, each from a different AWG channel. The AWG laser has a standard structure, based on as-cleaved facets, and incorporates in the resonator additional components. We have used a Boost SOA to increase the optical power of the dual mode signal.

We demonstrate for the first time to the best of our knowledge the relation between the channel SOA bias currents (I_{ch}) and the Boost SOA bias current (I_{Boost}) to generate a dual-wavelength mode operation regime. We found that the combination of currents where dual-wavelength is establish is narrow..

We also observed lasing on lower and higher FSR orders of the AWG, which means the device is sensitive to changes of the bias current in both channels' SOA and the boost amplifier. Biasing only the boost amplifier with a DC current level greater than its threshold current level and setting the channel SOAs at 0 mA, single optical lasing modes in all FSR orders of the AWG were observed. In order to achieve lasing modes from the upper channels (by geometric location), a DC current level greater than used from the central channels should be used. Therefore, the dual-wavelength mode operation regimes are reduced, since the Fabry-Perot modes of the extended cavity of each channel in the AWG will modify the shape of the emitted wavelength at the device output.

From these results we recommend that it would be advisable that the Boost amplifier is to be located outside the AWG cavity. Furthermore, we have also observed the importance of the FSR spacing, since it needs to be as large as possible in order to increase the achievable frequency difference between the two wavelengths for the optical heterodyne signal.

Moreover, the linewidth of any laser source can be reduced if the electrical noise added by the current source is reduced. Ultra-low noise current sources are suitable for these purposes, which allowing us to achieve a linewidth measurement closer to the real value of the laser linewidth.

In this kind of structure, if the bias current of the boost amplifier is set at a fixed value as the bias current of the channel SOA is swept from I_{min} to a bias current similar to the boost amplifier, a reduction of the measured linewidth value is achieved. While if the bias current of the channel SOA goes above the boost amplifier current and beyond, the laser linewidth become wider.

In comparison with other different structures, the device reported by [5], with a similar linewidth, 150 kHz, was fabricated on the same technological platform as our circuit, but with a different operational principle: using filtered feedback for wavelength locking. Several lasers with extended cavity and linewidth below 100 kHz were reported [6], [7].

3.6 References

[1] L. Chusseau, F. Philippe, P. Viktorovitch and X. Letartre, "Mode competition in a dual-mode quantumdot semiconductor microlaser", *Physical Review Applyed*, Vol. 88, No. 1, 2013.

[2] K. Lawniczuk, R. Piramidowicz, P. Szczepanski, P. J. Williams, M. J. Wale, M. K. Smit, and X. J. M. Leijtens, in Proceedings of the 23rd International Conference on Indium Phosphide and Related Materials (IPRM) (IEEE, 2011).

[3] Guzmán M., Robinson C.; Jimenez, Álvaro; Lawniczuk, Katarzyna; Corradi, Antonio; Leijtens, X aveer J. M.; Bente, Erwin A. J. M.; Carpintero, Guillermo ."Dual wavelength operation of monolithically integrated arrayed waveguide grating lasers for optical heterodyning". Proceedings of the SPIE, Volume 8781, id. 87810F 8 pp. (2013).

[4] L. A. Coldren, S. W. Corzine, and M. L. Mashanovitch, Diode Lasers and Photonic Integrated Circuits. JohnWily & Sons, 2012.

[5] J. Zhao, D. Lenstra, R. Santos, M. Wale, M. Smit, and X. Leijtens, "Feedback phase influence on an integrated filtered-feedback laser," *IEEE Photon. Technol. Lett.*, Vol. 24, No. 23, pp. 2195–2197, 2012.

[6] N. Wang, M. Feng, Z. Feng, M. Y. Lam, L. Gao, B. Chen, A. Q. Liu, Y. H. Tsang, and X. Zhang, "Narrow-linewidth tunable lasers with retro-reflective external cavity," *IEEE Photon. Technol.Lett.*, Vol. 24, No. 18, pp. 1591–1593, 2012.

[7] D. Zhang, J. Zhao, Q. Yang, W. Liu, Y. Fu, C. Li, M. Luo, S. Hu, Q. Hu, and L. Wang, "Compactmems external cavity tunable laser with ultra-narrow linewidth for coherent detection," *Optics Express*, Vol. 20, pp. 19670–19682, 2012.

On-chip multiwavelength AWG laser source

4.1 Multimode Interference reflectors

In the previous chapter we found that including additional elements into an AWG laser using the chip facet as mirrors, it introduces serious limitations in the dual-wavelength signal generation performance. The main problem that we have found is the mode competition that appears in the common arm, when new elements are included to add functionalities on the chip, which must be included within the Fabry-Perot cavity. Thus it would be a great advantage in improving the performance, as well as in adding functionalities to the chip, to use on-chip mirrors to enable a full integrated structure without the need of the cleaved facets.

In the AWG laser structure presented in the previous chapter, as-cleaved mirrors were key elements to define the Fabry-Perot (F-P) resonator. The F-P modes were filtered by the AWG to produce the lasing modes of the structure.

As-cleaved facets present several drawbacks. First of all determine the minimum cavity length to the separation distance between opposite cleaved facets of chip. As this distance cannot be accurately defined, the longitudinal mode spacing cannot be controlled. Most importantly, from a photonic integrated circuit perspective, since the light is emitted from the facets, out of the chip, no light is available on-chip to be further processed on additional components on the chip.

A solution to this problem is on-chip reflectors. Several on-chip reflectors have been used and reported, such as deeply etched DBR mirrors [1], [2] and Sagnac loop reflectors [3], [4]. The main advantage of on-chip reflectors is that can be positioned at any location within the chip defining resonator structures with lithographic accuracy.

Recently, a novel on-chip reflector for photonic integrated circuits, known as multimode interference reflector (MIR), has been demonstrated developing Fabry-Perot laser structures [5].

This reflector is fabricated using deeply-etched waveguide structure in any integration process flow that allows deeply-etched waveguides without the need for extra processing steps. These reflectors have relatively small size, and are therefore very promising reflection building blocks for large-scale photonic integration.

MIR structures derive from a standard multimode interference (MMI) coupler, in which deeply etched 45° mirrors at suitable locations reflect back the light by total internal reflection. The reflection to transmission ratio of the MIRs can be chosen by taking into account both the application and the physical geometry of the MIR [6].

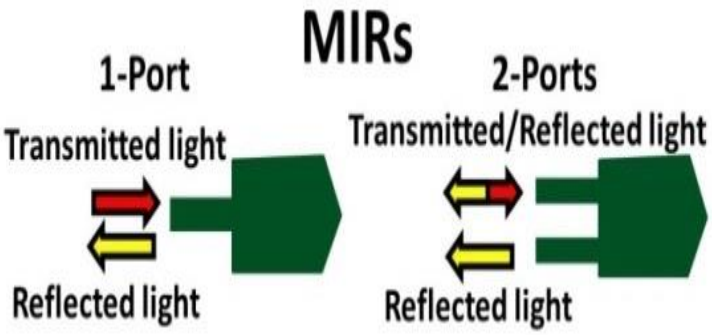

Figure 4.1. 1-port (left) and 2-ports (right) MIRs

There are different versions of these mirrors, being the most common those shown in Figure 4.1, differentiated by the number of access ports in the MMI region. The first structure that we will describe is the 1-port MIR (also known as 1x0 MIR), in which there is only one access port. All the incoming light at this port is reflected back, constituting a mirror with 100% reflectivity.

This mirror structure drawback is that it does not provide any light output. This problem is addressed by the alternative 2-port MIR (2x0 MIR), based in a 2x2 MMI structure. The incoming light enters through one port, known as reflection port, and is split in two halves. One half of the light is reflected back at the reflection port, while the other half is reflected to another port (known as transmission port).

The reflection achieved by this new building block is about 50% The main advantage is that this structure now offers an output port enabling laser structures on-chip with output on a waveguide for further processing on-chip. Due to its importance, we present in Figure 4.2 a 3D schematic and a SEM picture showing the top view of a 2-port MIR. In general, the width of MIR reflectors is chosen by considering the size and fabrication limitations, for example, the wider the width, the lower the device loss, but longer the device, and the minimum lithographical gap width also determines the minimum width of the MMI reflector.

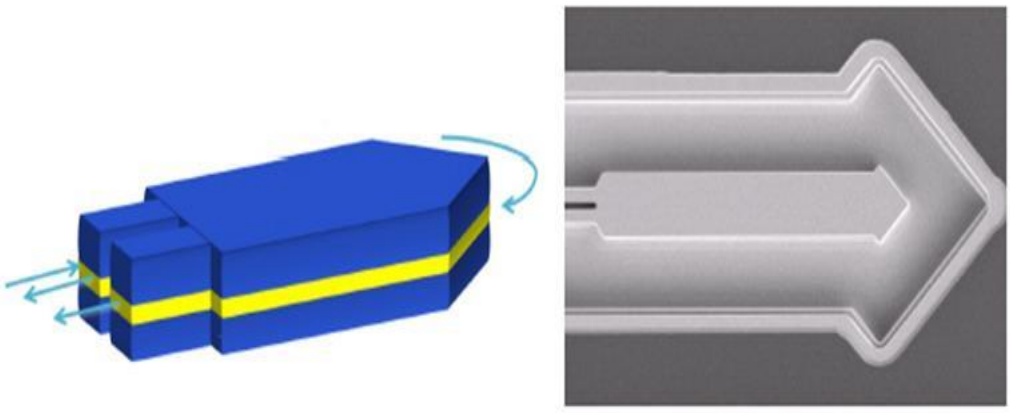

Figure 4.2. 3D schematic drawing of a 2-port MIR, and the corresponding SEM picture. To obtain highly reflective mirrors the device has to be deeply etched with vertical sidewalls

4.2 Linear AWGL with multimode interference reflectors

In this section we present our novel design for an AWG laser based on replacing the facet mirrors which for the Fabry-Perot cavity by on-chip reflectors.

The designed device consists of an AWG with 4 channels, one SOA per channel labelled SOA N (with N = 1 to 4) and one common output. In addition, two of the channels implement electro-optical phase modulators (EOPMs), as shown in Figure 4.3 (a). The electro-optical phase modulators are intended for fine tuning the lasing wavelength

An important feature, in order to compare the results from the cleaved facets structure, is the inclusion of a Boost SOA, located after the on-chip mirror at the AWG's common output. All the SOAs used both for the channel selection and for the boost amplifier are 400 μm long. The lengths of the EOPMs are 1000 μm The AWG central wavelength is λ = 1550 nm, the channel spacing $\Delta\lambda_{ch}$ = 0.961 nm (ΔF_{ch} = 120 GHz) and the FSR is 5.61 nm (700 GHz). From Eq. 2.7, the lasing mode spacing ΔF, generated by the longer laser cavity is around 8.8 GHz whilst for the shorter laser cavity is around 12 GHz.

The device was fabricated using InP-based active and passive integration technology within JePPIX multi-project wafer run using COBRA generic foundry process platform. A microscope photograph of on-chip structure 4-channels AWGL is shown in Figure 4.3 (b). In order to avoid reflections at the cleaved facets we have:

- Used 7º angled waveguides at the facets.
- Use anti-reflective (AR) coating on the cleaved facets.

Both are key to avoid creating undesired lasing cavity between the cleaved facets of the chip and the transmission port of each MIR which would result affecting the behaviour of each separate channel and the boost amplifier of the AWGL.

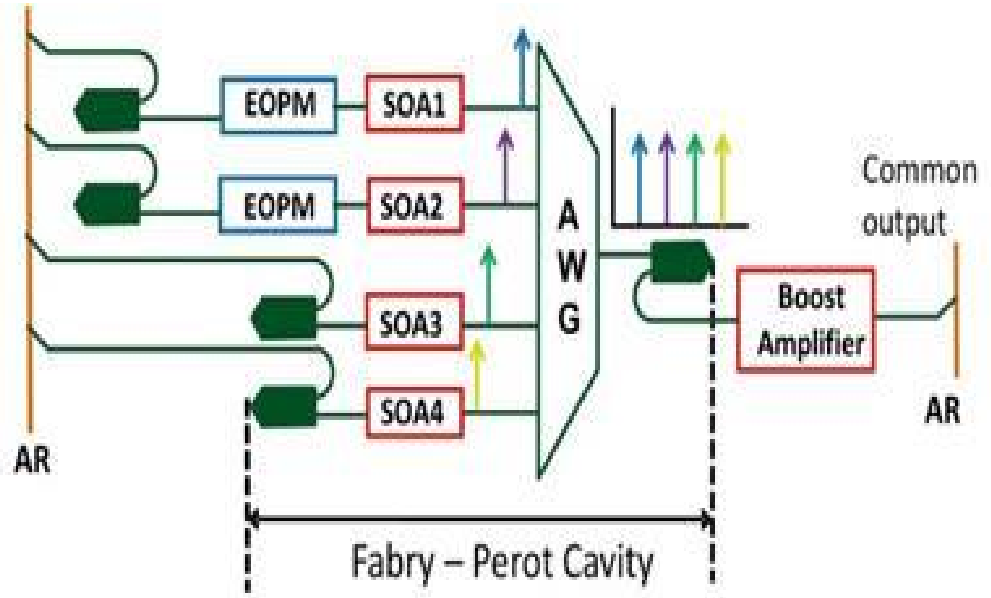

(a)

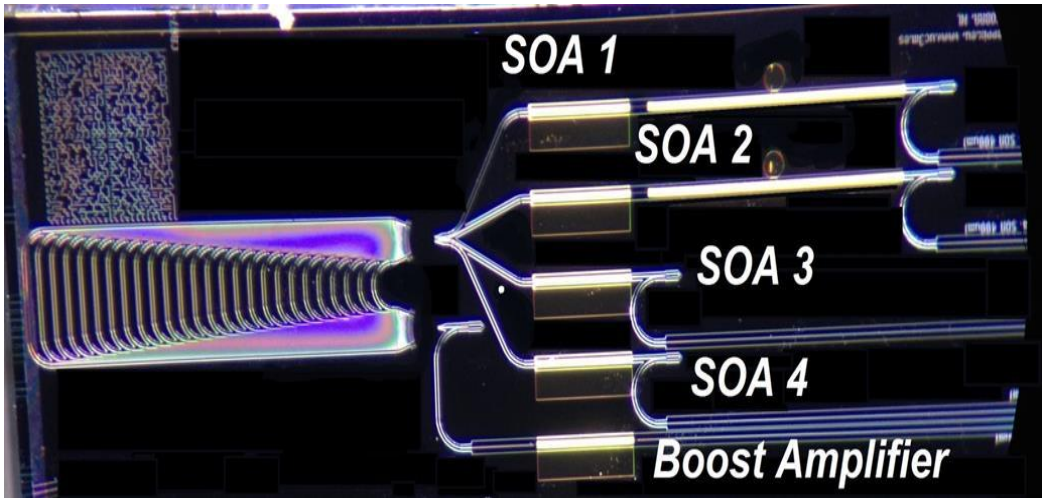

(b)

Figure 4.3. (a) Schematic of 4-channels AWGL. The cleaved facets of the chip use an anti-reflective (AR) coating in order to avoid undesirable reflections. (b) Microscope photograph of cleaved facet structure of 4-channels AWGL.

As well as in the first device, a boost amplifier is placed in the output common waveguide of the chip in order to increase the output optical power. However, it is very

important note that in this occasion the boost amplifier is placed outside the lasing cavity thanks to the MIR structures, which even allow us to have a precisely control of the total cavity length.

In this device a taper connected to the input waveguides and to the waveguides of the array of the AWG on both FPR regions is used. This optical component allows us to avoid the reflections caused by the gap between the waveguides located on the FPR region, by reducing this gap. Doing this, the performance of the device has been improved regarding the drawback that the first device had when only the boost amplifier was biased.

4.3 Measurements of LI curves and optical spectrum characteristics

This device is characterized in the same probe station that we used for the previous design. A lensed fiber is used to couple the light out from the chip, carrying it to the measurement devices, as shown in in Figure 4.4 (a). For this laser, with an angled facet, the lensed fiber has to be tilted with respect to the cleaved facet of the chip at a 23º angle. An optical isolator located at the other end of the lensed fiber in order to avoid and reduce any undesired back-reflections is used.

The block diagram of the experimental setup isshown in Figure 4.4 (b).

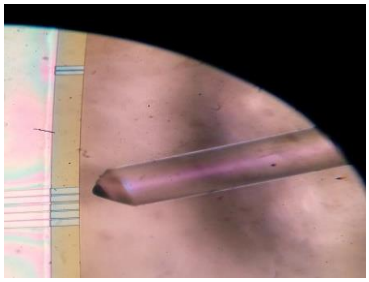

(a)

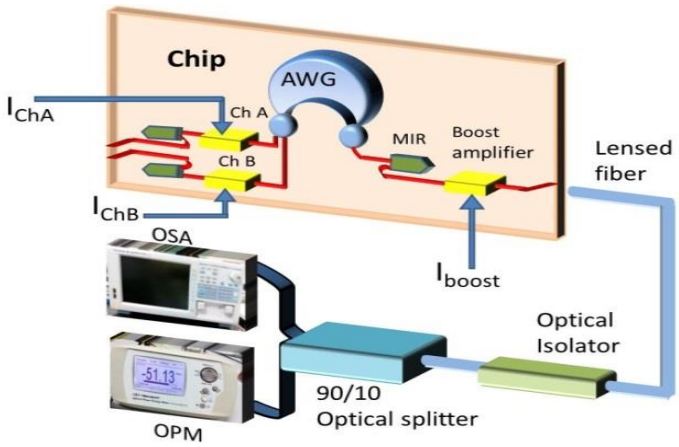

(c)

Figure 4.4. (a) Microscope photograph of how the lensed fiber is placed and aligned close to the cleaved facet of the chip. (c) General block diagram of the arranged setup for the L-I curve and optical spectrum measurements.

4.3.1 Boost amplifier characteristics

The first measurement that we have performed with this device aims to determine the existence of reflections when the Boost amplifier is biased. Only the boost amplifier is biased whilst all of the channel SOA's are not biased. The resulting Light-Current characteristic curve when the current is swept from 0 to 120 mA in 2 mA steps, as well as the mapping of the optical power spectrum, are shown in Figure 4.5.

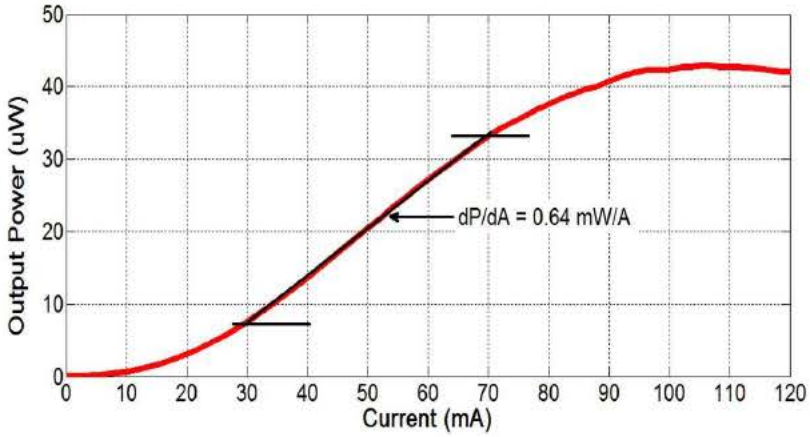

(a)

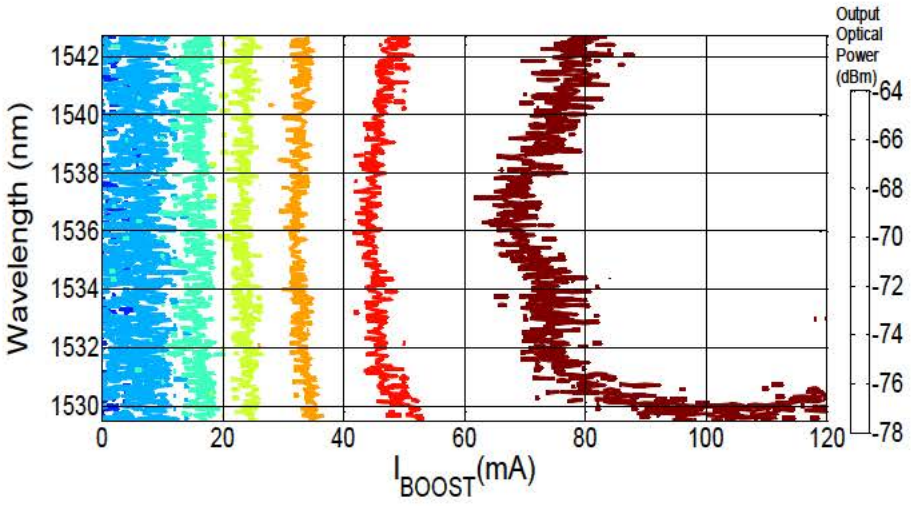

(b)

Figure 4.5. (a) LI curve of the boost amplifier. (b) Detected output optical spectrum at the common output of the chip. Broad spectrum beacuase of the spontaneous emission is achieved. No lasing modes at the chip output are generated.

Figure 4.5 (a) demonstrates that there is no Fabry-Perot cavity between the cleaved facet of the chip and the transmission port of the MIR located at the common waveguide of the AWG, as well we can see that there is no threshold current. Therefore, lasing modes at the common output waveguide of the chip are not generated, as shown in Figure 4.5 (b).

Furthermore, its optical response shows a broad spectrum characteristic of the spontaneous emission noise without lasing. This result also shows that the AR coating and the angled waveguide located at the common output of the chip help it to enhance the performance of the AWG laser.

4.3.2 Individual channel SOA characteristic

The next step in the characterization is to inject current into the Channel SOAs to trace the Light-Current characteristic curve. The boost amplifier has to be set at some bias. We have trace the curve for one of the channels (Channel 1) that includes electro-optic phase modulator (EOPM) and also one of the channels without EOPM (Channel 3).

When the boost amplifier is unbiased, the Light-Current characteristic curve is shown in Figure 4.6, when the current on the Channel SOA is swept from 0 to 120 mA, in 2 mA steps. The threshold current level for each channel is shown on the figure, resulting in similar values for all the channels independent on weather include or not an EOPM. The maximum optical output power around 0.3 mW is achieved as the channel 2 and 4 are biased with a fixed current value of 120 mA.

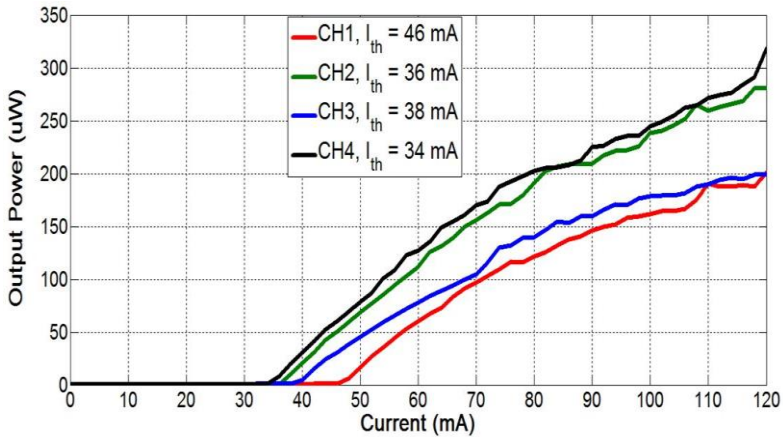

Figure 4.6. L-I characteristic curve of each individual channel. The outgoing light is collected at each individual output port.

The mapping of the output optical spectrum of each individual channel is shown in Figure 4.7, showing lasing modes at different FSR orders. From this measurement we found that the experimental free spectral range is5.59 nm (698 GHz), which is a closer value to the design target.

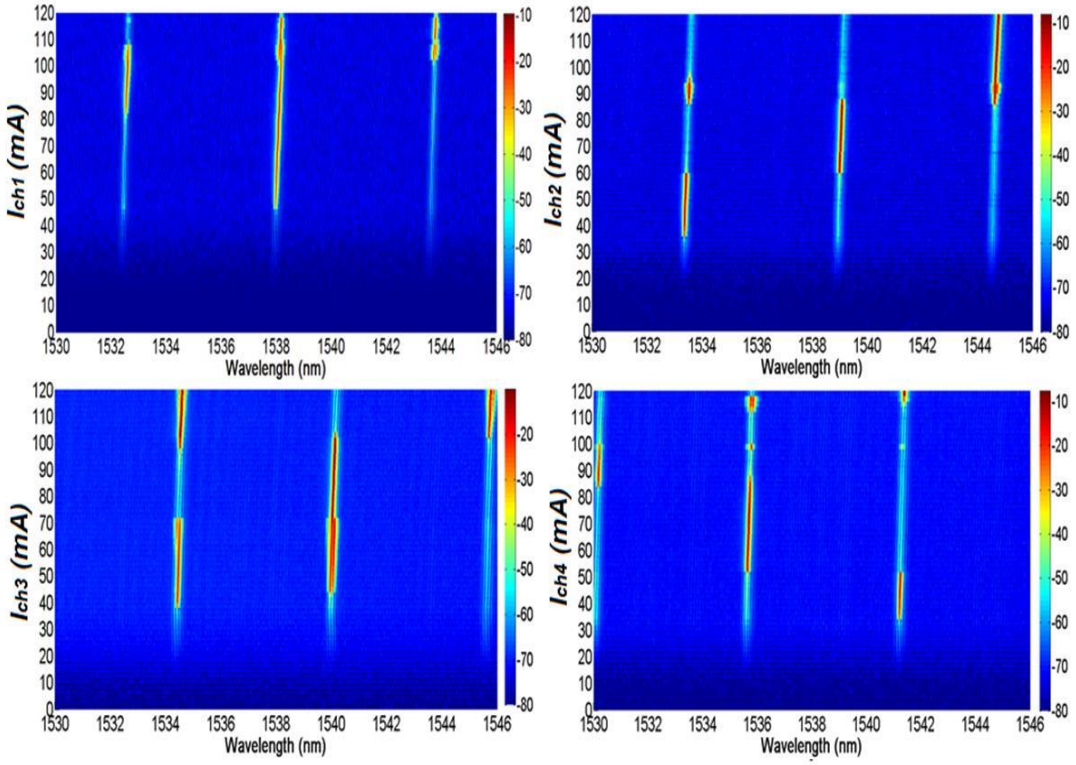

Figure 4.7. Detected optical spectrum of each individual channel measured at their output port.

We observe mode hops among different FSR orders as the channel SOA bias current is increased, as well as current values in which lasing takes place on different FSR orders simultaneously. On this device we have adjusted the channel SOAs bias currents in order to achieve the same optical power on each lasing mode, balancing the different losses at each channel.

Figure 4.8 shows the optical spectrum from the different channels, injecting 70 mA for the channels #1, # 2 and #3, and 50 mA at channel #4, achieving a peak amplitude value of -11.78, -11.03, -10.89 and -12.97 dB for each individual lasing mode. Each lasing mode was recorded and measured at the output waveguide of each individual channel. Individually biasing each channel we observe that the minimum and maximum frequency spacing that we can potentially achieved between wavelengths is 112 GHz for adjacent channels and 390 GHz for the furthest channels.

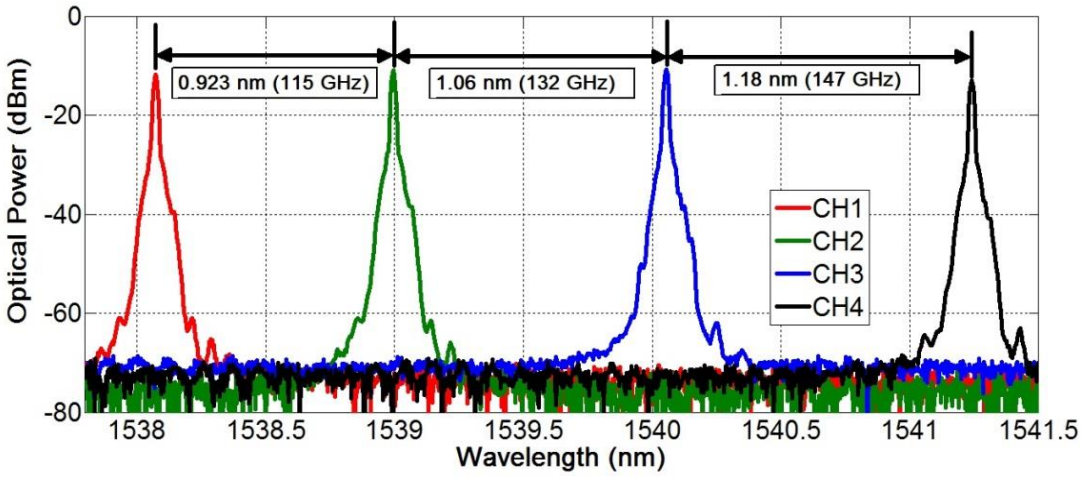

Figure 4.8. Optical spectrum showing lasing modes of each individual channel. The frequency spacing between two adjacent channels is 115, 132 and 147 GHz of channel 1-2, channel 2-3 and channel 3-4, respectively.

We now turn to bias two SOAs simultaneously. The channel SOA is swept from 0 to 100 mA, in 2 mA steps, whilst the boost SOA is set at five fixed values, from 0 to 40 mA in 10 mA steps. Measuring at both outputs, from the channel and the common

output waveguide, we have found that when the bias current injected into the Boost SOA is 15 mA, the optical power at the channel waveguide output port is the same as the optical power in the common output. Thus at this current level, the Boost SOA is transparent.

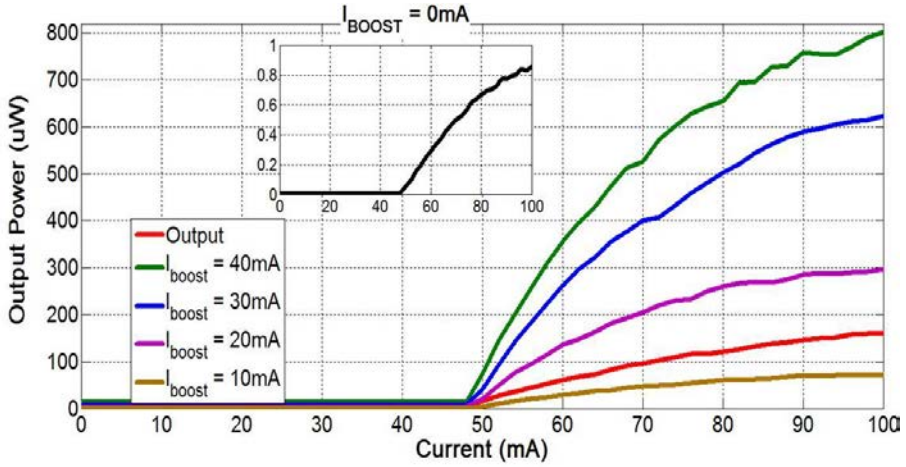

(a)

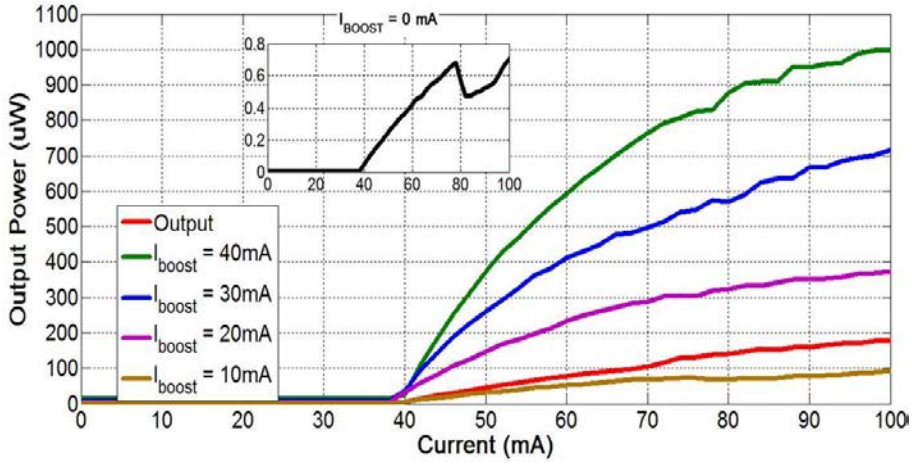

(b)

Figure 4.9. L-I characteristic curve of channel #1 (a) and channel #3 (b). The bias current injected into each channel is swept from 0 to 100 mA. For both cases the boost amplifier is biased at five different fixed current values of 0, 10, 20, 30 and 40 mA.

On Figure 4.9 (a) we present the Light-Current results from Channel 1, which includes an EOPM, while the results on Figure 4.9 (b) correspond to Channel 3, which does not include EOPM. It is worth to mention that the main difference that we observe

is the 10 mA current difference on the threshold current. The maximum output optical power saturates at high currents, being the maximum power 0.8 mW and 1 mW at channels 1 and 3 respectively, when the boost amplifier is biased at 40 mA. This value is higher than the cleaved facet device despite the fact that the SOAs lengths of all the channels of this device are shorter.

An important experiment was to study the effect of the EOPM. We expect that the changes in the refractive index of the EOPM allow tuning of the lasing wavelength. The initial bias conditions are 70 mA on the Channel SOA and 20 mA on the Boost amplifier while we sweep the EOPM reverse voltage from 0 to -3.5 V. Figure 4.10 (a) and (b) shows the optical spectrum, from which we observe that:

- For small (< 1 V) voltage variations of the reverse bias voltage, fine tuning of the lasing wavelength can be achieved. Figure 4.11 (a) shows the tuning of the lasing wavelength around 1536 nm. When EOPM bias voltage goes from 0 to -1V, a minimum and maximum tuning range of 0.6 and 2.4 GHz/V was founded.
- For larger variations (>1V) we achieve a hop of the lasing wavelength to a lower FSR order of the AWG. We observe a jump from a lasing mode around 1536 nm to 1530 nm. The EOPM can have an important function, allowing us to force that all the channels emit in the same FSR order. Figure 4.14 shows a case in which the channels 1 and 2 generate lasing modes at different FSR orders when the EOPMs are set at 0 V. As the reverse bias voltage of the EOPM of channel 2 is set at 1 V, a new lasing mode appears in the same FSR order of the lasing mode of channel 1.

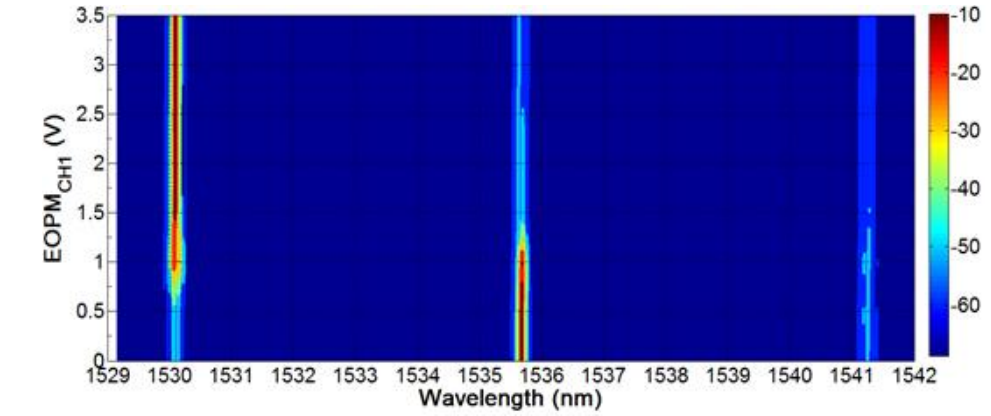

(a)

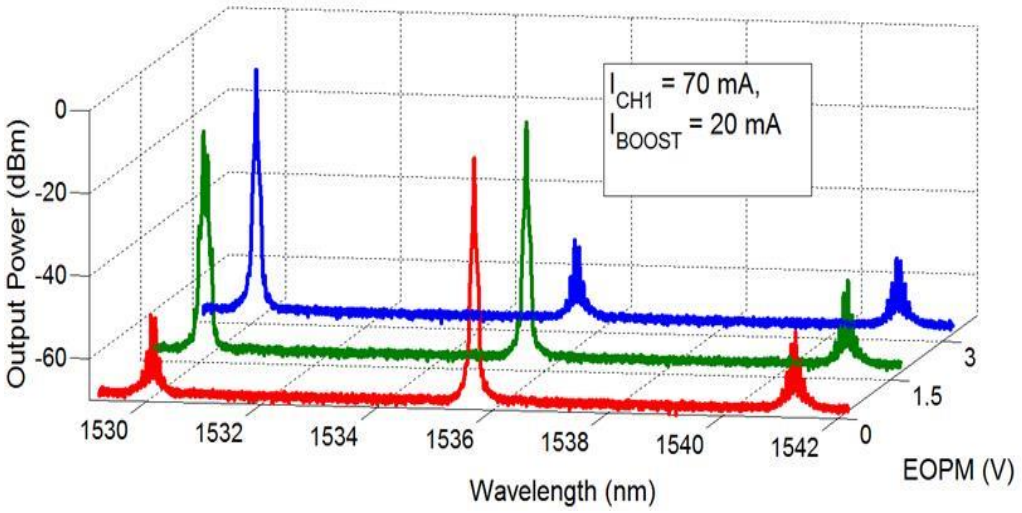

(b)

Figure 4.10. (a) Mapping of the detected output optical power spectrum at the common output of the chip. The channel 1 and boost amplifier are biased with a fixed current value of 70 and 20 mA, respectively. While the EOPM's reverse bias voltage of channel 1 is swept from 0 to 3.5 V. (b) Output optical spectrum as EOPM's reverse bias voltage is set at 0, 1.5 and 3 V.

The change of the refractive index of the EOPM makes that the lasing cavity becomes longer, and thus, leading to the generation of lasing modes with a lower frequency spacing. Some of these lasing modes enter in the channel bandpass of the AWG, being amplified by the gain section of the channel. A competition between these lasing modes in order to establish only one lasing mode into the channel passband of the AWG is yielded, as shown in Figure 4.11 (b).

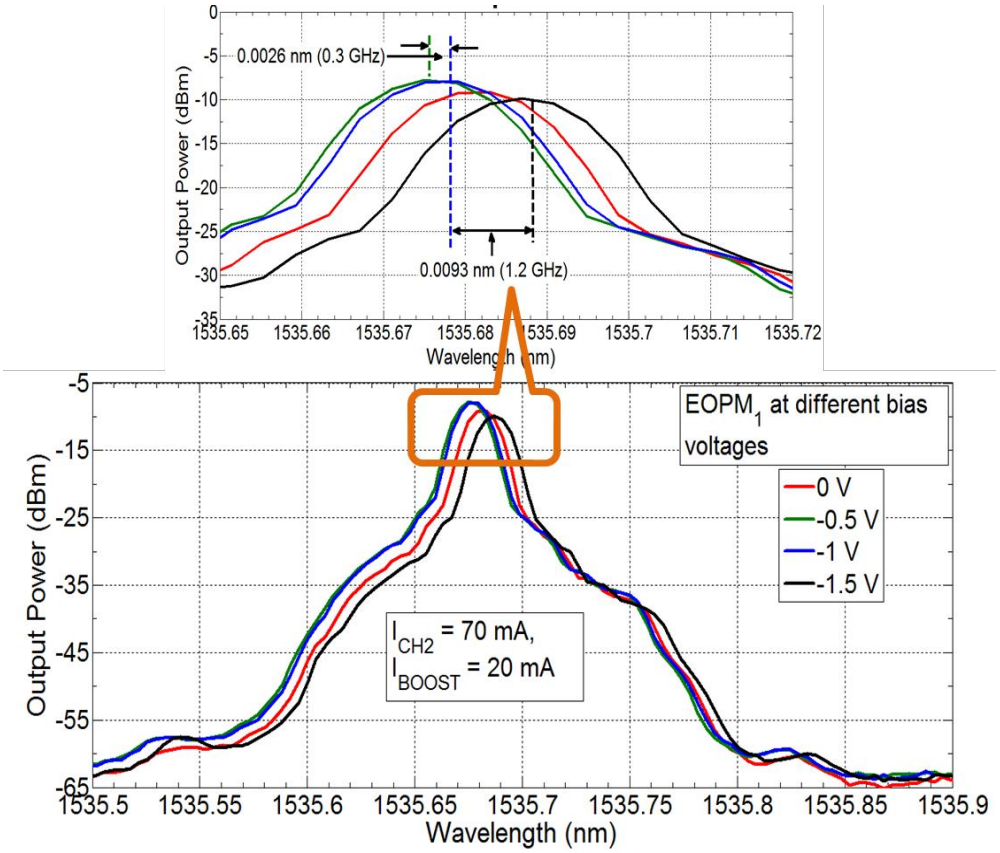

(a)

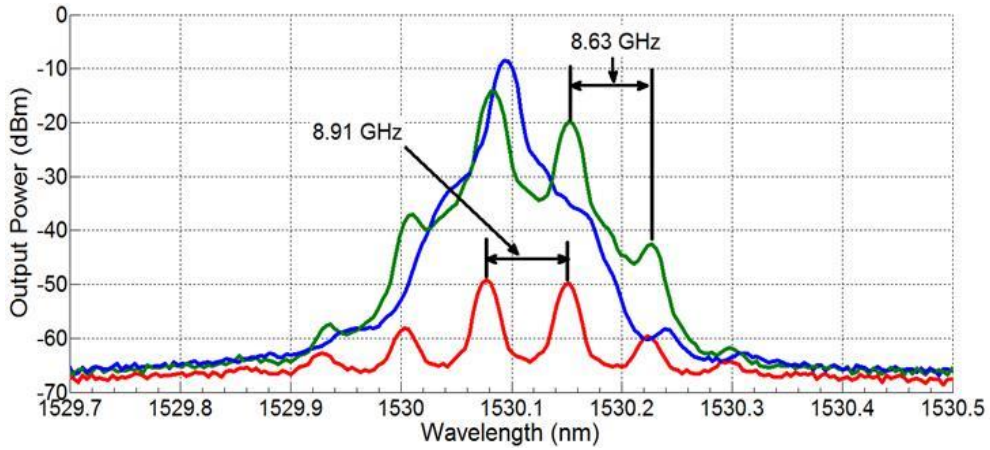

(b)

Figure 4.11. (a) Output optical spectrum as EOPM's reverse bias voltage is swept from 0 to 3V. (d) Zoom in on the lasing mode around 1530 nm as EOPM's reverse bias voltage is set at 0, 1.5 and 3 V reverse bias voltage

4.4 Dual-wavelength mode operation

After having characterized each single channel, the next step is set a dual-wavelength mode of operation biasing two channels simultaneously. This section presents these results.

For optical heterodyne signal, we have selected two channels that generate a frequency spacing corresponding to twice the channel spacing of two adjacent channels. For this scenario, the selected channels were #1 and #3. Channel #1 bias current is set at a fixed current value of 74 mA whilst the channel 3 (I_{th} = 38 mA) bias current is swept from 42 to 84 mA in 2 mA steps.

Channel #1 EOPM reverse bias voltage is set at 0 V, and the Boost amplifier is set at two fixed values, 30 mA, shown in Figure 4.12 (a) and 40 mA, shown in Figure 4.12 (b). Both optical spectrums are similar, despite the fact that the boost amplifier is biased at different current values, showing a frequency spacing of about 238.6 GHz.

This is an important demonstration showing that the Boost amplifier does not influence the optical spectrum, and the dual-wavelength mode of operation is maintained.

An extended map of the dual-wavelength mode operation regimes where two channels are selected is shown in Figure 4.13, demonstrating that the dual-wavelength mode operation regimes of this device are wider than the cleaved-facets AWGL. The boost amplifier, placed outside of the lasing cavity, fulfils its function to just amplify the optical signal.

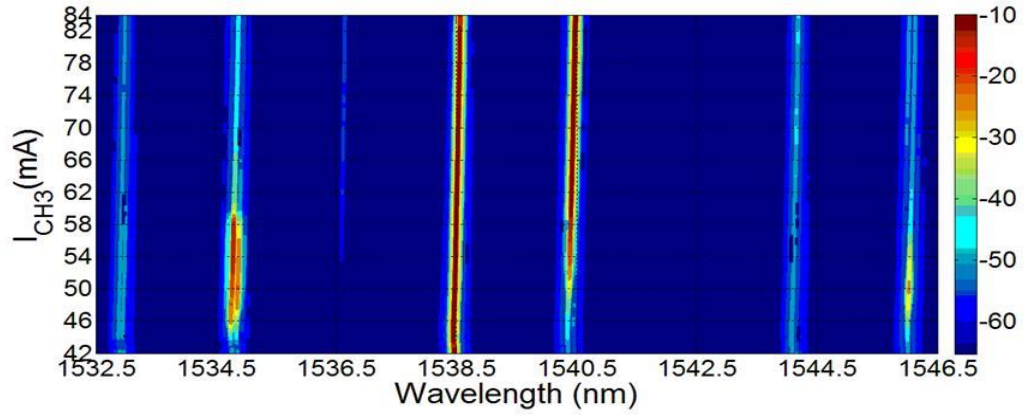

(a)

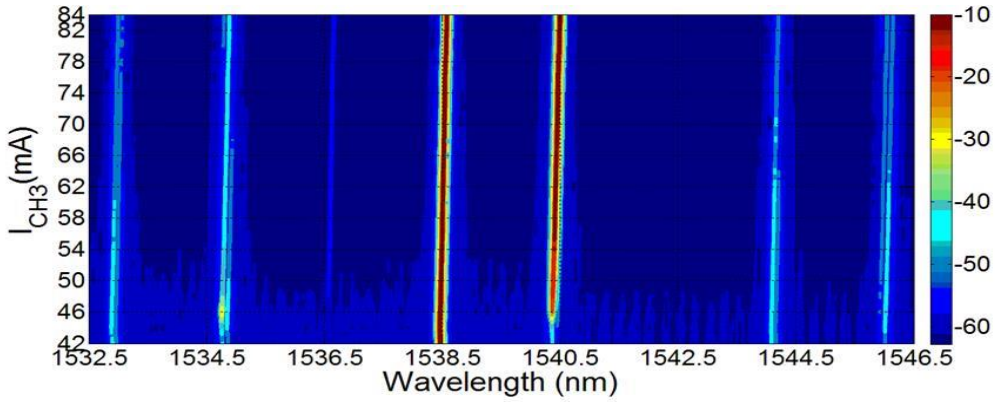

(b)

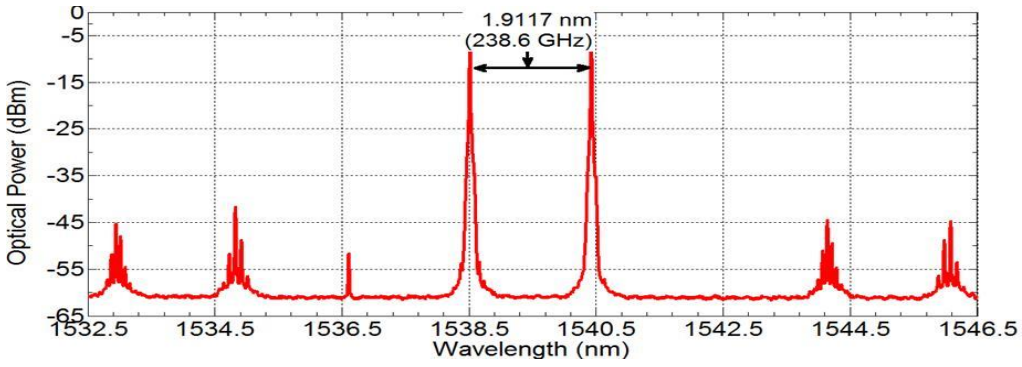

(c)

Figure 4.12. Detected output optical power spectrum at the common output of the chip as the channel 1 is biased at fixed value of 74 mA. The bias current of the channel 3 is swept from 42 and 84 mA, in 2 mA steps. The boost amplifier is set at two different fixed values of 30 mA (a) and 40 mA (b). (c) Optical spectrum of dual-wavelength mode operation, channel 3 and boost amplifier are biased at 62 and 40 mA.

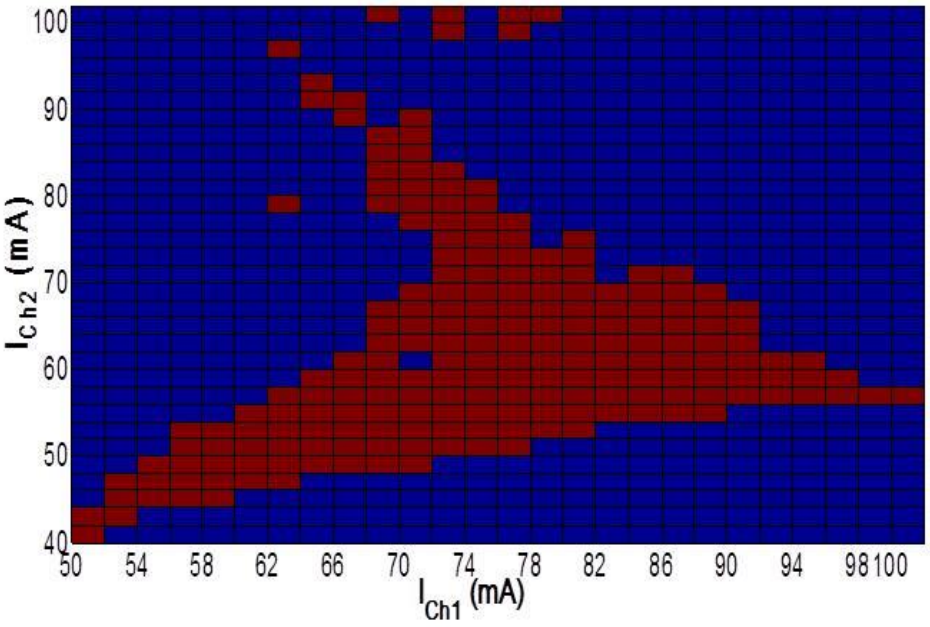

(a)

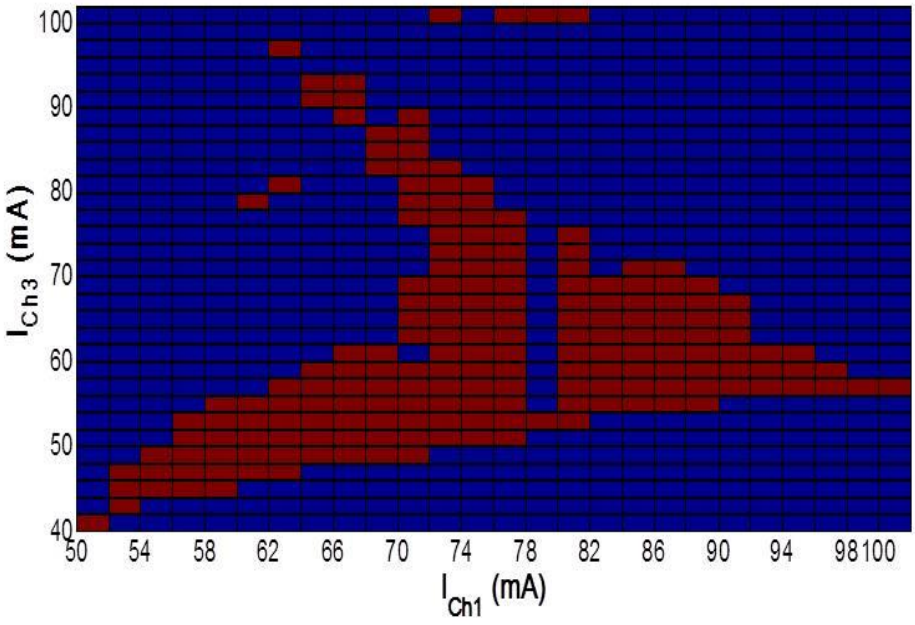

(b)

Figure 4.13. Mapping of dual-wavelength operation regimes. The peak diiference between the two lasing modes is ≤ 3 dB. The boost amplifier is biased at 30 mA for both cases.

Figure 4.14 shows the importance of having an EOPM within the Fabry-Perot lasing cavity in order to achieve a dual-wavelength operation regime, pushing the lasing

wavelength located at a higher or lower FSR order to emit in the same FSR order where the other lasing wavelength is.

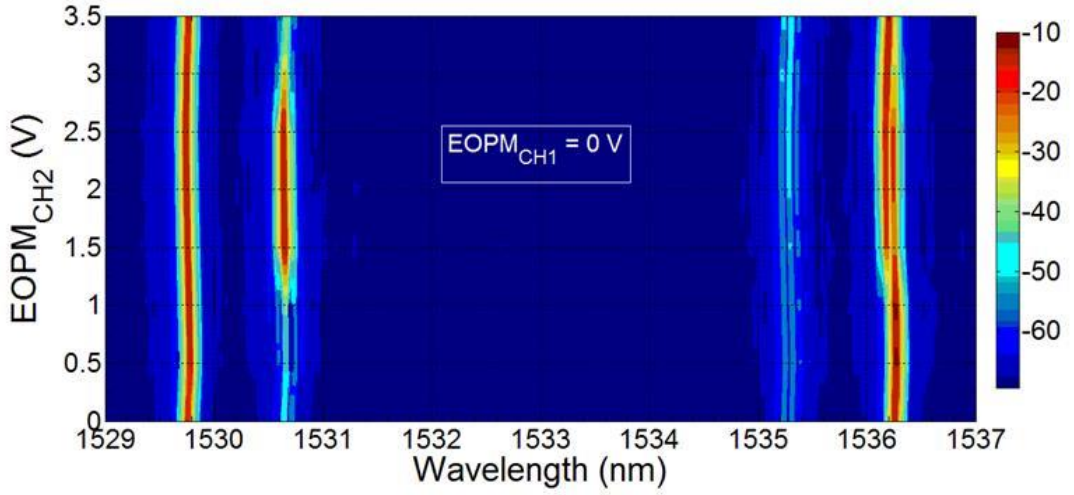

Figure 4.14. Optical spectrum of two independent channels generating lasing modes at different FSR orders. The EOPM of channel 1 is set at 0 V as the EOPM of channel 2 is swept from 0 to -3.5 V. The channel 1 and 2 are biased at 60 mA whilst the boost amplifier is biased at 20 mA.

From Figure 4.15, the channel 1 and 2 are biased at 60 mA, simultaneously. The boost amplifier and the EOPM of channel 1 are set at 20 mA and -1 V, respectively. The EOPM 2 reverse bias voltage is swept from 0 to -3.5 V. The dual-wavelength operation is achieved, even though the EOPM 2 is set at 0 V, however the lasing wavelength of channel #2 located at 1530.65 nm has some adjacent lasing modes, as shown in Figure 4.15 (bottom). While the reverse bias voltage of EOPM 2 increased up to -1V, only one strong lasing mode is kept into the channel passband of the AWG. The peak difference between the lasing modes is about 0.2 dB. In fact, if the voltage injected into the EOPM 2 goes on increasing up to -3 V, the lasing mode will get higher peak amplitude giving as result that the peak difference is about 3.5 dB. Therefore, using the EOPMs a reduction of the peak difference between the lasing modes in dual-wavelength mode operation can be achieved.

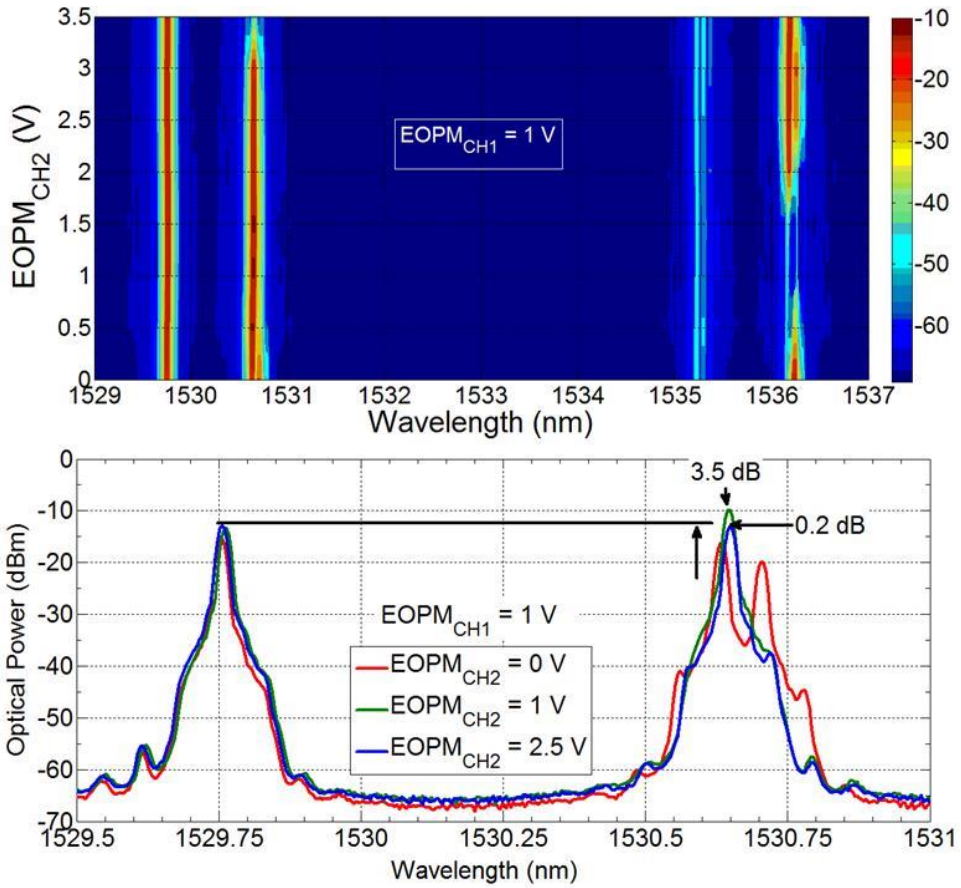

Figure 4.15. Optical spectrum of two independent channels generating lasing modes at different FSR orders. The EOPM of channel 1 is set at -1 V as the EOPM of channel 2 is swept from 0 to -3.5 V. The channel 1 and 2 are biased at 60 mA whilst the boost amplifier is biased at 20 mA. (bottom) Zoom in on the optical spectrum (top) of channel 1 and 2 as EOPM 2 is set at different reverse bias voltage.

This study demonstrates that the EOPM helps to push the lasing wavelength into the channel passband increasing the SMSR between the main lasing wavelength and its adjacent ones through a fine tuning of the EOPM reverse bias voltage. Furthermore, it also allows us to reduce or increase the amplitude difference between both lasing wavelengths.

4.5 Linewidth measurements

The linewidth measurements performed on the on-chip AWGL are developed using the current source PRO-8000 from ThorLabs. As we studied in chapter 3, we are aiming to assess the trend of the laser linewidth in this structure. Therefore, two different experiments are developed. The linewidth measurement results are shown in Figure 4.16 and Figure 4.17, which demonstrate that:

- The laser linewidth value decreases as the boost amplifier bias current increases, while the bias current of the channel SOA is set at a fixed value. Furthermore, the laser linewidth becomes narrower as the bias current of boost amplifier goes above the channel SOA bias current.
- The laser linewidth value increases as the channel SOA's bias current increases, achieving a wider laser linewidth when the bias current of boost amplifier goes above the channel SOA bias current.

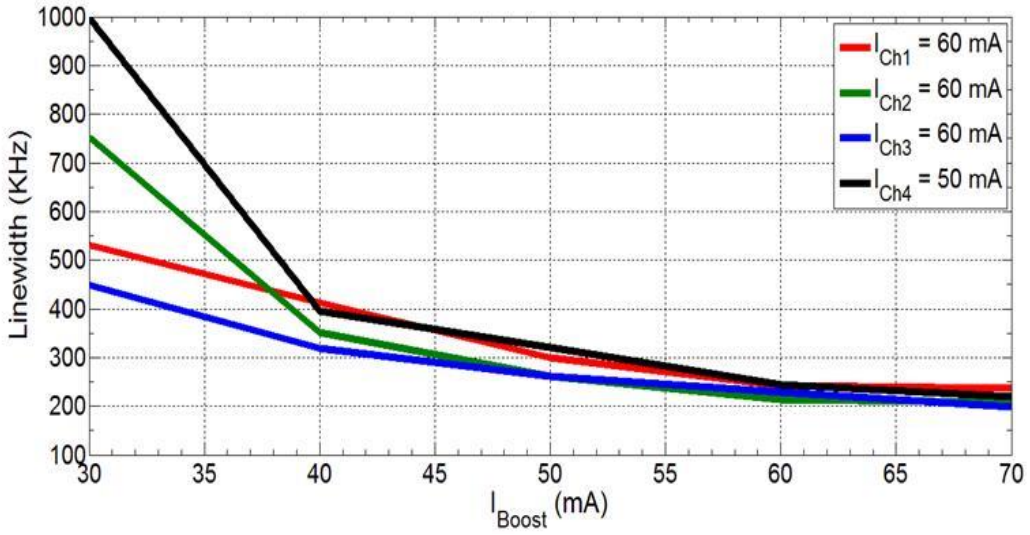

Figure 4.16. Linewidth vs I_{boost} curve. The bias current of the SOAs of channels 1, 2 and 3 is set at 20 mA, whilst for the channel 4 the bias current is set at 50 mA. The current injected into the boost amplifier is swept from 30 to 70 mA in 10 mA steps. The channel SOA and boost amplifier are biased using the PRO-800 current source.

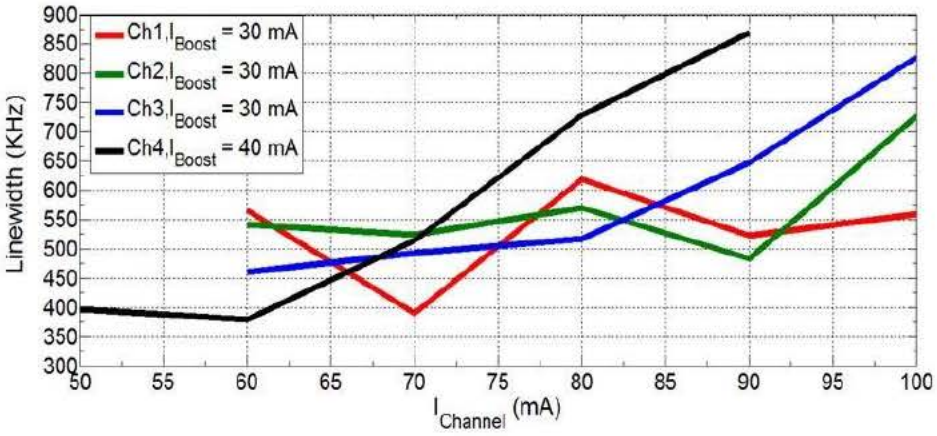

Figure 4.17. Linewidth vs $I_{channel}$ curve. The bias current of the SOAs of the channels 1, 2 and 3 is swept from 30 to 70 mA in 10 mA steps, whilst for the channel 4 it is swept from 50 to 90 mA, whilst for the channel 4 the bias current is set at 50 mA in 10 mA steps. The current injected into the boost amplifier is 30 mA for the channels 1, 2,and 3, while for the channel 4 is 40 mA. The channel SOA and boost amplifier are biased using the PRO-800 current source.

The linewidth measurement results for different bias settings of the boost amplifier whilst the channel SOA is set at a fixed bias current are presented in Table 4.1. The obtained linewidth is less than 250 kHz, with the best result of 199 kHz from channel #3. In the other way round, sweeping the bias current of the channel SOA whilst the boost amplifier is set at a fixed current value, the laser linewidth become wider and greater than 400 KHz

		Boost amplifier	
Channel	**I (mA)**	**30 mA**	**70 mA**
1	60	531 KHz	237 KHz
2	60	752 KHz	207 KHz
3	60	449 KHz	199 KHz
4	50	997 KHz	219 KHz

Table 4.1. Linewidth measurments of the on-chip AWG laser for different bias settings of channel SOA and boost amplifier

4.6 Conclusions

A relation between I_{ch} and I_{Boost} to generate a dual-wavelength mode operation regime in any of the FSR regions orders of the AWG exists as in chapter 3. However, a dual-wavelength operation regime wider than the AWG laser using cleaved facet as mirrors is found.

The use of on-chip mirrors, MIRs, and placing the boost amplifier out of the lasing cavity has enhanced the performance of the device. Also, optical power levels higher than the first structure has been measured and recorded, despite the fact that the channels SOAs length of this device are shorter.

In conclusion, we have proposed ***for the first time to our knowledge*** an on-chip AWG laser based on MIR mirrors. We demonstrated the advantages of this structure for millimeter and Terahertz wave signal generation by optical heterodyning

This device was produced on an InP technology multi-project wafer run, with great potential to develop low cost and compact sources and with the possibility to integrate further functionality.

4.7 References

[1] B. Docter, J. Pozo, S. Beri, I. Ermakov, J. Danckaert, M. Smit, and F. Karouta, "Discretely tunable laser based on filtered feedback for telecommunication applications," *IEEE J. Sel. Topics in Quantum Electron*., Vol. 16, No. 5, pp. 1405–1412, 2010

[2] M. Maximov, E. Ramushina, V. Skopina, E. Tanklevskaya, V. Solov'ev, Y. Shernyakov, I. Kaiander, M. Kaliteevski, S. Gurevich, N. Ledentsov, V. Ustinov, Z. Alferov, C. Sotomayor Torres, and D. Bimberg, "Edge-emitting In-GaAs/GaAs lasers with deeply etched semiconductor/air distributed bragg reflector mirrors," *Semicond. Sci. Technol*., Vol. 17, pp. 69–71, 2002.

[3] P. Muñoz, R. García-Olcina, C. Habib, L. Chen, X. Leijtens, T. de Vries, M. Heck, L. Augustin, R. Notzel, and D. Robbins, "Sagnac loop reflector and arrayed waveguide grating-based multi-wavelength laser monolithically integrated on InP," *IET Optoelectronics*, Vol. 5, No. 5, pp. 207–210, 2011.

[4] Y. Zheng, D. Keh-Ting Ng, Y. Wei, W. Yadong, Y. Huang, Y. Tu, C.-W. Lee, B. Liu, and S.-T. Ho, "Electrically pumped heterogeneously integrated Si/IIIV evanescent lasers with micro-loop mirror reflector," *Appl. Phys. Lett*., Vol. 99, No. 1, p. 011103, 2011.

[5] L. Xu, X. Leijtens, B. Docter, T. de Vries, E. Smalbrugge, F. Karouta, and M. Smit, "MMI reflector: A novel on-chip reflector for photonic integrated circuits," in Proc. *35th European Conference on Optic. Communications*. (ECOC '09), Vienna, Austria, Sep. 20—24 2009.

[6] E. Kleijn, "MMI reflectors with free selection of reflection to transmission ratio," *Proc. the 15th Annual Symposium of the IEEE Photonics Benelux Chapter*, Nov.18-19, 2010, Delft, The Netherlands.

Wireless data transmission link

5.1 Communication systems

After having designed, characterized and done a deep study of the behavior of two different AWG laser structures based on cleaved facet and on-chip mirrors, we have designed and setup a communication system. The objective of this communication system is to evaluate the performance of our devices as millimeter-wave and terahertz signal carrier frequency sources for a wireless data transmission link. In this section an overview of some general aspects of such a communication system which are relevant to build a wireless link are studied.

The main purpose of a communication system is transmitting information over a physical medium –as well known as the communication channel- to the receiver. This information may be either an analog signal or a set digital data which are transmitted to the communication channel through a transmitter component.

The transmitted signal can be encoded and modulated. The encoding add security to the information while modulation is used to up-convert the low-frequency baseband data from the data source to a bandpass signal at a higher carrier frequency which will be transmitted over the physical medium. The modulated signal is sent from the transmitter (Tx) block over the communication channel to the receiver (Rx) block where a receiver module detects the transmitted signal and lead it to the demodulator which recovers the baseband data from the received signal.

In wireless communications systems, the signal is radiated from an antenna to the communication channel, e.g. air or free space. The employed carrier frequencies range goes from several cents of MHz up to 300 GHz and beyond. At some carrier

frequencies, the wireless transmission link distance is significantly influenced by the atmospheric attenuation and weather conditions (seeSection 1.1).

Furthermore, other prevalent effects in wireless communication are multipath propagation and signal fading. At very high frequencies (millimeter wave and THz frequencies) mostly line of sight (LOS) connections are used, since highly directional antennas are needed to overcome the atmospheric losses and the free space path loss.

In order to know the data rate that can be transmitted over the communication channel the Shannon – Hartley theorem [1] is used. This theorem state that for a communication system without bandwidth limitation, the maximum channel capacity is related to the average transmitted signal power and power spectral density of the communication channel. The relationship of these two parameters is as well named as signal-to-noise ratio. However, generally, the bandwidth of communication system is limited due to the physical limitations of the medium and the components which are used to build the transmitter and receiver. Typically, the amount of available bandwidth increases with the carrier frequency of the electromagnetic signal which carries the data.

Before sending the information to the communication channel, it must be modulated. Several kind of modulation formats exist such as OOK, QAM, FSK, FM, etc. the On-Off Keying (OOK) modulation format is the simplest digital modulation format as the binary data sequence is directly encoded by the presence (“on”) or absence (“off”) of the carrier. The OOK modulation format is widely used in wireless communications before using higher modulation formats in order to assess the performance and the quality of the wireless link. The OOK format is phase-insensitive which it can easily be detected using an analog heterodyning receiver or an envelope detector.

5.2 Channel modelling for a wireless link

Channel modeling for a wireless link is performed with respect to wireless path length, frequency as well as further environmental conditions. Three main contributors can be identified for computing the total path losses are:

- The free-space path loss (FSPL).
- The atmospheric gaseous attenuation.
- The attenuation induced by rain fall.

Other effects that also may contribute to the loss are fog or mist. Calculation of the propagation losses of the wireless Line-Of-Sight (LOS) link is developed by the free-space path loss model. The free-space path denotes a linear, lossless and isotropic propagation medium without any current sources and charges. The relationship of received signal power P_{rx} and transmitted power P_{tx} for a wireless link is given by the Friis equation [2], [3].

$$P_{rx}(dBm) = P_{tx}(dBm) + G_{tx}(dB) + G_{rx}(dB) - 20Log_{10}\left(\frac{d}{4\pi\lambda}\right) \quad \text{Eq. 5.1}$$

Where P_{rx}, G_{rx}, G_{tx} are the received average power on the receiver module, receiver and transmitter antenna gain, respectively. Moreover, Eq. 5.1 is only valid for a line-of-sight path with perfectly matched antennas. Therefore, the free-space path loss can be expressed as:

$$L_{fsp}(\text{dB}) = 20Log_{10}(F_{RF}d) - 147.6 \quad \text{Eq. 5.2}$$

Where F_{RF} is the carrier frequency in GHz and d is the LOS distance between the transmitter and receiver module in meters.

The free space path loss in Eq. 5.2 demonstrates that there is a direct relationship between the carrier frequency and FSPL. By increasing the carrier frequency, the free space path loss is increased as well. In Figure 5.1 is depicted the free-space path loss for different carrier frequencies from 90 to 120 GHz in 5 GHz steps

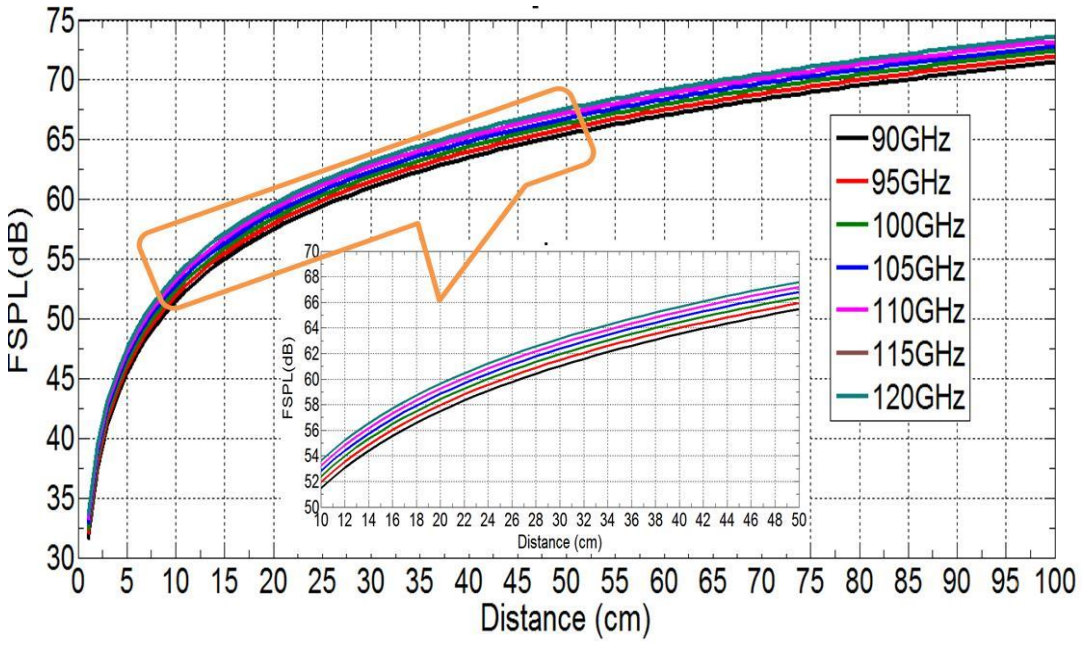

Figure 5.1. Free space path loss for different carrier frequencies from 90 to 120 GHz in 5 GHz steps.

The free-space path loss assumption is only valid in the far-field denoted as Fraunhofer's region taking into account that the transmitted signal can be described approximately as a plane wave. This distance of interest is calculated by [4].

$$d_f = \frac{2D_a}{\lambda_{tx}} \qquad \text{Eq. 5.3}$$

Where d_f is the Fraunhofer's distance, D_a the largest antenna dimension and λ_{tx} the carrier wavelength.

As this formula describes the loss of an ideal line-of-sight path without obstacles and without any multipath propagation due to reflective surfaces, it is barely applicable for indoor communication over longer distances. Here, path loss can be e.g. modeled by the exponential-loss model, where the exponent is adapted to the corresponding environment like a corridor, or hallway.

5.3 Wireless transmission link system setup

We have developed a wireless data transmission link system using the AWG lasers as photonic sources of the optical heterodyne signal for the generation of the carrier wave at the millimeter-wave frequency range. As a benchmark, we have also used two External Cavity Lasers (ECLs) supplied by Sacher Lasertechnik. The ECL lasers can tune their wavelength over a 200 nm range, and have -3 dB optical linewidth less than 25 KHz, being suitable for the millimeter wave signal generation in wireless transmission link systems and other applications. The block diagram of the wireless transmission link system is shown in Figure 5.2

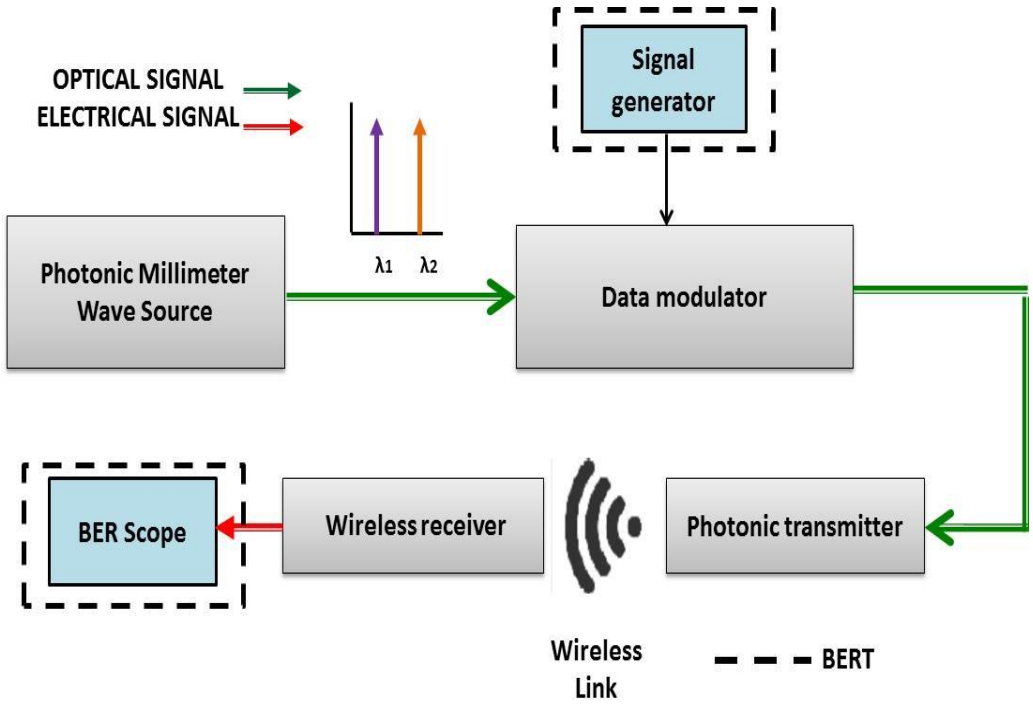

Figure 5.2. General block diagram of the wireless transmission link system setup

The optical heterodyne signal from the photonic integrated circuit is collected on a single mode fiber, fed onto the data modulator block. A pattern generator (generating a

pseudo-random bit sequence (PRBS) with a word length of 2^{23}-1) is connected to the optical modulator with a non-return to zero on-off keying (OOK). The modulated dual wavelength signal is shined onto a high speed photodiode, which converts the optical signal into an electrical radio-frequency signal.

This radio signal is launched to free space using a horn antenna. The receiver module is a direct detection Schottky receiver that rectifies the millimeter wave carrier signal, down-converting the data signal to baseband. The received baseband signal generated by the signal generator is amplified in order to lead it to the Bit error rate (BER) scope, which measures the quality of the wireless link. Both the BER scope and the signal generator make part of equipment well-known as BER tester (BERT).

5.4 Wireless transmitter

The wireless transmitter is composed of a photonic millimeter-wave source, data modulator and a photonic transmitter, as shown in Figure 5.3. The optical signal from the photonic millimeter wave source is collected by a lensed fiber followed by an optical isolator (to avoid the unwanted reflections back to the laser source), followed by an optical splitter with 99/01 splitting ratio. The one percent optical output is carried to an optical power meter (OPM) providing a measurement to estimate the optical power launched from the laser source. The other arm goes to the data modulator module.

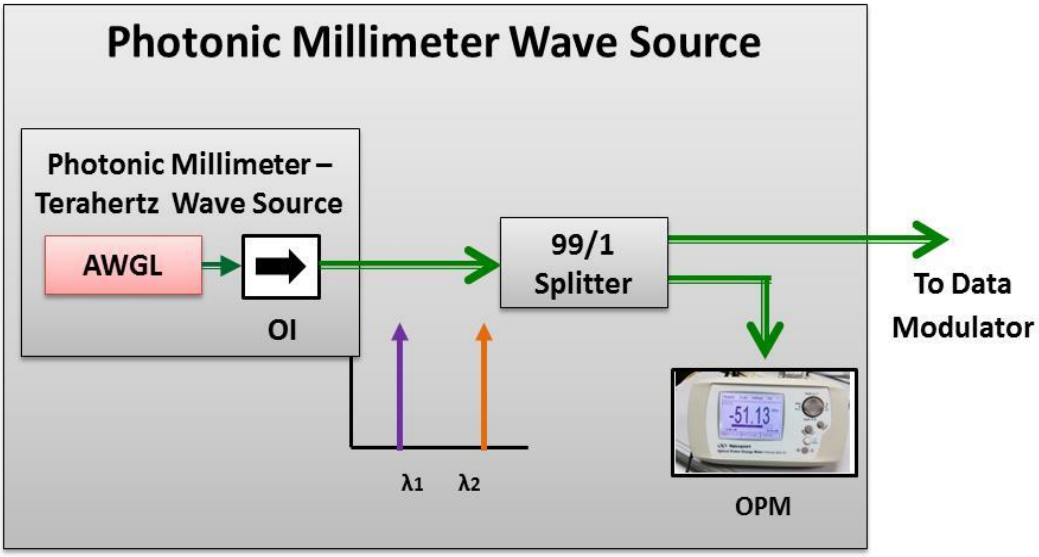

Figure 5.3. Block diagram of the photonic millimetre wave source

The data modulator block first includes an Erbium-Doped Fiber Amplifier (EDFA), raising the optical power up to 0 dBm, to increase the modulation efficiency of the following Electro-Optic Intensity Modulator (EOAM). A polarization controller adjusts the polarization into the modulator. The modulator is an EOAM biased at -6 V and modulated by a 1Gbps non-return to zero on-off keying data signal. The pseudorandom

bit sequence (PRBS) with a word length of 2^{23}-1 with NRZ-OOK modulation format is generated by a pulse pattern generator (PPG) with a maximum output voltage of 2 Vpp. The two wavelengths generated by the dual-wavelength laser source are modulated at the same time, thus a double sub-carrier modulation is done. The total attenuation generated by the EOAM is around 8 dB.

The modulated optical signal is lead to a second optical splitter, with 90/10 splitting ratio. The 10% output is carried to an optical spectrum analyser, with the purpose of measuring and monitoring the dual-wavelength signal. The 90% output is carried to a second EDFA to compensate the modulation losses of EOAM. An optical attenuator allows controlling the optical power launched into the high speed photodiode, measured with an in-line optical power meter, as shown in Figure 5.4.

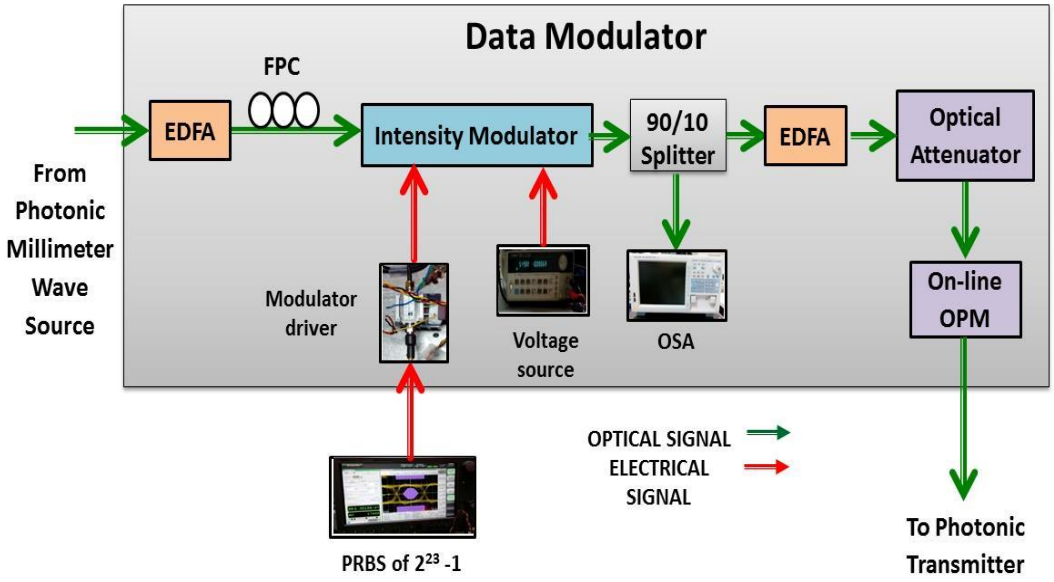

Figure 5.4. Block diagram of the data modulator block.

The optical signal from the data modulator module is led to the photonic transmitter. The key element is a Uni-Travelling Carrier Photodiode (UTC-PD) provided by NTT. The input optical signal is converted to an electrical signal by Photodiode (PD). At the

UTC-PD's output port a standard WR8 conical horn antenna with about 25.5 dBi gain is connected to launch the electrical radio-frequency signal to free space, as shown in Figure 5.5.

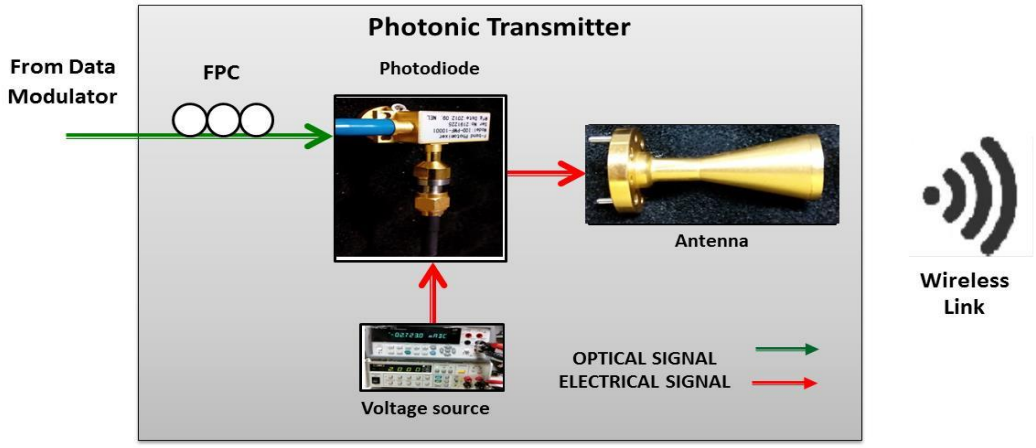

Figure 5.5. Block diagram of photonic transmitter

The photonic transmitter module has been characterized using two tunable ECLs, generating an optical millimeter-wave from 75 to 160 GHz. Figure 5.6 shows the characterization of this module, the average RF power generated by the UTC-PD is 1 mW (0 dBm) which is radiated to free space.

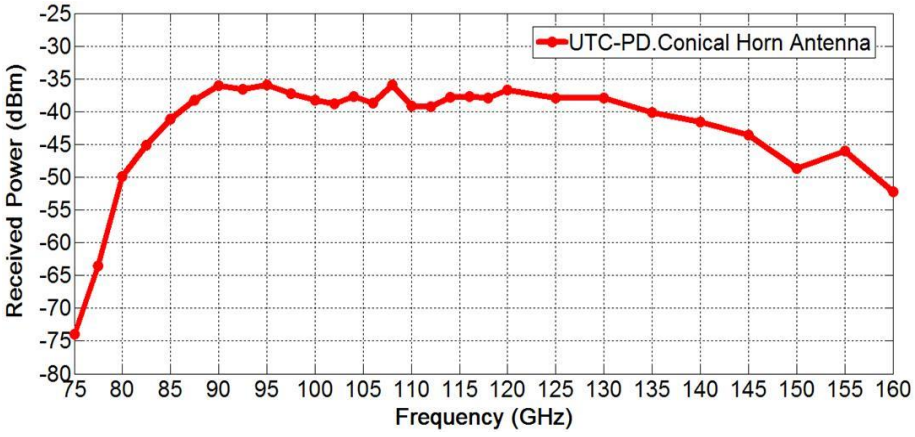

Figure 5.6. Characterization of the photonic transmitter showing the frequency response applying a carrier frequency which is swept from 75 to 160 GHz in 2.5 GHz steps. The average RF power generated by the UTC-PD is 1 mW (0 dBm).

5.5 Wireless receiver

After the transmitted millimeter-wave signal is received, the signal is down-converted to base band. Some of the electronic components used in this block in order to get the original modulated data are as shown in Figure 5.7. A photograph of all the electronic components used in this block is shown in Figure 5.8.

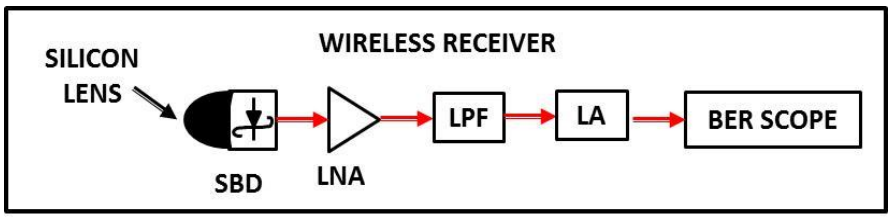

Figure 5.7. Block diagram of wireless receiver.

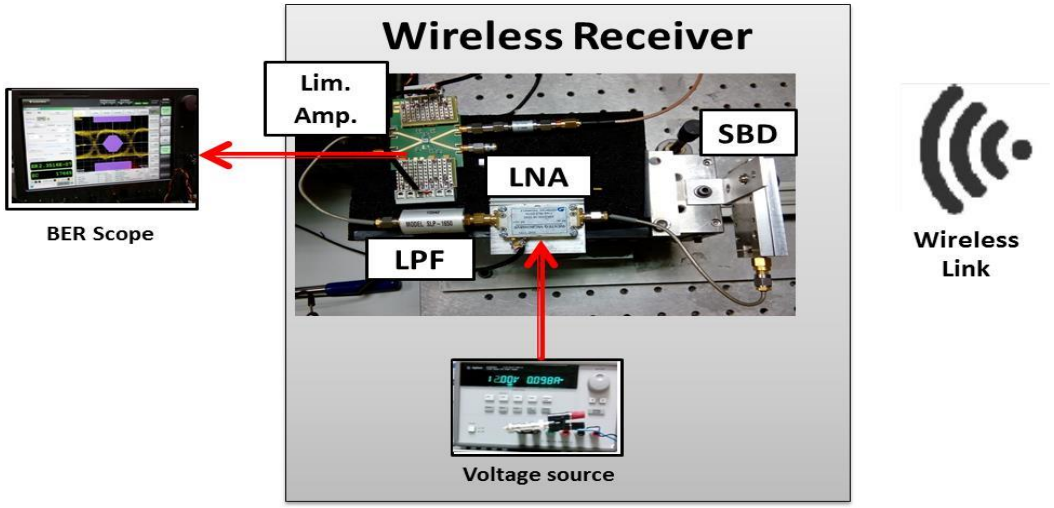

Figure 5.8. Photograph of the electronic components used in the wireless receiver block

Two electronics-based approaches can be done. The first one is direct detection where a diode detector such as a broadband Schottky-Barrier Diode (SBD) is used. And the second approach is heterodyne detection, a mixer and a local oscillator (LO) signal source with a high sensitivity and a wider bandwith for the recovery of the transmitted

data are used. In our wireless receiver unit a Schottky-Barrier Diode develop in [5] is used, as shown in Figure 5.9.

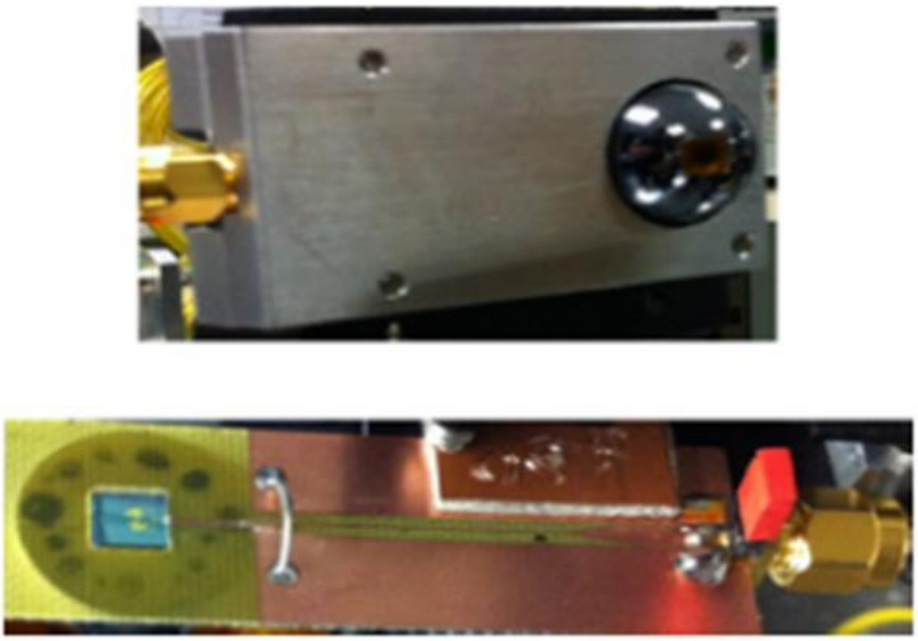

Figure 5.9. Photograph of receiver module: (top) front view of case module showing Si lens and (bottom) back view of uncased module, showing log periodic antenna on HR-Si and impedance matching transition to SMA output connector.

The data signal transmitted using an F-band carrier frequency is demodulated and down-converted to a base band data signal by the SDB detector. The responsivity of the antenna-integrated Schottky-Barrier Diode module with the silicon lens is about 500 V/W and 100 V/W, for an 101 GHz and 114GHz RoF signal, respectively.

A low-noise amplifier (LNA) connected in a series way and with 34 dB gain and 9 KHz~3GHz bandwidth, is effective to increase the receiver sensitivity. Therefore, the demodulated baseband signal is amplified by the LNA. An additional low-pass filter (LPF) with -3 dB cut-off frequency of 1.5 GHz is added to the output plug of the low-noise amplifier in order to smooth and eliminate the damping oscillations of the transient response yielded by the LNA due to the transition states of the baseband data

digital signal i.e from 0 to 1 and vice versa. A limiting amplifier (LA) in order to amplify and keep suitable voltage levels at the input plug of BERT is used. Finally, the transmitted digital data signal is input to the bit error rate (BER) scope to compare the transmitted data with the received data.

The enveloped detector has been characterized in order to know its maximum bandwidth. It is a very important parameter on the receiver block, so that it will indicate us the maximum data rate that can be transmitted by our communication system. In Figure 5.10 is depicted the baseband frequency response of the designed Schottky-Barrier Diode. It shows that the -3 dB cut-off frequency is 1.5 GHz having a 65 dB roll-off from 1.8 to 2 GHz. Therefore, it demonstrate that data rate beyond 1.5 Gbps cannot be transmitted.

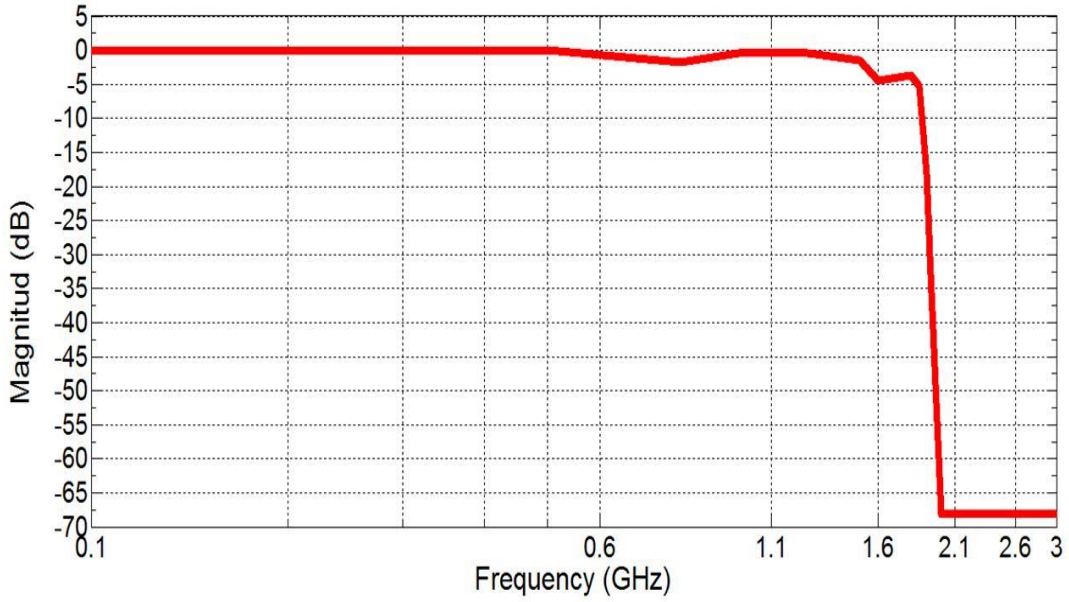

Figure 5.10. Photograph of receiver module: (top) front view of case module showing Si lens and (bottom) back view of uncased module, showing log periodic antenna on HR-Si and impedance matching transition to SMA output connector.

5.6 Experimental results

This section describes the achieved experimental results for photonic wireless data transmission of up to 1 Gb/s. Photonic millimetre-wave sources used for this experiment are the aforementioned in this thesis. Furthermore, a wireless transmission link at 100 and 110 GHz using two ECLs has been done in order to take this measurement as reference information to compare the quality of our system with another different type of laser. Indoor measurements within a laboratory environment have been performed.

The frequency spacing generated by AWG laser based on cleaved facets and on-chip mirrors is about 100 and 113 GHz, respectively. Therefore, dual-wavelength mode operation from both lasers is achieved for the optical millimeter-wave signal generation.

BER characterizations have been carried out without RF amplifier connected to the UTC-PD's output and the WR-8 conical horn antenna. Plano-convex lenses ideally suited for THz applications with low insertion loss is used in this experiment. These lenses are placed in front of the SBD envolved detector and the conical horn antenna.. The separation distance between the transmitter and receiver module is 50 cm. A photograph of the implemented experimental setup in this thesis for the wireless link is shown in Figure 5.11.

BER characterization at 1 Gbps to measure the quality of our system has been done. The results that show the BER characterization using the three mmW sources is depicted in Figure 5.12.

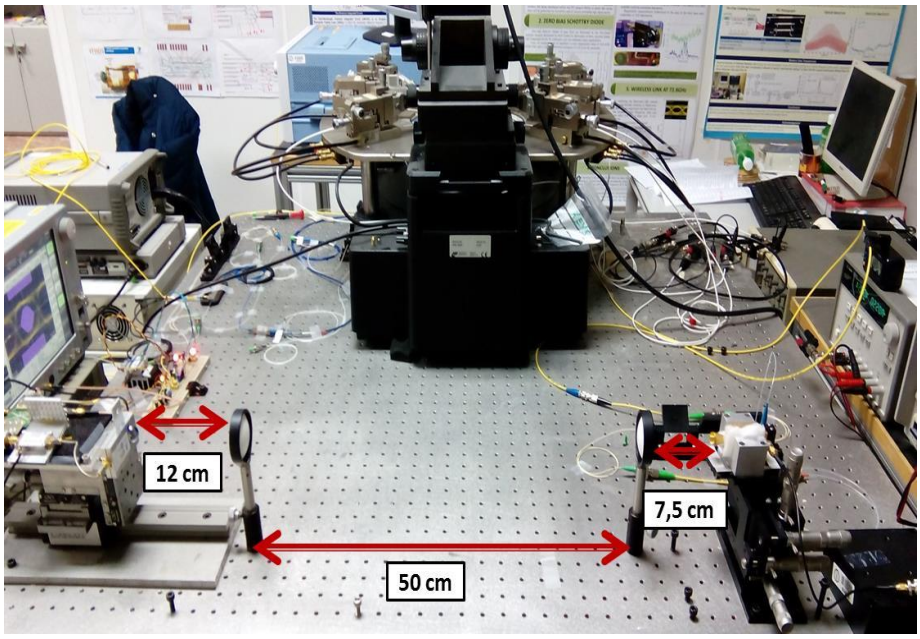

Figure 5.11. Photograph of experimental physical setup. Convex lenses are used to increase the distance between the transmitter and receiver module. The separation distance between the modules is 50 cm. the distance of SBD and conical horn antenna from the lenses in front each of them is 12 and 7.5 cm.

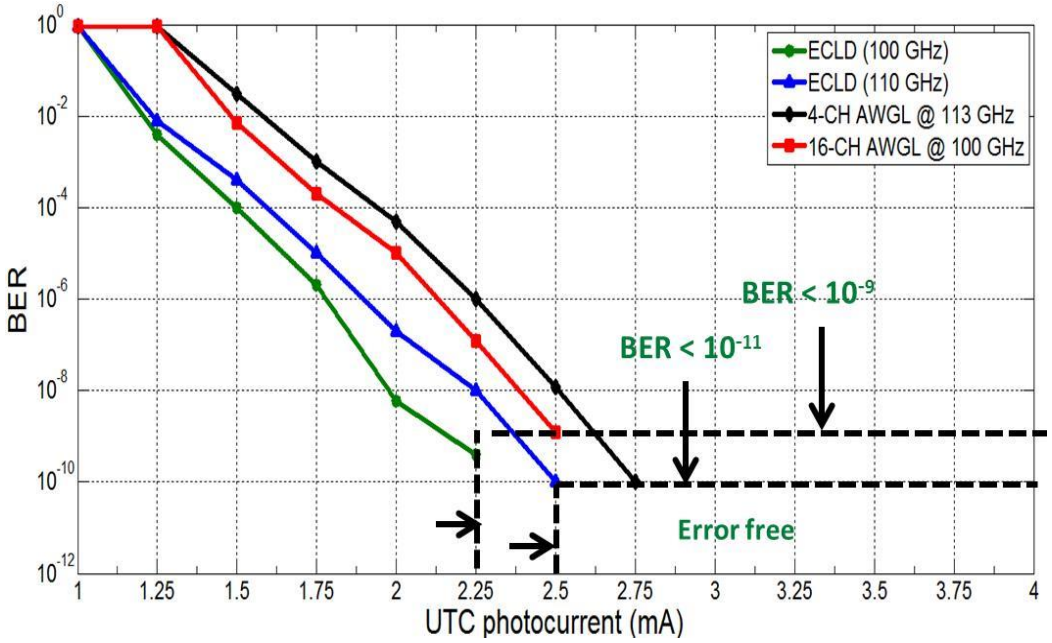

Figure 5.12. BER characterization at 1 Gbps. The frequency spacing generated by 16 and 4 channel AWG based laser is about 100 and 113 GHz. BER measurement less than 10^{-9} and 10^{-11} getting eror has been achieved

The bandwidth limitation on the wireless data link is determined mainly by the Low-Noise Amplifier (LNA) bandwidth and the Schottky-Barrier Diode detector in the receiver. The UTC-PD has a bandpass RF characteristic, with a -3 dB RF bandwidth from 90 to 140 GHz. The baseband signal bandwidth of the SBD detector module including the silicon lens is about 120 GHz (from 40 GHz to 160 GHz), having its peak responsivity (7129 V/W) at 75.7 GHz.

To evaluate the bit error rate, different optical power launched into the photodiode varying the optical attenuator is done. UTC-PD's responsivity is about 0.4 A/W.

From Figure 5.12, the BER measurement less than 10^{-9} and 10^{-11} are achieved; even error free is also achieved. Both lasers are working in a free running mode; it means that there is not any extra locking system enhancing their performance. The BER measurement difference between ECLs and AWGL sources is the order of 10^{-2} for the same optical power launched into the UTC-PD. The eye pattern generated by the BERT of received data is shown in Figure 5.13 and Figure 5.14 for the 16 and 4 channel AWG based laser, respectively. The optical power launched into the UTC-PD is 10 dBm and 5 dBm, thus the UTC-PD generates a photocurrent of 4 and 2 mA.

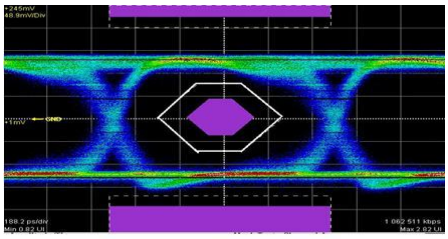

I_{UTC-PD} = 4 mA

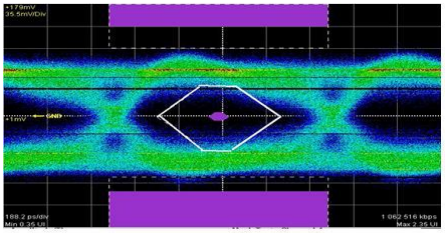

I_{UTC-PD} = 2 mA

Figure 5.13. Eye-Pattern of the received PRBS data, n =23, at 1Gbps after the transmission of the wireless link.. The carrier frequency is about 100 GHz using a non-return zero digital (NRZ) signal digital format

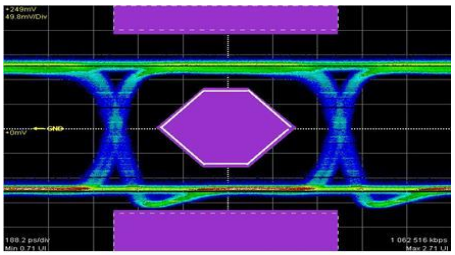

I_{UTC-PD} = 4 mA

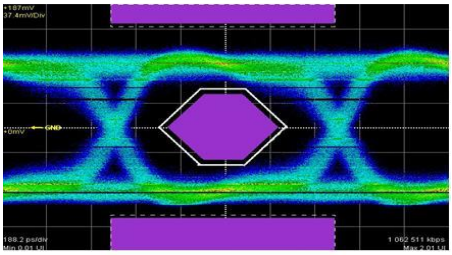

I_{UTC-PD} = 2mA

Figure 5.14. Eye-Pattern of the received PRBS data, n =23, at 1Gbps after the transmission of the wireless link.. The carrier frequency is about 113 GHz using a non-return zero digital (NRZ) signal digital format

5.7 Conclusions

We have also demonstrated 'error-free' transmission over a photonic enabled wireless link at a data rate of 1 Gbps with BER < 10^{-11} and over 50 cm distance without observing an error floor using carrier frequencies of 100 GHz and 113 GHz. The system uses two key components, a UTC-PD and a receiver. Both have a great potential to realize compact transmitter and receiver modules.

The maximum data rate is limited by the zero-bias Schottky barrier diode which has -3 dB cut-off frequency of 1.5 GHz. Therefore, data rate beyond 1.5 Gbps cannot be transmitted by our communication system.

The separation distance between the transmitter and receiver can be extended using some components such as RF amplifier, bigger Teflon lenses and low-noise amplifier with a amplification gain greater than 35 dB

5.8 References

[1] C. E. Shannon, "A mathematical theory of communication", The Bell System Technical Journal, vol. 27, no. 3, pp. 379-423, 1948.

[2] H. T. Friis, "A note on a simple transmission formula," *Proceedings of the IRE*, Vol. 34, no. 5, pp. 254–256, 1946.

[3] H. Hashemi, "The indoor radio propagation channel," *Proceedings of the IEEE*, Vol. 81, no. 7, pp. 943–968, 1993.

[4] T. Rappaport, *Wireless communications: principles and practice*. Prentice Hall, 2001.

[5] Javier Montero de Paz, Matthias Hoefle, Ion Oprea, Oleg Cojocari, Luis Enrique García-Muñoz, Daniel Segovia-Vargas, Rolf Jakoby, Guillermo Carpintero. "Compact Schottky Barrier Diode Receiver for E-Band (60 – 90 GHz) Wireless Communications". IEEE International Topical Meeting on Microwave Photonics (MWP) 2012, pp. 244-247

Conclusions and future work

6.1 Final conclusions

In this work has been characterized and demonstrated the performance of two dual-wavelength laser source based on AWG for the continuous millimetre wave signals generation. One of this photonic integrated circuits use the cleaved facets while the second one uses on-chip mirrors which are well-known as multimode interference reflectors (MIRs). This optical component is very useful and important for the laser cavity design where the lasing cavity length is not determined by the distance of the cleaved facet of the chip. In fact, this optical component can placed at anywhere into the chip.

A boost amplifier placed at the output common waveguide in order to increase the optical power of laser is used. An advantage of this kind of structure is that the two generated optical modes shall be correlated at the output of the chip, generating a high spectral purity and absolute frequency stability. Moreover, the two wavelengths generated at the AWG's common output from each separate channel are amplified by the same Boost amplifier; it means that we must equalize the power in the two channels which is limited by the SMSR required in the output of each channel of the AWG giving as result a drawback for this kind of structure. A drawback is that, locating a boost amplifier into of the laser cavity generates lasing modes at the common output of the chip as the channel SOAs are disabled.

Therefore, regarding the structure which uses on-chip mirrors, the boost amplifier can be located outside the FP cavity, giving a result that the optical power at the AWGL output may be increased in the order of milliwatts. In addition, neither residual optical power nor optical modes are yielded at the AWGL output as the one from the first

device. An anti-reflective (AR) coating placed on each of the cleaved facets improves the performance of the chip, by eliminating all the unwanted reflections. A wider dual-mode operation region from the 4-channel AWG based laser structure that the one from the 16-channel AWG based laser structure is achieved. Optical FWHM linewidth less than 250 KHz were achieved on both devices, despite the fact that both laser sources were working in a free running mode.

We have also demonstrated 'error-free' transmission over a photonic enabled wireless link at a data rate of 1 Gbps with BER < 10^{-11} over 50cm distance without observing an error floor. The system uses two key components, a UTC-PD and a zero-bias Schottky barrier diode receiver. Both have a great potential to realize compact transmitter and receiver modules.

These AWG lasers were fabricated on an InP-based technology multi-project wafer run, with great potential to develop low-cost and compact sources and with the possibility to integrate further functionality.

6.2 Future work

In order to continue to explore and investigate the possibility to develop dual-wavelength laser sources for millimetre and terahertz generation based on an AWG with a common SOA at the chip output for two wavelengths, a new generation of devices may be designed. The new structures ought to have on-chip mirrors, MIRs. It will allow us to design also laser sources with different cavity lengths.

The position of the boost amplifier should be out of the Fabry-Perot cavity laser. It would let to get higher optical power from the chip. Besides, reflection caused by the boost amplifier will be avoided.

The fabrication of these structures can be made using different platform technology, combining InP based platform with either Polymer technology or Triplex technology in order to reduce the losses caused by the passive section lengths such as the AWG.

Publications based on this work

List of Publications

[1] (INVITED) Guillermo Carpintero, Robinson Guzman, Carlos Gordon, Frédéric Van Djik, Gaël Kervella, Mourad Chitoui. "Photonic Integrated Circuits for Radio-Frequency Signal Generation". Journal of Lightwave Technology. Vol. 34, No. 2, p.p 508-515.2016

[2] (INVITED) Guillermo Carpintero, Robinson Guzmán, K. Balakier, Gaël Kervella, Martyn Fice, Mourad Chitoui, Frederic Van Dijk, Cyril Renaud, Xaveer Leijtens and A. J. Seeds. "Photonic-Enabled Millimetre-Wave Wireless Data Transmission Based On Photonic Integrated Circuits". Proceedings of Optical Fiber Communications Conference and Exhibition (OFC). Los Angeles, California, USA. March 22nd – 26th, 2015.

[3] Guillermo Carpintero, Robinson Guzman, Carlos Gordon, Xaveer Leijtens, Katarzyna Ławniczuk. "Photonic-Enabled Millimeter-Wave F-Band Wireless Link Using Photonic Integrated Circuits". Proceedings of 20th European Conference on Network and Optical Communications (NOC). London, United Kingdom. June 30nd – July 2nd, 2015.

[4] Carlos Gordón, Robinson Guzmán, Guillermo Carpintero, Vinicio Corral , Xaveer Leijtens. "On-Chip Photonic Integrated Circuits Structures for Millimeter and Terahertz Wave Signal Generation". Proceedings of International Topical Meeting on Microwave Photonics (MWP). Paphos, Cyprus – European Union. October 26th -29th, 2015.

[5] Robinson Guzman, Guillermo Carpintero, Carlos Gordon, Xaveer Leijtens, Katarzyna Ławniczuk. "Wireless Link using On-Chip Photonic Integrated Millimeter-Wave Sources". Proceedings of International Topical Meeting on Microwave Photonics (MWP). Paphos, Cyprus – European Union. October 26th -29th, 2015.

[6] Vinicio Corral, Robinson Guzmán, Carlos Gordón, Guillermo Carpintero, Xaveer Leijtens. "Optical Frequency Comb Generator based on a Monolithically Integrated Ring Laser". Proceedings of European Semiconductor Laser Workshop. September 24nd – 25th, 2015.

[7] Vinicio Corral, Robinson Guzmán, Carlos Gordón, Guillermo Carpintero. "Simulación y Caracterización del Laser DBR, Monolíticamente Integrado en un Circuito Fotónico". Proceedings of URSI 2015- XXX Simposium Nacional de la Unión Científica Internacional de Radio. September 2nd – 4th, 2015.

[8] Carlos Gordón, Robinson Guzmán, Guillermo Carpintero, Vinicio Corral , Xaveer Leijtens. "E-band Wireless Link Using an On-Chip Colliding Pulse Passive Mode-Locked Laser Diode Structure". Proceedings of URSI 2015- XXX Simposium Nacional de la Unión Científica Internacional de Radio. September 2nd – 4th, 2015.

[9] (KEYNOTE) Carlos Gordon, Robinson Guzman, Guillermo Carpintero, Xaveer Leijtens. "Millimeter and Sub-terahertz Wave Colliding Pulse Mode-Locked Laser Diode". Proceedings of 40th International Conference on Infrared, Millimeter, and Terahertz Waves (IRMMW-THz). Hong Kong, China. August 23th -28th , 2015.

[10] Robinson Guzman, Guillermo Carpintero, Carlos Gordon, Xaveer Leijtens, Katarzyna Ławniczuk. "F-Band Millimeter-Wave Signal Generation for Wireless Link Data Transmission using On-Chip Photonic Integrated Dual-Wavelength Sources".

Proceedings of the 38TH Progress In Electromagnetics Research Symposium, p.p 866-869. Prague – Czech Republic – European Union. July 6th -9th, 2015.

[11] Carlos Gordon, Robinson Guzman, Guillermo Carpintero, Vinicio Corral, Xaveer Leijtens." On-chip Colliding Pulse Mode-Locked Laser Diode (OCCP-MLLD) Using Multimode Interference Reflectors". Optics Express. Vol. 23, Issue 11, pp. 14666-14676

[12] Carlos Gordon, Robinson Guzman, Guillermo Carpintero, Xaveer Leijtens." On-chip Mode-Locked Laser Diode Structure Using Multimode Interference Reflectors". Photonics Research. Vol. 3, Issue 1, pp. 15-18, ID223478.

[13] Guillermo Carpintero, Robinson Guzman, Carlos Gordon, Xaveer Leijtens, Frédéric Van Djik, Gaël Kervella, Martyn J. Fice, Katarzyna Balakier, Cyril C. Renaud. "Comparison of Photonic Integrated Circuits for Millimeter-Wave Signal Generation Between Dual-Wavelength Sources for Optical Heterodyning and Pulsed Mode-Locked Lasers". Proceedings of the SPIE Optics + Optoelectronics, Vol. 9357, id. 935719. Physics and Simulation of Optoelectronic Devices XXIII. San Francisco – California – United States. February 7th -12th , 2015.

[14] Guillermo Carpintero, Robinson Guzmán, Carlos Gordón, , Xaveer Leijtens. "Photonic Integrated Dual Wavelength Source Using an On-Chip Mode Locked Laser Diode and Arrayed Waveguide Grating Optical Filter". 5th International Symposium on Terahertz Nanoscience (TeraNano V). Martinica. December 1st – 5th, 2014.

[15] Carlos Gordón, Robinson Guzmán, Álvaro Jiménez, Guillermo Carpintero, Xaveer Leijtens." Fully Monolithic Colliding Pulse Mode-Locked Laser Diode using Multimode Interference Reflectors". Proceedings of URSI 2014- XXIX Simposium Nacional de la Unión Científica Internacional de Radio. Escuela Técnica Superior de

Ingenieros de Telecomunicación de la UPV de Valencia, Valencia, Spain. September 3th – 5th, 2014.

[16] Robinson Guzmán, Álvaro Jiménez, Vinicio Corral, Guillermo Carpintero, Xaveer Leijtens, Katarzyna Ławniczuk." Narrow Linewidth Dual-Wavelength Laser Sources Based on AWG for the Generation of Millimeter Wave". Proceedings of URSI 2014- XXIX Simposium Nacional de la Unión Científica Internacional de Radio. Escuela Técnica Superior de Ingenieros de Telecomunicación de la UPV de Valencia, Valencia, Spain. September 3th – 5th, 2014.

[17] Carlos Gordón , Robinson Guzmán, Álvaro Jiménez, Guillermo Carpintero, Xaveer Leijtens. "olliding Pulse Mode-Locked LaserDiode using Multimode Interference Reflectors". Proceedings of 17th ECIO 2014 – European Conference on Integrated Optics and Technical Exhibition, 19th Micro-optics Conference. Université Nice Sophia Antipolis, Nice, France. June 24th – 27th, 2014.

[18] Robinson Guzmán, Álvaro Jiménez, Guillermo Carpintero, Xaveer Leijtens, Katarzyna Ławniczuk. "Dual-Wavelength AWG based Lasers for Narrow Linewidth Heterodyne Beat-Note Generation". Proceedings of 17th ECIO 2014 – European Conference on Integrated Optics and Technical Exhibition, 19th Micro-optics Conference. Université Nice Sophia Antipolis, Nice, France. June 24th – 27th, 2014.

[19] Guillermo Carpintero, K. Balakier, Z. Yang, Robinson Guzmán, Antonio Corradi, Álvaro Jiménez, Gaël Kervella, Martyn Fice, Marco Lamponi, Mourad Chitoui, Frederic Van Dijk, Cyril Renaud, A. Wonfor, Erwin Bente, R.V. Penty, I.H. White and A. J. Seeds. "Fully Monolithic Photonic Integrated Circuits for Microwave and Millimeter Wave Signal Generation". Progress In Electromagnetics Research Symposium Proceedings, p.p 1711-1714. Guangzhou, China. August 25th – 28th, 2014.

[20] Guillermo Carpintero, Robinson Guzmán, K. Balakier, Z. Yang, Antonio Corradi, Álvaro Jiménez, Gaël Kervella, Martyn Fice, Marco Lamponi, Mourad Chitoui, Frederic Van Dijk, Cyril Renaud, A. Wonfor, Erwin Bente, R.V. Penty, I.H. White and A. J. Seeds. "Microwave Photonic Integrated Circuits for Millimeter-Wave Wireless Communications". Journal of Lightwave Technology Vol. 32, No. 20 -p.p 3495-3501.

[21] Álvaro Jiménez, Robinson Guzmán, Guillermo Carpintero, Daniel Segovia, Luis Enrique Garcia-Mujioza. "Continuous Wave Millimeter and Tera-Hertz generation using a Photonic Integrated Circuit". Proceedings of 38th International Conference on Infrared, Millimeter, and Terahertz Waves (IRMMW-THz. Mainz on the Rhine, Germany. September 1st -6th, 2013.

[22] Robinson Guzmán, Guillermo Carpintero, Alvaro Jiménez, Katarzyna Ławniczuk, Antonio Corradi, Xaveer Leijtens, Erwin Bente. "Dual-Wavelength Operation of Monolithically Integrated Arrayed Waveguide Grating Lasers for Optical Heterodyning". Proceedings of the SPIE Optics + Optoelectronics. Vol. 8781, id. 87810F. Prague, Czech Republic. April 15th -18th, 2013.

[23] Robinson Guzmán, Guillermo Carpintero. "Digital Filtering Model of an Arrayed Waveguide Grating Device". Proceedings of URSI 2012 - XXVII Simposium Nacional de la Unión Científica Internacional de Radio. p.p 73-76. Universidad Miguel Hernández de Elche. Elche, Alicante, Spain. September 12th – 14th, 2012.

[24] Robinson Guzmán, Luis Jorge Orbe, Guillermo Carpintero, Antonio Corradi, Erwin Bente. "Traveling Wave Model of an AWG-based Multiwavelength Laser". Proceedings of 16th ECIO 2012 - European Conference on Integrated Optics and Technical Exhibition. Sitges, Barcelona, Spain. April 18th – 20th, 2012.

[25] Luis Jorge Orbe, Robinson Guzmán, Guillermo Carpintero. "Modelo de Propagación de un Láser Semiconductor en Anillo". Proceedings of URSI 2011 - XXVI Simposium Nacional de la Unión Científica Internacional de Radio. p.p 31-34. Universidad Carlos III de Madrid. Leganés, Madrid, Spain. September 6th – 9th, 2011.

[26] Robinson Guzmán, Luis Jorge Orbe, Pablo Acedo, Guillermo Carpintero. "Diseño de un AWGL Basado en Modelo de Propagación". Proceedings of URSI 2011 - XXVI Simposium Nacional de la Unión Científica Internacional de Radio. p.p 31-34. Universidad Carlos III de Madrid. Leganés, Madrid, Spain. September 6th – 9th, 2011

[27] Luis Jorge Orbe, Robinson Guzmán, Guillermo Carpintero. "Traveling Wave Model of a Twin Ridge Semiconductor Laser". Proceedings of the 2010 Annual Symposium of the IEEE Photonics Benelux Chapter. p.p 281-284. Delft, the Netherlands. November 18th and 19th, 2010.